NAVAL POSTGRADUATE SCHOOL

MONTEREY, CALIFORNIA

THESIS

LONG-RANGE STATISTICAL FORECASTING OF KOREAN SUMMER PRECIPITATION

by

Robert C. Tournay, Jr

March 2008

Thesis Advisors:	Tom Murphree
	David Smarsh
Second Reader:	Zhuo Wang

Approved for public release; distribution is unlimited

THIS PAGE INTENTIONALLY LEFT BLANK

REPORT DOCUMENTATION PAGE			Form Approved OMB No. 0704-0188
Public reporting burden for this collection of information is estimated to average 1 hour per response, including the time for reviewing instruction, searching existing data sources, gathering and maintaining the data needed, and completing and reviewing the collection of information. Send comments regarding this burden estimate or any other aspect of this collection of information, including suggestions for reducing this burden, to Washington headquarters Services, Directorate for Information Operations and Reports, 1215 Jefferson Davis Highway, Suite 1204, Arlington, VA 22202-4302, and to the Office of Management and Budget, Paperwork Reduction Project (0704-0188) Washington DC 20503.			
1. AGENCY USE ONLY ***(Leave blank)***	**2. REPORT DATE** March 2008	**3. REPORT TYPE AND DATES COVERED** Master's Thesis	
4. TITLE AND SUBTITLE: Long-Range Statistical Forecasting of Korean Summer Precipitation		**5. FUNDING NUMBERS**	
6. AUTHOR(S) Tournay, Robert, C.			
7. PERFORMING ORGANIZATION NAME(S) AND ADDRESS(ES) Naval Postgraduate School Monterey, CA 93943-5000		**8. PERFORMING ORGANIZATION REPORT NUMBER**	
9. SPONSORING /MONITORING AGENCY NAME(S) AND ADDRESS(ES) N/A		**10. SPONSORING/MONITORING AGENCY REPORT NUMBER**	
11. SUPPLEMENTARY NOTES The views expressed in this thesis are those of the author and do not reflect the official policy or position of the Department of Defense or the U.S. Government.			
12a. DISTRIBUTION / AVAILABILITY STATEMENT Approved for public release; distribution is unlimited		**12b. DISTRIBUTION CODE**	

13. ABSTRACT (maximum 200 words)

We examined long-range statistical forecasting methods for Korean summer precipitation (KSP). We reviewed existing literature on the East Asian summer monsoon to develop a background on current KSP research and on the relationship of KSP to climate variations. Second, we explored interannual variability of KSP using composite and correlation analyses. We found that circulation anomalies in the spring prior to the monsoon in the tropical northwest Pacific alter sea surface temperatures (SST). These SST anomalies then persist into the following summer, leading to summer circulation anomalies that alter the flow into Korea and the precipitation on the seasonal scale. From this relationship, we developed a seasonal forecasting index. Third, we looked at KSP on the intraseasonal scale, to develop statistical forecast methods with five to thirty day leadtimes. We found that the Korean summer monsoon onset, break and withdrawal are positively correlated to the El Niño / La Niña state. We found that the Madden-Julian Oscillation (MJO), when conditioned with our seasonal index, showed skill in forecasting with lead times out to 20 days. Last, we found that tropical cyclone activity in Korea is impacted by ENSO on the interannual scale, and MJO on the intraseasonal scale.

14. SUBJECT TERMS Climate, climate variations, Korea, monsoon, precipitation, El Niño, La Niña, teleconnections, index development, smart climatology, flooding, drought, statistical forecasting, long-range forecasting			**15. NUMBER OF PAGES** 145
			16. PRICE CODE
17. SECURITY CLASSIFICATION OF REPORT Unclassified	**18. SECURITY CLASSIFICATION OF THIS PAGE** Unclassified	**19. SECURITY CLASSIFICATION OF ABSTRACT** Unclassified	**20. LIMITATION OF ABSTRACT** UU

NSN 7540-01-280-5500 Standard Form 298 (Rev. 2-89)
Prescribed by ANSI Std. 239-18

THIS PAGE INTENTIONALLY LEFT BLANK

Approved for public release; distribution is unlimited

LONG-RANGE STATISTICAL FORECASTING OF KOREAN SUMMER PRECIPITATION

Robert C. Tournay, Jr
Captain, United States Air Force
B.S., University of Maryland, College Park, 2000

Submitted in partial fulfillment of the
requirements for the degree of

MASTER OF SCIENCE IN METEOROLOGY

from the

NAVAL POSTGRADUATE SCHOOL
March 2008

Author: Robert C. Tournay, Jr

Approved by: Tom Murphree
Thesis Advisor

David Smarsh
Co-Advisor

Zhuo Wang
Second Reader

Phillip Durkee
Chairman, Department of Meteorology

THIS PAGE INTENTIONALLY LEFT BLANK

ABSTRACT

We examined long-range statistical forecasting methods for Korean summer precipitation (KSP). We reviewed existing literature on the East Asian summer monsoon to develop a background on current KSP research and on the relationship of KSP to climate variations. Second, we explored interannual variability of KSP using composite and correlation analyses. We found that circulation anomalies in the spring prior to the monsoon in the tropical northwest Pacific alter sea surface temperatures (SST). These SST anomalies then persist into the following summer, leading to summer circulation anomalies that alter the flow into Korea and the precipitation on the seasonal scale. From this relationship, we developed a seasonal forecasting index. Third, we looked at KSP on the intraseasonal scale, to develop statistical forecast methods with five to thirty day leadtimes. We found that the Korean summer monsoon onset, break and withdrawal are positively correlated to the El Niño / La Niña state. We found that the Madden-Julian Oscillation (MJO), when conditioned with our seasonal index, showed skill in forecasting with lead times out to 20 days. Last, we found that tropical cyclone activity in Korea is impacted by ENSO on the interannual scale, and MJO on the intraseasonal scale.

THIS PAGE INTENTIONALLY LEFT BLANK

TABLE OF CONTENTS

THIS PAGE INTENTIONALLY LEFT BLANK

LIST OF FIGURES

LIST OF TABLES

LIST OF ACRONYMS AND ABBREVIATIONS

ACC	Accuracy
AFCCC	Air Force Combat Climatology Center
AH	Azores High
AO	Arctic Oscillation
ASM	Asian summer monsoon
BOB	Bay of Bengal
BOM	Australian Bureau of Meteorology
CAF	composite analysis forecast
CCA	canonical correlation analysis
CDC	Climate Diagnostics Center
CMAP	Climate Prediction Center's Merged Analysis of Precipitation
CPC	Climate Prediction Center
CRI	Changma Rainfall Index
CSEOF	cyclostationary empirical orthogonal function
CZ	convergence zone
DMI	Dipole Mode Index
DoD	Department of Defense
E	east
EASM	East Asian Summer Monsoon
EN	El Niño
ENLN	El Niño/La Niña
ENSO	EL Niño/Southern Oscillation
EOF	empirical orthogonal function
ESRL	Earth Systems Research Laboratory
FAR	false alarm rate
FNMOD	Fleet Numerical METOC Detachment
GFS	Global Forecast System
GHCN	Global Historical Climatology Network
GPH	geopotential height
GSOD	Global Summary of the Day

hPa	hectopascal
HSS	Heidke skill score
IO	Indian Ocean
IOZM	Indian Ocean Zonal Mode
IRI	International Research Institute for Climate and Society
ISO	intraseasonal oscillation
ISV	intraseasonal variability
KSM	Korean summer monsoon
KSP	Korean summer precipitation
LLJ	low-level Jet
LTM	long term mean
MC	maritime continent
MEI	Multivariate ENSO Index
MJO	Madden-Julian Oscillation
MT	monsoon trough
N	north
NAM	North Atlantic Annular Mode
NAO	North Atlantic Oscillation
NCAR	National Center for Atmospheric Research
NCEP	National Centers for Environmental Prediction
NH	northern hemisphere
NE	northeast
NW	northwest
OLR	outgoing longwave radiation
PNA	Pacific-North American
POD	probability of detection
RMMI	real-time multivariate MJO index
PRATE	precipitation rate
PSAC	Philippine Sea anticyclone
S	south
SASM	South Asian summer monsoon
SCS	South China Sea

SD	standard deviation
SLP	sea level pressure
SPWG	seasonal prediction working group
SST	sea surface temperature
SE	southeast
SW	southwest
TC	tropical cyclone
UDEL	University of Delaware
W	west
WP	West Pacific Oscillation
WPZI	West Pacific Zonal Index
WS	weather squadron
ZMI	Zonal Mode Index

THIS PAGE INTENTIONALLY LEFT BLANK

ACKNOWLEDGMENTS

My heartfelt thanks to my advisors, Prof. Tom Murphree, Col Dave Smarsh and Dr Zhuo Wang. Without your guidance and knowledge none of this would have been possible. Of course, my thanks go to my family. To my wife Meredith for putting up with my sometimes short temper brought on by too many hours working towards dead ends. To my daughter Charlotte for always being able to change my attitude — after a day of academic annoyance — with her (mostly) positive three-year-old's attitude. And last, to my dog Brutus for being the best pet one could ask for, despite his constant complaining about the frequent military moves.

THIS PAGE INTENTIONALLY LEFT BLANK

I. INTRODUCTION

A. IMPORTANCE

Between 5 and 9 August 1998, over 40 inches of rain fell in vicinity of the Demilitarized Zone (DMZ) in Korea. Over 230 people were killed, including three U.S. soldiers. Over 100 million dollars in flood damages was assessed at regional U.S. Army camps. Ammunition was swept away as hundred of buildings were destroyed (Hawthorne 2008). Cleanup continued for months as the U.S. force's focus was taken from its primary mission. Untold numbers of North Koreans died, with the heaviest of the precipitation falling north of the DMZ. This single event underpins the importance of summer precipitation forecasting on the Korean peninsula during the Changma, or Korean Summer Monsoon (KSM). During the KSM, from late June through early September, Korea receives over 55% of its annual total rainfall. Short-term effects of flooding rains can be devastating, but longer term, more widespread implications exist as well. Seasonal floods and droughts can wreak havoc on the rice crop, which supplies the majority of the diet for the 72 million inhabitants of the peninsula. In addition to the direct effect of precipitation on the mission of U.S. and Republic of Korea forces, the secondary effects of reduced visibility, ceilings and trafficability are the worst during the summer rains.

B. THE MONSOON ANNUAL CYCLE

The word *monsoon* is derived from the Arabic *mausim*, meaning season. Today, the monsoon is defined generally as a seasonal reversal of winds (Ramage, 1971). The northern hemisphere (NH) monsoon is specifically the change from winter, in which the low level winds are northerly, out of the Asian continental high, to summer, in which the low level winds are southerly, from the tropics into the migratory convergence zones (CZs) stretching from Pakistan in the west to Japan in the east. The summer CZs essentially follow the solar maximum heating, moving to their most southern positions during the middle of the austral summer and to their most northern positions during the

boreal summer. Due to the much greater amount of land in the NH and the distribution of topography, which provides an elevated tropospheric heat source in the Tibetan region, a strong meridional temperature gradient develops in the boreal spring and summer, and the transition from the Asian winter monsoon to the Asian summer monsoon is much more abrupt than the reverse transition. The two primary subsystems of the Asian summer monsoon (ASM) system are the South Asian summer monsoon (SASM) and the East Asian summer monsoon (EASM).

1. The South Asian Summer Monsoon

As the SASM develops during the boreal spring, the monsoon CZ shifts northward to the Maritime Continent (MC). This convection induces large-scale subsidence over the northern Indian Ocean (IO), allowing for abundant solar heating of the waters as well as the Subcontinent and Tibetan Plateau (Goswami 2005). This low-level heating is capped by the subsidence, allowing for "potential convective instability" to accrue as the CZ slowly moves northward. Normally, the meridional gradient of tropospheric temperature will reach a critical level and switch from a north-to-south gradient, to a south-to-north gradient, causing the CZ to move rapidly northward into the Bay of Bengal and the west coast of India through the month of May. This period also heralds the reversal of the low-level wind field over the northern IO from easterlies or northeasterlies to monsoon westerlies, as low level air flows out of the southern hemisphere Mascarene High pressure system, through the Somali jet and into the northern IO. Through subsequent weeks in late May and early June, the CZ moves further north into Bangladesh and western Indochina. Finally, the CZ moves into central and northern India and Pakistan through the month of June. The average start dates for all sectors of the ASM monsoon are illustrated in Figure 1. Figure 2 shows the peak rainfall by pentad. Pentads are a method of breaking the year into 72 five-day periods, making six pentads per month. The first pentad in June is pentad 31 while the last whole pentad in August is pentad 48. Figure 3 (a) shows a latitude-time cross-section of mean precipitation along 70-80 E longitude. Note the rapid northward movement of the precipitation during May-June, and a much more gradual southward movement during September-December.

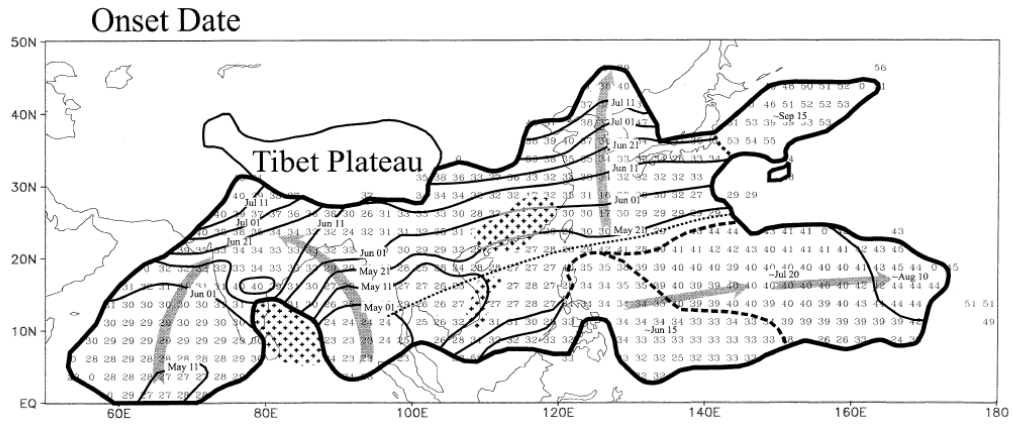

Figure 1. Average dates at which Asian summer monsoon precipitation begins, shown by dates along thin black contour lines (from Wang and Linho 2002).

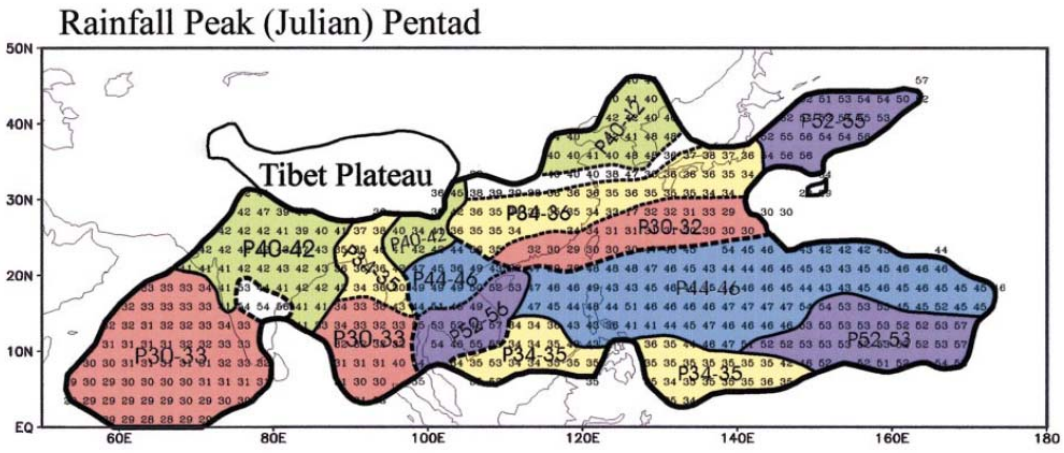

Figure 2. Peak precipitation by pentad (P30 - P55) for each major subsystem of the Asian summer monsoon (shown by colored regions) (from Wang and Linho 2002).

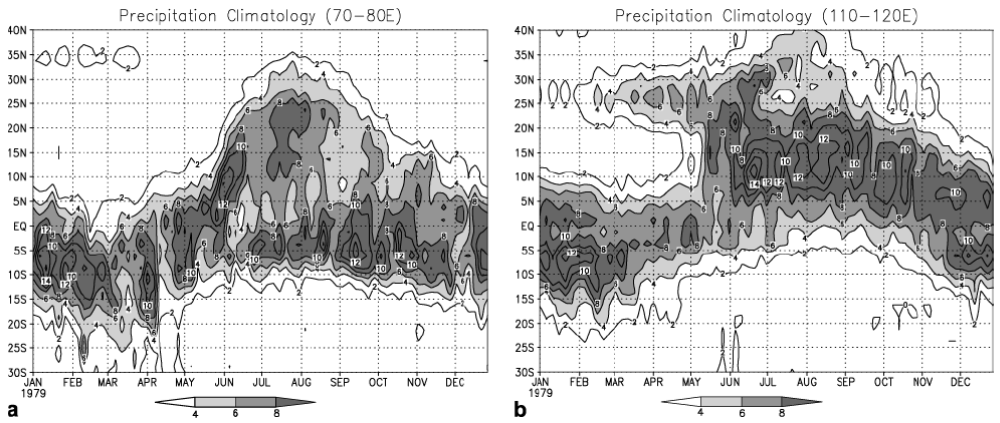

Figure 3. Latitude-time cross-sections of precipitation for (a) 70-80 degrees E longitude and (b) 110-120 degrees E longitude. Data from Climate Prediction Center's Merged Analysis of Precipitation (CMAP) dataset for 1979-2001. Units are mm s^{-1}. From Sun (2002).

2. The East Asian Summer Monsoon

The East Asian summer monsoon (EASM) develops in the boreal spring as the convection moves northward from the MC into the South China Sea (SCS). The start date of the SCS monsoon has been a source of controversy in recent literature, but the appearance of steady 850 hPa westerlies in the SCS is a commonly used indicator of the start (Wang, et. al. 2004). The SCS is the only subsystem of the EASM that is purely tropical. There is also controversy on whether to include the SCS monsoon in the EASM system. The older school of thought (Tao et al 1987) defines the EASM as a subtropical system that commences with the appearance of the rain band in the Yangtze River valley and progresses north and eastward. Wang et al. (2004) showed that the SCS subsystem does lead into the subtropical subsystems of the EASM as it shifts northward through the summer. The SCS monsoon begins an average of 15 days after the rains begin in the Bay of Bengal, in mid May and reaches its peak in late May through early June.

The EASM typically shifts abruptly northward from the SCS into the heart of China and southern Japan during early to mid June. During this shift, the monsoon moves from a purely tropical system driven primarily by diabatic heating fields and low level winds, to a subtropical system that also interacts with transient baroclinic eddies, increased vertical wind shear, and baroclinicity. Figure 3 (b) shows a latitude-time cross-

section of mean precipitation along 110-120 E longitude. Note the rapid move northward during May-July. The EASM reaches its northward maximum in Korea during August and, just as in the SASM, shifts gradually equatorward during September-December.

The onset time and peak rainfall time of mid to late June are about the same for the Yangtze River valley to the west and southern Japan in the east (Figures 1-2). However, the major summer monsoon precipitation, referred to as the "Meiyu" in China and the "Baiu" in Japan, shows distinctly different characteristics between east and west. Chen and Chang (1980) noted that the eastern portion showed the hallmarks of a midlatitude polar frontal system, which stacks to the north with height and shows a strong horizontal temperature gradient in the low-levels; while over China, the vertical structure was more barotropic, with little system stacking with height and negligible horizontal temperature gradients in the low levels. These differences were later expounded upon in detail by Ding (1992). While these differences are still accepted, there are cases in the literature describing transient waves causing heavy rainfall over China (Chang 1998) and Meiyu frontogenesis (Cho and Chen 1998). Figure 4 provides a schematic of the Meiyu/Baiu in the context of upper and lower level flow and regional geography.

The Meiyu is the most studied subsector of the EASM. While there is not a large horizontal temperature gradient across the Meiyu precipitation boundary, and both sides are moist, there is weak gradient that provides enough low level convergence to support heavy rains. Figure 5 shows a north to south vertical profile schematic of the Meiyu. As in the Baiu region, the development of a southerly low-level jet (LLJ) is prominent and key to the heavy rainfalls. The Meiyu LLJ is broad in scale and pulls in deep tropical moisture. Mesoscale convective complexes are frequent during the peak rainfall period (Ding 2005).

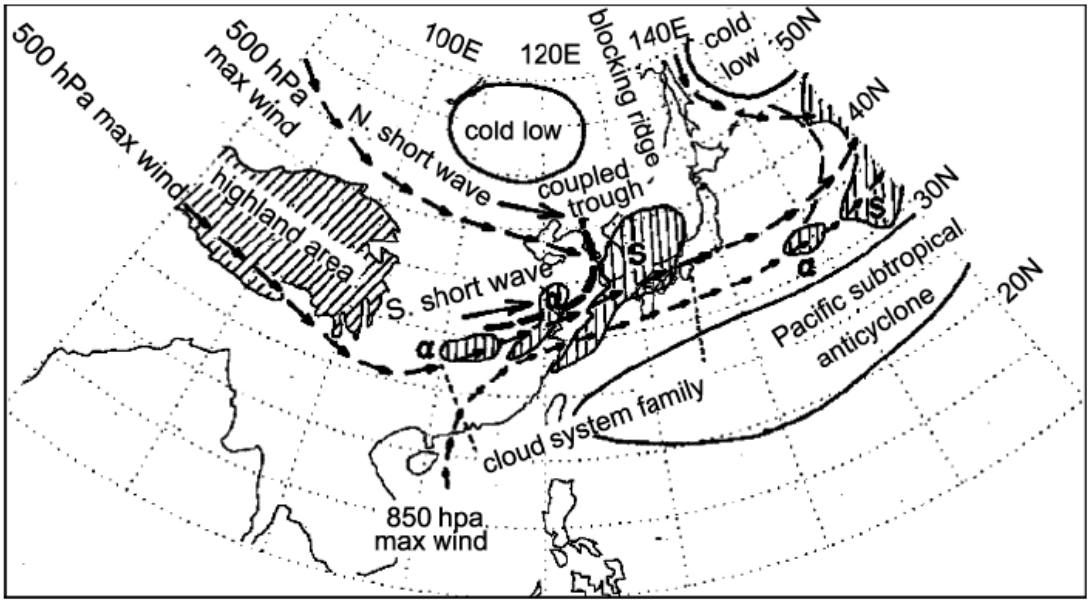

Figure 4. Conceptual model of the Meiyu/Baiu system. Shaded "S" area over Korea is associated with a shortwave trough with associated mesoscale alpha systems trailing over China (from Ninoyama 2004).

Because Japan is further downstream than China from the Tibetan High, which deflects the maximum upper tropospheric winds to the north, more vertical shear and baroclinic structure is present over Japan than China during the onset of the summer monsoon (Ding and Chan 2005). As a result, mesoscale depressions moving in from the west often undergo baroclinic development as they move into this baroclinic zone. The LLJ is also key to heavy rainfalls in the Baiu, but shows the characteristics associated with a midlattitude system, namely a stronger maximum and a smaller horizontal scale than that associated with the Meiyu.

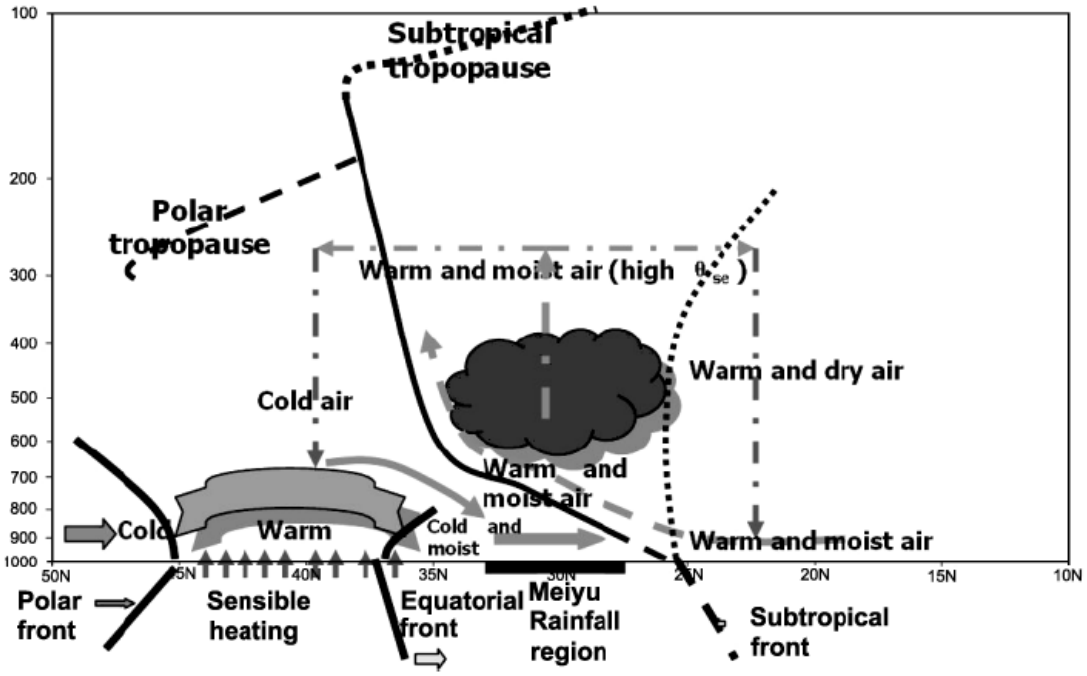

Figure 5. Schematic model of the Meiyu in East China (from Liu et al 2003).

C. THE KOREAN PENINSULA AND THE KSM

1. Geography

The Korean Peninsula is comprised of two states: the Democratic People's Republic of Korea to the north and the Republic of Korea to the south. The peninsula stretches from the Yalu River in the north, at an average latitude of 41 N to its southern tip at 34 N. The peninsula is an average of 260 kilometers (160 miles) wide, though it is much wider at the northern edge. The entire peninsula is mountainous, with a distinctly higher range running along the east coast, the Taebek Range, with fewer mountains and plains and arable land on the west coast. To the north is the mountainous Chinese region of Manchuria, with elevations ranging from 500 ft to 3000 ft (150m to 900m). To the west is the Yellow Sea (called the East Sea by Koreans) with a west-east extent of roughly 600 km (380 miles). To the south, is the East China Sea (called the South Sea)

and to the east is the Sea of Japan (East Sea), and beyond is Japan, 180km (115 miles) from the Korean Peninsula at its closest point. Figure 6 shows a map of the Korean peninsula with the features above listed.

Figure 6. Map of Korean Peninsula and surroundings. Accessed from http://www.globalsecurity.org/ (10 January 2008).

2. The Korean Summer Monsoon

The final northward movement of the EASM is into the Korean Peninsula region. The Korean portion of the EASM, the Korean summer monsoon (KSM), is not nearly as well studied as other sectors of the ASM system (especially when considering research published in US journals), with most KSM studies having been published after 1996.

There are considerable differences in the determination of the KSM start date. For example, at the southern tip of the peninsula, Tanaka (1992) proposed a start date of 1 June, while Chen (1987) proposed 30 June. We investigated the start date in this study, but assume for now the start dates proposed by Wang and Linho (2002) of 21 June for the

southern Korean Peninsula to 11 July for the northern part of the Korean Peninsula. The peak intensity of the KSM underwent a large decadal scale shift in peak intensity in the late 1980s and early 1990s, with the peak occurring on average in mid-July during 1979-1992, 20 days later than during 1993-2001 (Ha 2005). This study also highlights the fact that, like other sectors of the ASM, the KSM shows a bimodal distribution of precipitation, with the first, and main, peak coming between late June through mid July and the second, and lesser, peak coming in August, with a monsoon break typically occurring in between.

A recent study by Wang et. al. (2007) studied the 227-year Seoul rain gauge dataset developed by Lim et al. (1996) and Jhun and Moon (1997) based on data collected from the Chukwookee ("rain-measuring device") from 1778 to 1907 and the modern instrument record from 1908-2004. They found that the onset date averaged 25 June (pentad 36), with a monsoon break typically around 5 through 15 August (pentads 44 and 45). A prominent mode of variability was the quasi-biweekly oscillation, to the surprise of the authors. The running 30-year mean fluctuated dramatically through the long record, indicating a large amount of low frequency variability.

D. INTERANNUAL VARIABILITY AND TELECONNECTIONS

Since Gilbert Walker's 19th century work on the linkage of the Indian summer monsoon to pressure patterns in the Pacific Ocean, scientists have made great efforts to identify linkages between weather and climate phenomena occurring far from each other. Such linkages between widely separated areas of the globe are referred to as *teleconnections.* Teleconnections tend to be associated with climate variations, such as El Niño/La Niña (ENLN), the North Atlantic Oscillation (NAO), the West Pacific Oscillation (WP), and the Indian Ocean Zonal Mode (IOZM) (Vorhees 2006). All of these interannual variations are potentially important for understanding interannual variability in the EASM in general and KSP in particular.

1. El Niño/La Niña

Numerous studies have demonstrated that the anomalous convection in the equatorial Pacific during ENLN periods leads to tropical and extratropical atmospheric

circulation anomalies (e.g., Ford 2000). Part of the mechanism by which this is accomplished was first advanced by Matsuno (1966) and Gill (1980), who found that the forcing induced by anomalous convection produced an equatorial Rossby-Kelvin wave response (Figure 7). Horel and Wallace (1981), and other studies, have documented a number of characteristic extratropical anomalies that occur during EN and LN events. Sardeshmukh and Hoskins (1988) proposed a mechanism by which anomalous tropical forcing could induce an extratropical Rossby wave train response. Nitta (1987) and others identified a Rossby wave train response to off-equatorial tropical convection anomalies during the summer that can extend across large portions of the extratropics (Figure 8).

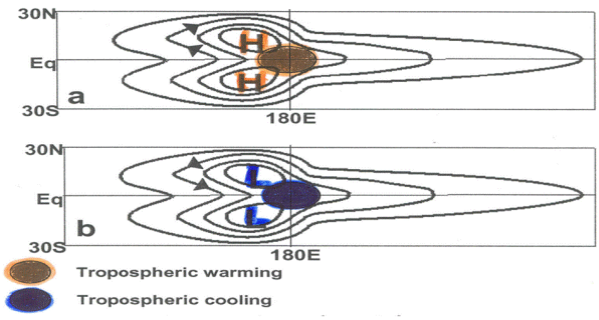

Figure 7. Schematic upper tropopheric response to anomalous (a) warming and (b) cooling of the tropospheric column about the equator. Contours show perturbation pressure isobars. There is a ridge in (a) and a trough in (b) at the equator and to the east of the forcing region. Note that the pressure to the west of the forcing region is different relative to its value off the equator. Note the paired (a) anticyclones and (b) cyclones to the NW and SW of the forcing region. From Ford (2000).

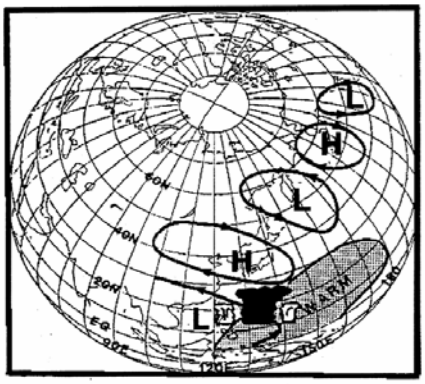

Figure 8. Schematic showing 500 hPa geopotential height (GPH) anomalies associated with increased convection over the warmer than normal SST in the tropical western Pacific. H (L) denotes a positive (negative) GPH anomaly. Adapted from Nitta (1987).

For the EASM system as a whole, the impact of ENLN has been shown to depend on the stage of ENLN development prior to and during the summer monsoon in question. Huang and Wu (1989) found that during summers in which an EN is developing, north and south China tended to experience drought, while central china tended experience wetter than normal conditions. In summers immediately after an EN has occurred, Meiyu/Baiu tended to be above average intensity (Huang Wu 1989, Zhang 1996, Kawamura 1998).

Wang, Wu, and Fu (2000) and Wang and Zhang (2002 attempted to explain increased rainfall throughout the EASM sector following an EN event. They proposed that ENLN impacts on the EASM occur through changes in the Philippine Sea Anticyclone (PSAC). The PSAC develops abruptly during the boreal fall of a developing EN event. The PSAC is then maintained through the boreal winter and spring of the EN event through positive thermodynamic feedback between atmospheric Rossby waves and an underlying cold SST anomaly east of the PSAC center. The anomalously anticyclonic circulation of the PSAC persists into the summer and provides increased southerly flow and moisture flux into the EASM, making the EASM precipitation greater following an EN event.

2. Indian Ocean Zonal Mode

The eastern portions of the Indian Ocean tend to be warmer (by approximately 1-2 °C) than the western portions (Black et al. 2003). During the late 1990s, in seeking a mechanism to explain anomalous rainfall in tropical east Africa, Saji et al. (1999) identified an interannual mode of variability in SSTs across the tropical Indian Ocean that creates an anomalous east-west temperature gradient, with positive (negative) SST anomalies in the western (eastern) Indian Ocean. This mode came to be called the IOZM, (also called the Indian Ocean Dipole), and is a phenomenon that occurs in the Indian Ocean basin but at times is intertwined with ENLN (Saji et al. 1999; Twigg 2007). Saji et al. (1999) described the dipole mode in terms of the difference in SST *anomaly* between the tropical western Indian Ocean (50 °E-70 °E, 10 °S-10 °N) and the tropical

southeastern Indian Ocean (90 °E-110 °E, 10 °S-equator) (near the west coast of Sumatra). A schematic of the IOZM is presented in Figure 9.

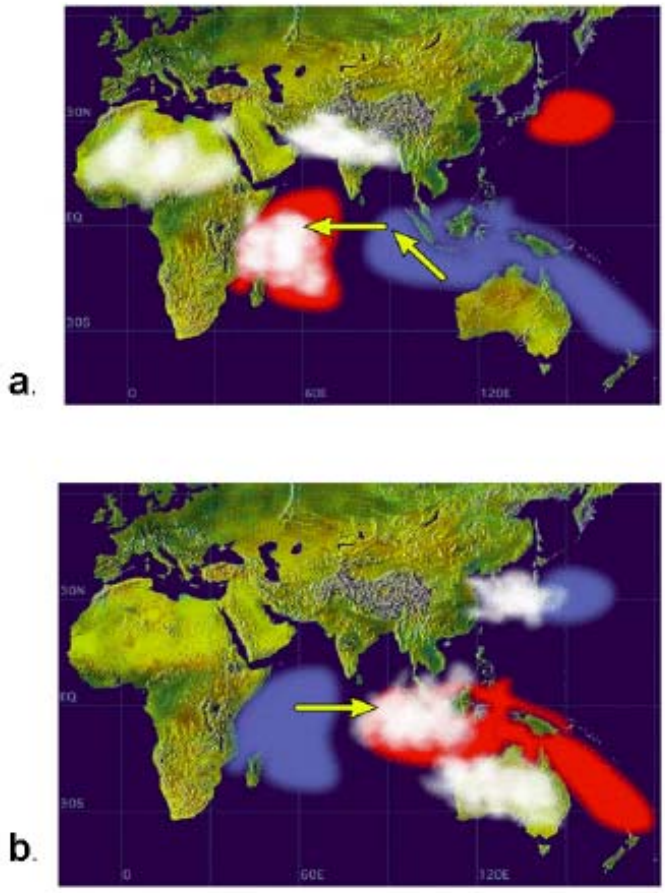

Figure 9. Schematics showing the SST anomaly patterns associated with the (a) positive and (b) negative phases of the IOZM. The red shading denotes positive SST anomalies and the blue denotes negative SST anomalies. Clouds are drawn in areas that experience above normal convection during the two phases. From http://www.jamstec.go.jp/frsgc/research/d1/iod/IOD1.html (Accessed 2 Feb 2008).

Little research has linked the IOZM with the EASM in general or the KSM in particular. Kripilani (2006) studied the relationship between the IOZM and total summer precipitation for the Chinese, Japanese, and Korean sectors of the EASM. Using a leading and lagging seasonal Zonal Mode Index (ZMI) versus sector averaged

precipitation values, the leading ZMI was shown to have the greatest correlation to Korean precipitation, in particular when the ZMI led Korean precipitation by one-year, for which the correlation was 62%, and for three-season lead, for which the correlation was 35%. The author offers two explanations for this possible long lead correlation. The first is dubbed the northern channel, in which anomalously heavy precipitation over India induces an anomalous anticyclonic Rossby wave response to the northwest, over Central Asia, which in turn induces an anomalous Rossby wave train response downstream. The Rossby wave train response manifests itself in snowfall/snowdepth anomalies over Eurasia. Heavy snow over western Eurasia and light snow over eastern Eurasia weakens the large-scale pressure gradient between high and low latitudes, and subsequently weakens the LLJ into Korea, thus dampening the amount of monsoon precipitation. The second, dubbed the southern channel, is premised on a strong SASM drawing more air in from the cross-equatorial flow which leads to upwelling on the East African coast. Walker circulation adjustment leads to warmer water over the eastern IO and the western tropical Pacific. The warmer water over western tropical Pacific causes the West Pacific Subtropical High pressure to develop earlier than normal, reducing moisture advection into, and precipitation over, Korea and Japan.

3. North Atlantic Oscillation, Arctic Oscillation, and the West Pacific Pattern

Halfway across the world from where the MJO, IOZM, and ENSO exert their influence, the most prominent and recurrent pattern of atmospheric variability in the middle and high latitudes of the northern hemisphere is the North Atlantic Oscillation (Hurrell et al. 2003; Trigo et al. 2002). The NAO corresponds to a large-scale alternation of mass in the North Atlantic between regions of subtropical high pressure (centered near the Azores) and subpolar low pressure (south and east of Greenland—located near the climatological position of the Icelandic Low) (Lamb and Peppler 1987; Trigo et al. 2002) as shown in Figure 10.

Similar in appearance, but closer to Korea is the West Pacific (WP) pattern. The WP is also a north-south dipole of alternating pressure centers over northeast Siberia and over the western north Pacific, south of Japan. Unlike the NAO, the WP is not prominent

during all months of the year, and tends to be relatively weak in the summer, but it is the second leading mode in the NH in April and May (Barnston and Livezey 1987).

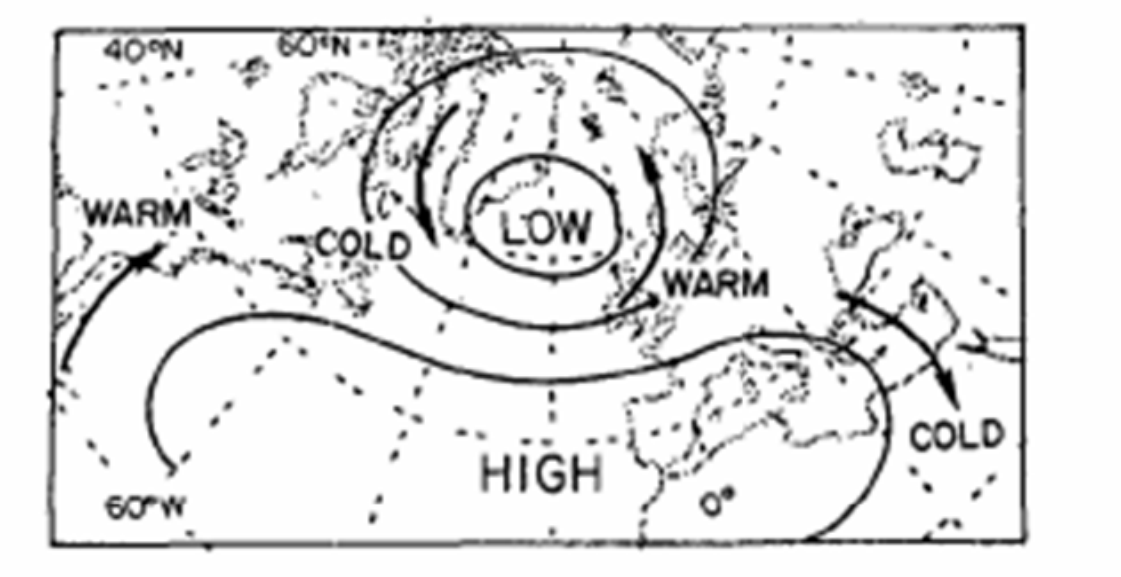

Figure 10. Schematic showing idealized relationships between pressure and temperature anomalies associated with the positive phase of the NAO. The opposite anomalies are associated with the negative phase. From Wallace and Gutzler (1981).

Hurrell et al. (2003) proposed that the NAO is the North Atlantic component of a northern hemisphere wide meridional seesaw in SLP between polar and mid-latitudes known as the Northern Hemisphere Annular Mode (NAM), and that the WP is the Pacific component of the NAM. The term NAM has come into favor recently to describe what has more commonly been called the Arctic Oscillation (AO). There is still a great deal of debate, however, as to whether the NAO is in fact the North Atlantic component of the NAM (Hurrell et al. 2003; Ambaum and Hoskins 2002). For example, Thompson and Wallace (1998, 2000) argued that the NAO "reflects the modification of the annular mode by zonally-asymmetric forcings, such as topography and land-ocean temperature contrasts."

Several scholars have studied the relationship between the NAO and the ASM system as a whole, usually with the SASM emphasized, including Chang, et al. (2001) and Dugam (1997, 2006). Yang et al (2004) examined the relationship between leading

and simultaneous AO, NAO, and ENSO on ASM intensity using the Webster and Yang Index (Webster and Yang 1992). They postulated that for a positive AO and NAO, the North African/Asian Jet is strengthened in the winter and spring, leading to higher than normal extratropical wave activity impinging upon the Tibetan Plateau, which leads to more precipitation over the plateau and colder temperatures at the start of ASM season and a later and weaker ASM. Correlations between March through May 200 hPa heights in a box over the Tibetan Plateau and surrounding area with June-August precipitation showed a -.61 correlation.

Only very recently has a relationship between the EASM and NAO been explored. Gong and Ho (2003) examined the relationship between EASM precipitation and the Arctic Oscillation (AO) over a 100-year period. Specifically, they examined the leading and simultaneous AO versus high pass filtered rainfall data at ten locations in the vicinity of the Yangtze River valley and southern Japan, as well as a mean rainfall for these stations representing the total EASM rainfall1. Correlation coefficients for individual stations for total summer rainfall (June-August) versus May AO ranged from .20 to .42, while the correlation between the mean and May AO was .45. Examining the problem in reverse, Gong and Ho performed a regression analysis of the mean summer rainfall on NH 1000 hPa GPH, which revealed a prominent annular mode between the polar region and the North Pacific. Regressions of the AO onto 200 hPA heights and mean rainfall onto 200 hPA heights produced very similar results over the region, as seen in Figure 11. The authors offer two possible explanations. First, they suggest that the strong correlation between the leading AO and EASM precipitation could arise from modification of surface boundary conditions on the Eurasian landmass leading into the EASM, which in turn modifies atmospheric circulation in the coming EASM. Second, they suggest a direct coupling between the AO and circulation features that impact the EASM, such as the EA jet and the Okhotsk High.

Ha and Lee (2007) studied the impact of teleconnection patterns on the strength of the summertime Bonin High, defined in their study as area averaged the 500 hPa GPH in a box south of Japan. They found that the WP pattern in the April preceding the EASM was correlated to the retreat of the Bonin high, and to the retreat of the EASM precipitation.

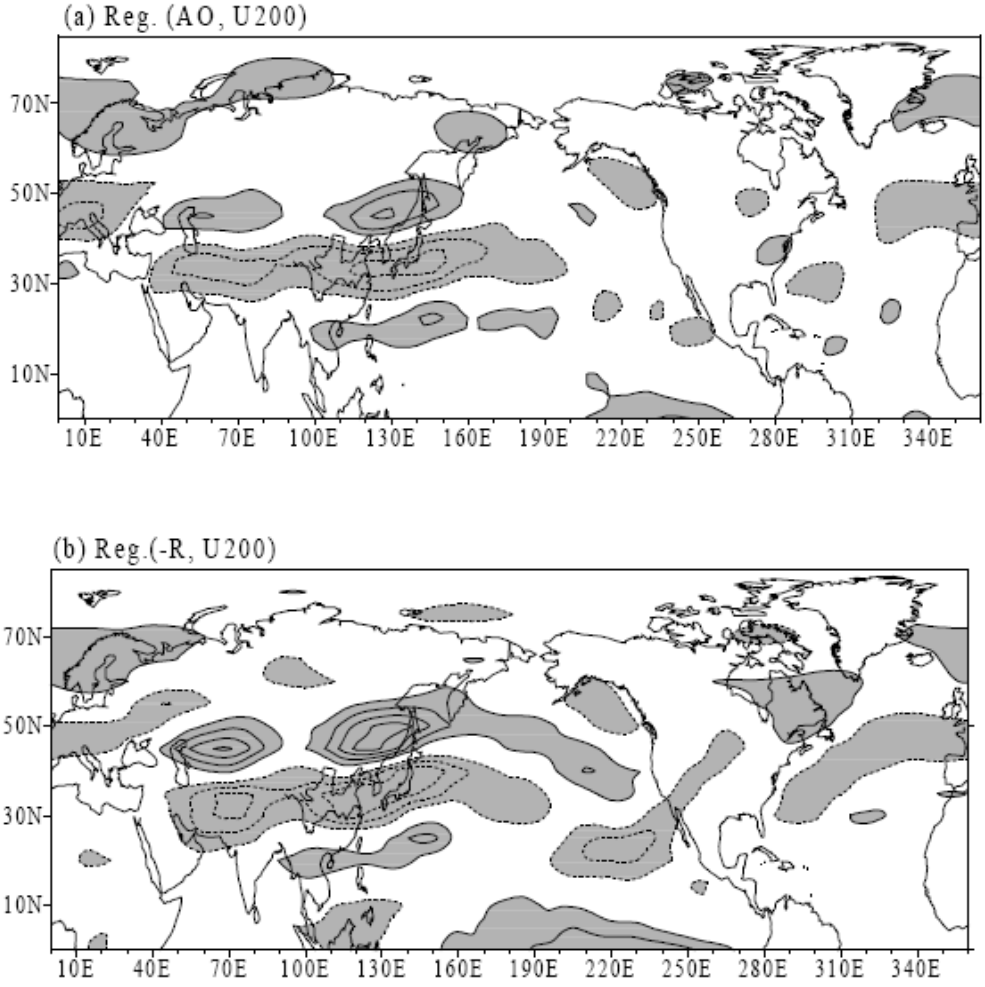

Figure 11. Changes in summer zonal wind at 200 hPa associated with (a) one standard deviation anomaly of the May AO index and (b) simultaneous ten-station-mean rainfall for summer for the period 1958-1999. Contour interval is 0.5 m s^{-1}. Regions below –0.5 m s^{-1} and above 0.5 m s^{-1} are shaded. From Gong and Ho (2003).

E. INTRASEASONAL VARIATION OF THE ASIAN SUMMER MONSOON

Intraseasonal oscillations (periods of 20-90 days) have been identified as critical to variations in the EASM (Waliser 2005). The most studied of these intraseasonal oscillations are related to weekly to monthly variations in different sectors of the ASM that can then affect the upper level circulation pattern over Korea. These include the Madden Julian Oscillation (MJO) in the equatorial region and subsequent intraseasonal

oscillations (ISOs) in the off-equatorial region, intraseasonal variations in the western North Pacific monsoon, and intraseasonal variations in the SASM.

The MJO is the dominant mode of tropical intraseasonal variability and is most active in the boreal winter (Jones et al. 2004). Madden and Julian (1971) first identified the MJO as a 40-50 day oscillation that propagated eastward from the west coast of equatorial Africa, through the Indian Ocean and Maritime Continent, and out into the equatorial Pacific Ocean. The MJO describes alternating regions of enhanced convective activity (the convective component) and enhanced subsidence (the subsidence component) (Figure 12). Variations in tropical outgoing longwave radiation (OLR) and upper and lower tropospheric wind anomalies are often used to identify the MJO. The MJO patterns of convection, subsidence, and upper and lower level height and circulation anomalies propagates eastward along with the MJO at about five meters per second (Hendon and Salby 1994).

While the MJO is typically limited in its meridional extent to within a few degrees of the equator, the influence of MJOs is felt throughout much of the extratropics. Sardeshmukh and Hoskins (1988) demonstrated that the horizontal divergence above a region of tropical convective heating (e.g., above the convective component of the MJO) can induce an extratropical wave train through Rossby wave dynamics. One important result Sardeshmukh and Hoskins (1988) demonstrated was that the upper level response to convection in the equatorial region was a pair of nearly symmetric *anticyclones* near the longitude of the forcing. The pair of anticyclones identified was very similar to the Rossby-Kelvin wave response found by Matsuno (1966) and Gill (1980).

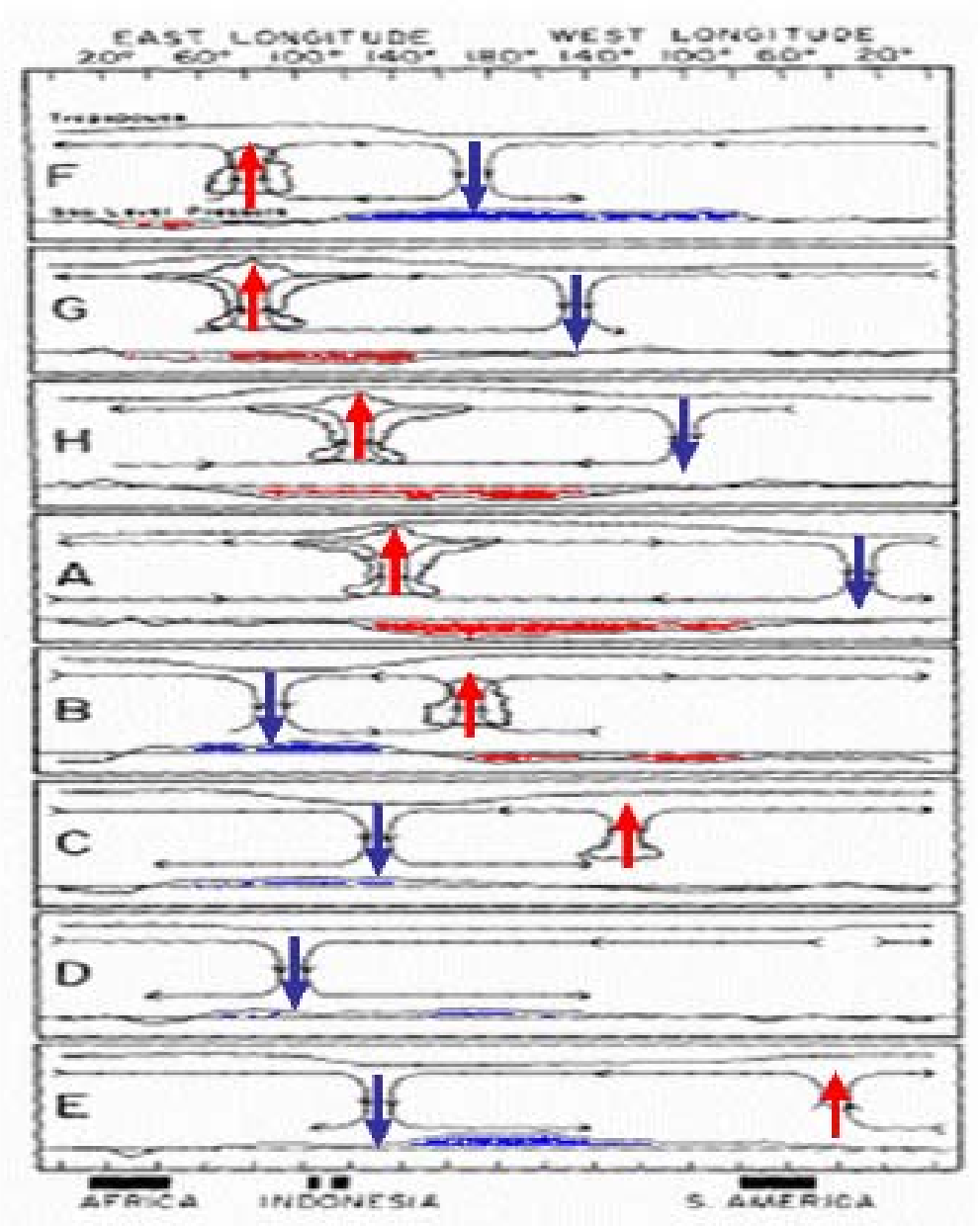

Figure 12. Schematic showing the eastward progression of the convective clouds (upward red arrows) and subsidence (downward blue arrows) components of the MJO across the Pacific and Indian Ocean. The red and blue arrows are indicative of the anomalous vertical circulation. The red and blue shading are indicative of negative and positive SLP anomalies respectively. Adapted from Madden and Julian (1994).

In addition, the authors demonstrated that the upper and lower level responses are relatively independent of the longitude of the forcing — similar responses were found when the tropical convection was in the Indian Ocean, Maritime Continent, and the central Pacific regions.

The extratropical wave trains generated by the MJO as it propagates through the Indian and Pacific Oceans impact numerous distant regions of the globe, from Australia to North America to South Africa (Stepanek 2006; Bond and Vecchi 2003; Whitaker and Weickmann 2001; Hendon and Liebmann 1990, Nogues-Paegle and Mo 1997). Understanding the teleconnections associated with the MJO is critical to long-range forecasting.

Yasunari (1979) and Lau and Chan (1988) described a 30-60 day ISO with eastward and poleward propagating components that was later related to active and break cycles of the boreal summer monsoon system (Wang 2006). Kemball-Cook and Wang (2001) produced a schematic of the synoptic evolution of this system (Figure 13).

In addition to this 30-60 day ISO, there is also a 10-20 day intraseasonal variation (ISV). The ISO accounts for roughly two-thirds of the intraseasonal variability, and the ISV accounts for another one quarter (Annamalai and Slingo 2001). The ISV appears to originate in the western North Pacific Ocean and travel westward in the form of Rossby waves at 5 m/s. As with the ISO, the ISV shows strong seasonal variation. Early in the boreal summer, with convective activity strongest in southern Asia, the 30-60 ISO is the dominant mode. As the season progresses and convective activity shifts northward and eastward, and with more convection in the western North Pacific Ocean, ISV activity intensifies.

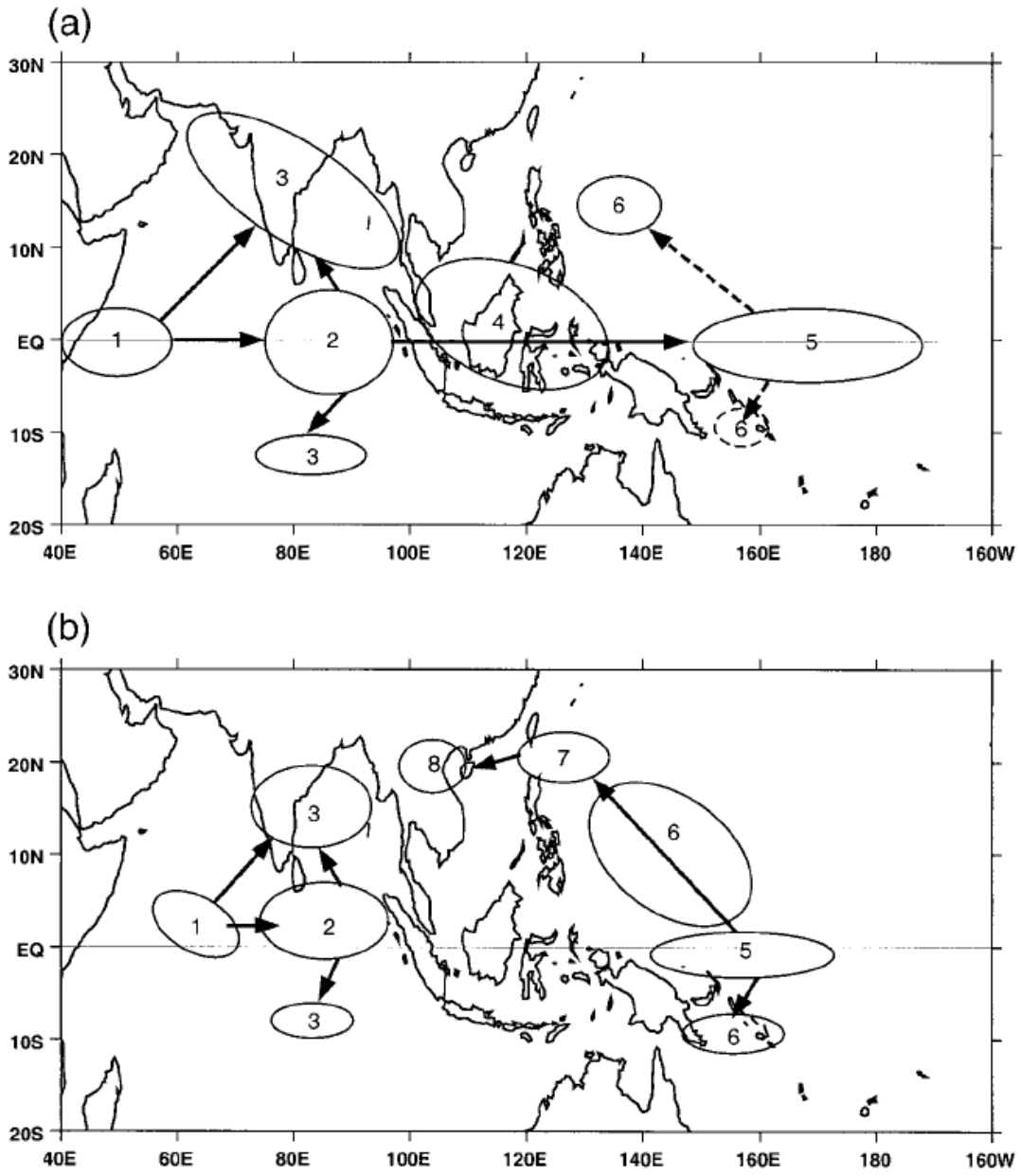

Figure 13. ISO convection life cycle schematic for (a) May-June and (b) August-October. Ovals indicate convection, with numbers indicating the evolution sequence. Arrows indicate the direction of propagation of convection. Poleward propagation of convection is associated with emanation of Rossby waves from equatorial convection. Dashed lines indicate low amplitude signal. From Kemball-Cook and Wang (2001).

Nitta (1987) proposed a connection between western Pacific convection and NH circulation patterns. He found that anomalously high sea surface temperatures near the Philippines are associated with overlying positive anomalies in atmospheric convection. This in turn causes a higher height anomaly in the upper levels along with upper level divergence. A Rossby wave response is then triggered and propagates to the northeast. This results in a trough in the wavetrain over East Asia, which inhibits convection. Using both 30-day average and 5 day average datasets, a much clearer picture of the Rossby wavetrains is exhibited on the 5-day average, suggesting that this response is more important and clear on the weekly versus monthly timescale.

F. EXISTING KOREAN CLIMATE PREDICTION METHODS

While a bevy of empirical prediction methods exist and have been tested against one another for the SASM (e.g., Kang and Shukla 2006; Wang and Fan 1999), few empirical models exist for the EASM in general or for the KSM in particular.

Hwang et al (2001) attempted a seasonal forecast of temperature and precipitation over East Asia (Korea and Japan) using canonical correlation analysis (CCA). The predictor fields for the CCA were SSTs, 700hPa GPH fields, and prior values of the temperature and precipitation. For every month and both predictand fields, Korea fared much more poorly than Japan, showing almost no statistical significance for temperature and none for precipitation forecasts during the summer months.

Kim et al. (2006) developed a seasonal prediction method using multivariate linear regression. A total of 16 climate indices provided on the Climate Diagnostic Center's and the Climate Prediction Center's website were correlated at leads of two to twelve months against South Korea monthly averaged temperature and precipitation for all months. Ten test models consisting of five grouped variables each at different leads were developed, each of which was statistically significant up to .01. These groups were then run against one another on 30 years of training data and 20 years of test data. An ensemble of the 10 models yielded performance correlation coefficients of .35, .48, and .63 for June, July, and August respectively.

Ha et al (2005) developed a non-predictive Changma Rainfall Index (CRI). The CRI consists of simultaneous correlation coefficients between total summer precipitation falling in a box surrounding Korea (developed from the CMAP dataset) and nearby GPH, SLP, or wind at various pressure levels. The CRI describes clear relationships between KSP and these other atmospheric variables. However, because it is based on simultaneous correlations, it is not prognostic and there is little predictive power in the CRI alone.

Lim and Kim (2006) used cyclostationary empirical orthogonal functions (CSEOFs) in the linear statistical forecasting technique developed by Kim and North (1998) to forecast precipitation on the pentad timescale for separate sectors of the ASM system. Using this system, the first 16 CSEOFs, the deterministic modes, were retained, which explained roughly 67% of the variance. The remaining hundreds of "noise" modes were discarded. The results of the system showed that skillful prediction of the EASM sectors up to six pentads forward could be made using this system, though the system does not describe the physical basis for the predictions.

G. EXISTING CLIMATE PREDICTION OF THE KSM

1. DoD Products

Within the DoD, 14th Weather Squadron (14 WS) and the Fleet Numerical METOC Detachment (FNMOD), both in Asheville, North Carolina, provide the majority of the climatological support to warfighters. A review of the products offered by these two centers shows their products are constructed largely with long term means (LTMs) of meteorological fields. The strengths of 14 WS and FNMOD lie in the collection, synthesizing, and visualization of LTM fields, in order to provide planning products for warfighters at all levels. Examples include atlases of ceilings, visibility, and icing; narratives describing the climate over the course of the year for numerous locations; and Operational Climatic Data Summaries — summaries of monthly and annual climate data for various cities and airfields. While it is critical to understand LTM patterns and processes, it is important to recognize that LTMs provide an incomplete picture of the climate system.

The climate variations discussed in the previous section all involve departures from LTMs and have been shown to strongly influence summer weather in Korea.

While 14 WS provides a suite of high-quality products focused on LTM conditions, it does not relate current climate conditions to these LTMs or attempt climate forecasting. 14 WS is currently exploring methods to correct this shortfall. These methods include adaptation of the types of climate analyses and forecasts produced by several different civilian agencies (particularly the Climate Prediction Center (CPC) and the International Research Institute for Climate and Society at Columbia University (IRI)). The 14 WS is presently generating experimental forecasts at lead times out to 75 days.

The 607th Weather Squadron, located on Yongsan Army Installation in Seoul, Republic of Korea, has produced a highly detailed climatological pamphlet that pulls together a large body of climate information for the Korean Peninsula. This pamphlet includes an overview of climatic regimes and forecasting rules of thumb. A major shortcoming of this pamphlet is that it accounts for only a negligible amount of scholarly work on Korean and East Asian weather and climate, especially the relatively large amount of work done in recent years.

2. Non-DoD Products

While climate prediction is still a relatively young field in the civilian community, there have been considerably more resources dedicated to this issue than in the DoD. A few of the major players in this field are the Climate Prediction Center (CPC) in Camp Springs, Maryland (www.cpc.ncep.noaa.gov, accessed 21 Feb 2008), the Earth Systems Research Laboratory (ESRL) in Boulder, Colorado (http://www.cdc.noaa.gov/index.html, accessed 21 March 2006), the International Research Institute for Climate and Society (IRI) in Palisades, New York, (http://iri.columbia.edu/, accessed 21 March 2008), and the Australian Bureau of Meteorology (BOM) in Melbourne, Australia (http://www.bom.gov.au/, accessed 21 March 2008). The various products provided by each center are discussed below. These are just a subset of the experimental and

operational monitoring and prediction products that are available, but they provide an overview on the state of climatology in the civilian sector.

a. Climate Prediction Center

CPC is the authoritative source of climate monitoring and prediction for the United States. CPC provides various indices for many of the climate variations and teleconnections discussed above. For ENLN, CPC provides numerous resources for assessing the current state of the atmosphere and ocean including plots of SST (both surface and subsurface), outgoing longwave radiation (OLR), and 850 hPa zonal winds. As the impacts of the IOZM on the US are largely unexplored, they do not include any resources for monitoring it. For the NAO, the CPC provides both graphical and tabular products to monitor this teleconnection using an index based on the rotated principal component analysis technique developed by Barnston and Livezey (1987). CPC also provides daily updates of an MJO index (based on an extended empirical orthogonal function (EEOF) applied to pentad 200 hPa velocity potential), and weekly discussions on the state of the MJO. Korea is not mentioned specifically in these products.

As its name implies, CPC also provides forecast products for some of the teleconnections discussed in the previous paragraph. CPC provides seasonal outlooks of precipitation and temperature to the public that incorporate the impacts of teleconnections. Their web page, however, contains forecast products tailored to the meteorology community, including discussions of the rationale they used to create the seasonal forecasts. For ENLN, they generate forecasts of SST (and numerous other parameters) using the NCEP coupled forecast system (CFS) model (CFS03). CPC uses the Global Forecast System (GFS) model and an 11-member ensemble model to generate seven, ten, and fourteen day outlooks of the NAO. CPC uses the GFS/Empirical Wave Propagation (EWP) model and CFS model to generate one and two-week forecasts of 200 hPa velocity potential and 45-day forecasts of 850 hPa zonal winds, respectively, to forecast the MJO. Again, Korea is not specifically addressed as the majority of CPC's customers are concerned with impacts in the US.

b. Climate Analysis Branch, Earth Systems Research Laboratory

According to their website, the ESRL Climate Analysis Branch (CAB; formerly the Climate Diagnostics Center) "strives to advance national capabilities to interpret the causes of observed climate variations, and to apply this knowledge to improve climate models and forecasts and develop new climate products that better serve the needs of the public and decision-makers." They are especially focused on climate variations causing major floods and droughts in the US and on global-scale impacts of ENLN. None of their products (monitoring or prediction) focus specifically on Korea. CAB provides tools to monitor the current state of ENLN at http://www.cdc.noaa.gov/ENSO/ (accessed 21 March 2008) and for NAO and the MJO in their "Map Room" (http://www.cdc.noaa.gov/map/, accessed 21 March 2008).

CAB also offers a wealth of climate prediction tools for ENSO, NAO, and MJO at the two websites listed above. The NAO forecasts are for seven, ten, and fourteen days. For details concerning CAB's experimental MJO prediction methodologies see their web page at http://www.cdc.noaa.gov/MJO/Predictions/ (accessed 21 March 2008).

c. International Research Institute for Climate and Society

IRI's mission, as stated at its web site, is to "enhance society's capability to understand, anticipate and manage the impacts of seasonal climate fluctuations, in order to improve human welfare and the environment, especially in developing countries."

To accomplish this, they provide numerous resources dedicated to monitoring, predicting, and investigating the impacts of climate variations. While it is impossible to discuss the full spectrum of resources here, this study will highlight a few of the most interesting and applicable products. For monitoring the climate, IRI has constructed an entire web page (http://iridl.ldeo.columbia.edu/maproom/.ENSO/, accessed 21 March 2006) dedicated to aggregating from various sources current (and recent) values of numerous quantities often used to assess ENLN, including SST, the Southern Oscillation Index, low level winds, and expert discussions. While the other

teleconnections are not discussed specifically, IRI accounts for them when issuing their outlook discussions, discussed below. For Korea specifically, one can access temperature, precipitation, and atmospheric circulation anomalies for the last month and last three months at http://iridl.ldeo.columbia.edu/maproom/.Regional/ (accessed 21 March 2006).

IRI issues probabilistic ENSO forecasts for the Niño3.4 region (120 to 170 W by 5 S to 5 N), and seasonal climate forecasts of precipitation and temperature for both regional and global domains. For additional products and details, see their web page at http://iri.columbia.edu/pred/productlist.html (accessed 21 March 2008). The seasonal climate forecasts (http://iri.columbia.edu/climate/forecast/net_asmt/, accessed 21 March 2008) are "net assessments of information from a variety of climate prediction tools, including dynamical models of the atmosphere, statistical models of climate variability related to sea surface temperature variability, and knowledge of the current state of the climate system." The forecasts are in the form of gridded maps showing the likelihood of a particular quantity falling within each of the three climatological terciles of "below-normal," "near-normal," and "above-normal," with an accompanying discussion detailing the rationale used.

d. The Korean Meteorological Administration

The Korean Meteorological Administration (KMA) runs an ensemble global spectral model at 2.5 x 2.5 degree resolution. It uses this model to produce one month, three month, and six month outlooks. The one-month outlook produces 10-day and 30-day average temperature and precipitation anomalies and is produced three times a month. The three-month forecast produces one month and three month mean temperature and precipitation forecasts at the end of every month. The six-month forecast is produced twice a year and provides one-month mean temperature and precipitation forecasts for the coming six months. Based on this numerical output, a seasonal outlook for tropical cyclones and the Changma are issued prior to summer (http://kma.go.kr/eng/lrwp/info_kma_lrf_sys.pdf, accessed 21 March 2008).

H. MOTIVATION

The overarching objective of this study is to develop long and mid-range empirical forecasting tools for the Korean summer rainy season. With this in mind, the main goals of this thesis are to:

1. Review existing literature on KSP.

2. Develop long-range prediction capabilities for the KSP

   a. Predict KSP at seasonal lead times using existing or new circulation and teleconnection indices.

   b. Predict KSP at intraseasonal lead times using circulation and teleconnection indices, and an understanding of intraseasonal oscillations of the ASM.

To fit within time constraints, this study focuses on climate variations and their relationships to circulation and precipitation patterns and anomalies. Note that precipitation fields can also be used to study cloud and moisture fields, in addition to many other variables (e.g., vertical motion, stability, etc.). Precipitation forecasting is also crucial to predicting flooding and drought. The populations in large portions of Korea, especially North Korea, lead a pastoral lifestyle in rugged mountain terrain. The potential impact of flooding and drought can be enormous. The impact of heavy rain, low level clouds, obscured mountain tops, and limited visibility can impact aviation and military operations. For this reason, being able to foresee these events will help to mitigate the impacts of climate-driven natural disasters, and improve humanitarian operations conducted by DoD in this part of the world.

Our hypotheses are that:

1. The upper and lower circulation anomaly patterns associated with ENLN, IOZM, MJO, and NAO are directly linked to *both* the primary climate variations of the region and anomalous KSP.

2. Many of the predictable impacts on KSP occur through changes in the strength and position of the Bonin subtropical high pressure system in the western North Pacific south of Korea.

3. ENLN, IOZM, AO, and MJO have impacts on the intraseasonal variations of KSP. The predictability of these large-scale circulation indices means that the intraseasonal variations in KSP also have a measure of predictability.

Chapter II presents our data and methods. Our results for seasonal forecasting and index development are detailed in Chapter III. Chapter IV contains the results of intraseasonal forecasting techniques, and Chapter V contains a summary of our results, discussions, and suggestions for future research.

II. DATA AND METHODS

A. DATA

1. NCEP/NCAR Reanalysis

The primary data source for this study was the NCEP/NCAR reanalysis data set (Kalnay et. al. 1996), acquired from the Earth Systems Research Laboratory via their website, http://www.cdc.noaa.gov (accessed 21 March 2008). The reanalysis process uses a fixed, state-of-the-art global data assimilation system to collect and analyze land surface, ship, rawinsonde, pibal, aircraft, satellite, and other observational data to produce a temporally consistent analysis of global atmospheric fields for a variety of variables (Kalnay et al. 1996). These reanalysis fields were available for most variables from 1948 through the present, and at 2.5° latitude x 2.5° longitude resolution, as of the time of this writing. As is inevitable for a project of such an immense scope, researchers have come across some questionable and erroneous data, and known problems in the dataset are documented at http://www.cdc.noaa.gov/cdc/reanalysis/problems.shtml (accessed 21 January 2008). Monthly and daily mean fields were used. To avoid potentially inconsistent data, we sought to limit our use of reanalysis data as much as possible to the era of meteorological satellites. So, for most purposes, we limited ourselves to data from 1979 and after.

2. Precipitation Data

There are numerous precipitation datasets, each with merits and faults for use in the study of Korea summer precipitation (KSP). The following issues were considered when we selected our precipitation dataset:

1. Availability of the dataset on a day-to-day basis for weekly forecasting
2. Ease of availability to end-users
3. Length of data record and completeness of the data over the period of record
4. Spatial and temporal resolution

5. Relationship to proven datasets at lower temporal resolution

6. Evidence of the accuracy of the data

7. Effectiveness of data in conducting climate forecasting for Korea

The main available datasets for assessing KSP are the University of Delaware precipitation data, NCEP/NCAR Reanalysis precipitation rate, Global Summary of the Day precipitation data, NOAA interpolated outgoing longwave radiation (OLR), and CPC Merged Analysis of Precipitation data (all described in the following section). Issues one through four were addressed for each dataset, then a comparison of the datasets at various time scales was made, followed by an assessment of the accuracy and effectiveness of the datasets for long-lead forecasting of Korean summer precipitation.

a. Precipitation Datasets

University of Delaware Precipitation (UDEL). This dataset, developed at the University of Delaware by Willmott et al. (1994), is comprised of a large number of stations, both from the Global Historical Climatology Network (GHCN) and, more extensively, from the archive of Legates and Willmott (1990).

1. Available from University of Delaware free of charge. (http://climate.geog.udel.edu/~climate/html_pages/archive.html, Accessed 10 January 2008)

2. Data delivered in large text files that require processing by user to extract useful climate information.

3. Data available for 1900 to 2006. Uses only rain gauge data. The number of stations changes over time, as do numerous other factors, such as insturmentation and instrument fielding.

4. Data available only over land every 0.50 degrees at a monthly resolution.

NCEP/NCAR Reanalysis Precipitation Rate (PRATE). The NCEP/NCAR reanalysis uses a numerical weather prediction model to consistently

reanalyze data from the past to the present so it can all be compared without bias from the model or analysis method. Precipitation rate data is not quality checked versus any other data set, but is the strict output of the reanalysis model.

1. Available at a time delay of two to three days

2. Easily available via internet from ESRL website.

3. Dataset exists from 1948 to present. Problems with compatibility of data pre and post 1970 arise due to the gradual introduction of satellite data through the 1970s.

4. Data is available globally at every 2.5 degrees and every 6 hours

Global Summary of the Day (GSOD) Precipitation. The World Meteorological Organization collects the GSOD from all stations that report. These then go through a quality check and are catalogued in a database. They are available from the National Climatic Data Center.

1. Available on a daily basis

2. Fairly lengthy and confusing menu system to get to dataset

3. Reliable data is available only from 1983 to present. Data from North Korea is questionable due to irregular reporting

4. Available where there are reliably reporting stations on a daily basis

NOAA Interpolated Outgoing Longwave Radiation (OLR). OLR can be used as a proxy for precipitation data, with, in general, lower (higher) OLR values indicating a higher (lower) probability of precipitation. NOAA collects daily values from a composite of polar orbiter data.

1. Daily data available, but with a 2-3 month lag. Data from polar-orbiters available daily.

2. Easily available at ESRL website

3. Data available from 1974 to present. Data truly uniform and available without significant gaps for 1979 to present

4. Data is available ever 2.5 degrees and every day

CPC Merged Analysis of Precipitation (CMAP). The CMAP data combines different types of satellite estimates of precipitation, rain gauge data, and NCEP Reanalysis precipitation rate data (in the enhanced version) in one product (Xie and Arkin 1997).

1. Available at irregular intervals. Appears to be about a year lag.
2. Easily available at ESRL website
3. Data available from June 1979 through September 2005
4. Available every 2.5 degrees at monthly and pentad (5-day) resolutions.

b. All-Summer Precipitation Comparison

Table 1 shows the linear correlations between the all-summer precipitation data from the five datasets. Note that, as expected, the correlations between the precipitation datasets are positive, and between the precipitation datasets and the OLR dataset are negative. However, the magnitude of the correlations varies considerably, and several are quite weak, indicating inconsistencies between the datasets. The least correlated to the other totals is PRATE, with a .51 correlation to UDEL and below .5 for all the other datasets, including an insignificant .16 correlation with GSOD. OLR is also weakly correlated with the other datasets, with a -.6 correlation to UDEL and a low correlation of -.31 to GSOD. CMAP and UDEL are very well correlated to all datasets, with UDEL having the highest average correlation of the five, with no correlation below .5.

	Crosscorrelation of Precipitation Datasets for All-Summer Totals			
	PRATE	OLR	CMAP	GSOD
UDEL	0.51	-0.60	0.78	0.80
PRATE		-0.39	0.42	0.16
OLR			-0.65	-0.31
CMAP				0.40

Table 1. Correlation of all-summer precipitation totals between the various precipitation datasets

The standardized anomalies of the all-summer precipitation for 1970-2006 from each of the five datasets is shown in Figure 14. Note that many of the larger and longer term variations are relatively consistently represented by all five datasets, but with some notable exceptions (e.g., the inconsistencies between PRATE and the other datasets during 2000-2006).

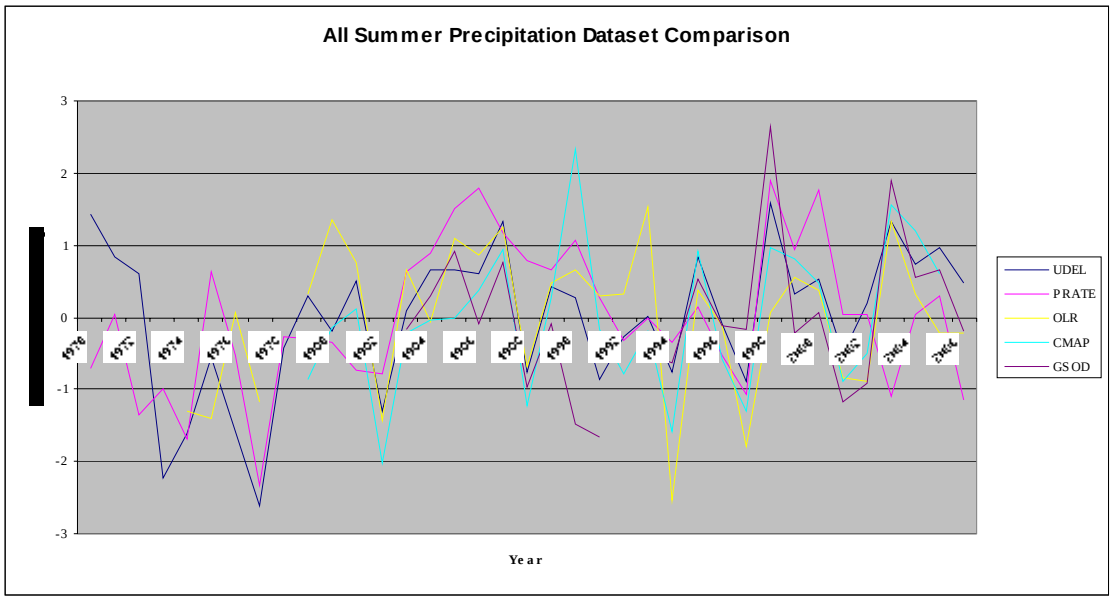

Figure 14. Graph of standardized anomalies of all-summer precipitation from all datasets.

c. Pentad Precipitation Comparison

Table 2 shows the linear correlations between the pentad summer precipitation data from the four datasets with pentad temporal resolution. A pentad value is a five day average, with, for example, pentad 1 representing 1-5 January and pentad 31 representing 31 May - 4 Jun, the first pentad of summer in this study. All four datasets show high correlations with each other. The highest correlations are between CMAP and GSOD, and CMAP and PRATE, and the lowest are those with OLR. Based on these comparisons of the datasets, and the dataset characteristics described in the preceding section, we chose to use CMAP as the precipitation dataset for this study. The key features of the CMAP dataset that make it suitable for this study are its relatively correlations with the other datasets, its integration of all types of precipitation data, from rain gauge to OLR, its relatively high temporal resolution to the pentad timescale, and its wide acceptance by the research community. From here on in this study, the precipitation results we present are based on CMAP precipitation data, unless otherwise noted.

	Crosscorrelation of Precipitation Datasets at the Pentad Timescale		
	OLR	CMAP	GSOD
PRATE	-0.50	0.79	0.69
OLR		-0.59	-0.56
CMAP			0.85

Table 2. Correlation of pentad precipitation totals between the various precipitation datasets

B. CLIMATE INDICES

1. El Niño-La Niña

ENLN phenomena have been researched extensively. There are several different methods used by researchers to classify ENLN events and quantify their strength. One of the most comprehensive measures of ENLN is the Multivariate ENSO Index (MEI) introduced by Wolter and Timlin (1993). This index monitors the six main observed variables over the tropical Pacific: SLP, zonal surface wind, meridional surface wind,

SST, surface air temperature, and total cloudiness fraction of the sky. The MEI is computed for each of twelve sliding bi-monthly seasons (e.g., Dec/Jan, Jan/Feb….Nov/Dec). Positive (negative) values of the MEI represent El Niño (La Niña) events. More information on the MEI can be found at: http://www.cdc.noaa.gov/people/klaus.wolter/MEI/index.html (accessed 21 March 2008). Because of the broad range of parameters included in the MEI, we chose to use it for our study. Positive (negative) MEI values above (below) a given threshold indicate EN (LN) events, with the threshold being determined by the user of MEI data. For our study, we set the threshold at zero, meaning that we defined EN (LN) as having occurred when the MEI was above (below) zero. We chose this low threshold because during the boreal summer, our season of interest, ENLN events tend to be relatively weak.

2. Indian Ocean Zonal Mode

The primary means for measuring the IOZM is the Dipole Mode Index (DMI), as defined by Saji et al. (1999). It is simply the difference in SST anomaly between the tropical western Indian Ocean (50 °E-70 °E, 10 °S-10 °N) and the tropical southeastern Indian Ocean (90 °E-110 °E, 10 °S-equator). Running tallies of this index are available on several different timescales, from weekly to monthly and longer. For this study, we required no finer scale than the monthly timescale. Therefore, we used the DMI as developed by Twigg (2007) based on the SST difference in the boxes above.

3. Madden-Julian Oscillation

It has only been during the last few years that methods to quantify the strength and location of the MJO in real-time have been introduced. The fundamental problem of real-time MJO-monitoring is extracting the frequency-limited signal without the use of a bandpass filter (Wheeler and Hendon 2004). Bandpass filters, typically used to identify MJO episodes, require information beyond the end of the time series, i.e., from the future when attempting to conduct real-time analyses. Researchers at the Australian Bureau of Meteorology overcame this limitation by projecting daily data onto spatial patterns characteristic of the MJO of selected meteorological variables. The details of their techniques are beyond the scope of this paper, but in essence they projected combinations

of daily meteorological fields onto two EOFs associated with the MJO. For a more detailed discussion of EOF analysis see Wilks (2006). The fields they chose to combine were OLR, 850 hPa zonal wind, and 200 hPa zonal wind, each averaged over the latitudes of 15 °S - 15 °N (Wheeler and Hendon 2004). The real-time projection of the data onto the two EOF fields yields two MJO indices—the Real-time Multivariate MJO series 1 (RMM1) and series 2 (RMM2).

In order to diagnose the state of the MJO, the RMM indices are combined into a two-dimensional phase space to display the MJO in a phase space diagram representing the location and intensity of the MJO at several consecutive times. The points representing the MJO location and intensity on sequential days are then joined by a line. These lines tend to trace a counter-clockwise circle around the origin of the phase space diagram, signifying the eastward propagation of the MJO through the global tropics (Wheeler and Hendon 2004). In order to further diagnose the state of the MJO and to facilitate compositing, the phase space is divided into eight numbered phases that are associated with the location of the convective component of the MJO. As the convective component of the MJO moves eastward from the east coast of Africa and transits the Indian Ocean into the Pacific and Atlantic regions, it moves from phase 1 through phase 8. Wheeler and Hendon (2004) noted that the nominal time between each of the numbered phases is six days for a total of 48 days (consistent with the 30-60 day period of the MJO), but that time can vary considerably from event to event.

Daily operational values of the RMM1 and RMM2 indices are available in near real-time from 1 June 1979 through the present from the Australian Bureau of Meteorology at http://www.bom.gov.au/bmrc/clfor/cfstaff/matw/maproom/RMM/ (accessed 21 March 2008). A gauge of the intensity of the MJO at any given time is obtained by taking the square root of (RMM1 + RMM2), referred to here as the magnitude of the MJO.

4. North Atlantic and West Pacific Oscillation

The NAO essentially measures the oscillation of mass between the subtropical Azores High and subpolar Icelandic Low (see chapter I). Like ENLN, the NAO has been

researched extensively, and there have been a number of different methods devised to quantify the positive and negative phases of the oscillation. Most of these methods involve measuring SLP differences between a point associated with the Azores High (either in the Azores Islands or in mainland Portugal) and a point in Iceland. This is a particularly effective means of measurement, as SLP records from these locations frequently extend far enough back in time to facilitate creation of a historical record of the NAO over at least the last century. Similar statements can be made about the WP, except that it is measured in terms of SLP differences between northeast Siberia and the southeast Asian – subtropical western North Pacific regions.

We chose for our study to use the NAO and WP indices calculated and compiled by CPC because they are more rigorous than simple SLP-differences between two locations. CPC maintains a monthly index of the NAO dating back to January 1950 and a daily index that stretches back 120 days. The monthly index we used can be found at http://www.cpc.ncep.noaa.gov/products/precip/CWlink/pna/norm.nao.monthly.b5001.current.ascii.table (accessed 21 March 2008). The method CPC uses to calculate the daily and monthly index is based on the rotated principal component analysis (RPCA) technique described in Barnston and Livezey (1987) and Wilks (2006).

C. METHODS

This thesis focuses on two major topics: (1) seasonal analysis and forecasting of KSP; and (2) intraseasonal analysis and forecasting of KSP. Each of the three methods described below below --- composite analysis, correlation analyses, and composite analysis forecasting --- were used to address each of the two main topics and are described in the following section. On the seasonal scale, composite anomalies and correlations were conducted first to provide a firm grounding on which to base a skillful composite analysis forecast. On the intraseasonal scale, a correlation analysis of the regional monsoon sectors was conducted with respect to KSP and then used to assess composite analysis forecast skill. MJO was then analyzed, first through composite analysis and then through composite anomalies and correlation analyses to identify the physical relationships between the MJO and KSP.

1. Composite Anomalies

We constructed composite anomalies of a variety of meteorological fields to highlight the impacts ENLN, IOZM, MJO, and NAO and other climate variations had on Korea. The anomalies were calculated as the difference between the actual values for a period and the LTM value for that period. For example, 200 hPa GPH anomalies for autumn of EN years were calculated by subtracting the LTM 200 hPa GPH from the mean 200 hPa GPH calculated for the selected EN years. The composite anomalies are constructed by averaging together all the anomalies associated with the climate variation (e.g., with EN). The resulting composite anomalies highlight the distinctive and characteristic climate system patterns that occur during the climate variation. For these calculations, we used as our LTM base period the mean value for 1979-2005.

2. Correlations Maps

Numerous correlation maps were developed to study the relationships between different climate system variables, especially between KSP and other atmospheric and oceanic variables in the Asian-Pacific region. Figure 15 shows the box region centered over the Korean Peninsula that we used to construct an area averaged KSP index. This box was chosen to include the entire Korean Peninsula and to capture the climatological signal of the east-west oriented EASM rain band. Picking a smaller box, one that included only Korea, would capture less variability associated with the KSM while introducing more variability due to noise in a small box. All sub-regions within the box were treated equally, with no weighting by sub-region. For each month or pentad, the CMAP values for the box region were averaged into a single monthly or pentad value. The resulting monthly and pentad KSP time series were then correlated with corresponding time series of other variables in the Asian-Pacific region (e.g., CMAP precipitation for other locations, 850 hPa GPH from the NCEP Reanalysis dataset).

3. Composite Analysis Forecast

We used the composite analysis forecast (CAF) method to develop probability forecasts for Korean summer precipitation on seasonal and intraseasonal timescales. Details on, and examples of, the CAF process can be found in Hanson (2007) and Moss

(2007). For these forecasts, the monthly and pentad KSP time series described in the preceding section were the predictands. KSP is defined through the rest of our study as the average precipitation over the box in Figure 15 below. The predictors varied according to the time scales of interest and are described in the subsequent chapters. In all cases, the forecasts are categorical for KSP values above or below the mean value for the given time period (e.g., above or below the mean summer precipitation total; above or below the pentad mean for pentad 31 (31 May - 4 June; etc.). Predictor thresholds were also used --- for example, thresholds for the ENLN or MJO index, or for other indices developed in this study. These thresholds are described in the subsequent chapters. The probability of the KSP exceeding or falling below the mean value is based on predictor values exceeding the predictor thresholds.

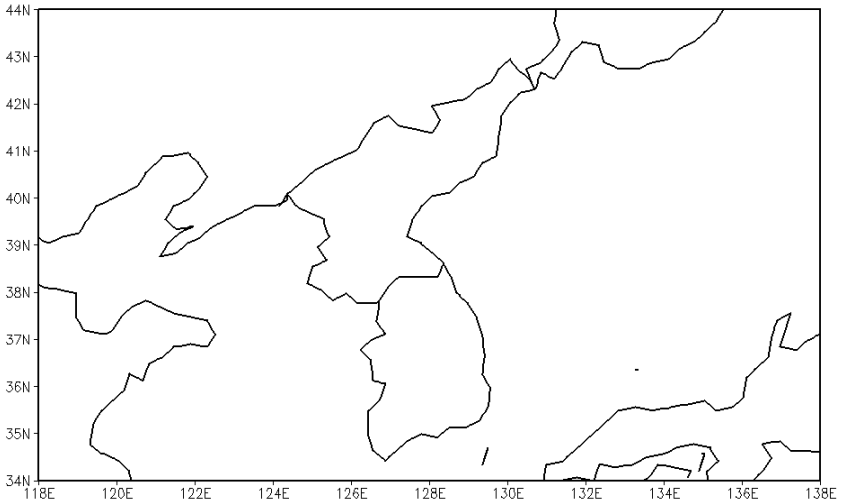

Figure 15. Box region used to construct the Korean summer precipitation (KSP) time series used in this study.

THIS PAGE INTENTIONALLY LEFT BLANK

III. RESULTS OF SEASONAL ANALYSIS AND PREDICTION OF KOREAN SUMMER PRECIPIATATION

A. KOREAN SUMMER PRECIPITATION (KSP)

Figure 16 shows several time series of KSP for 1979-2005 for the Korean box shown in Figure 15. All the time series show substantial interannual variability. The precipitation for all of the KSP period (31 May – 23 September) we refer to as the *all-summer KSP*, which is shown in Figure 16 by the brown curve. The bold black line in this figure shows a positive long term trend in all-summer KSP of about 0.5 mm/day during 1979-2005. It is also clear that July and August contribute more to KSP than June and September, making up a total of 60% of KSP versus 40% for June and September.

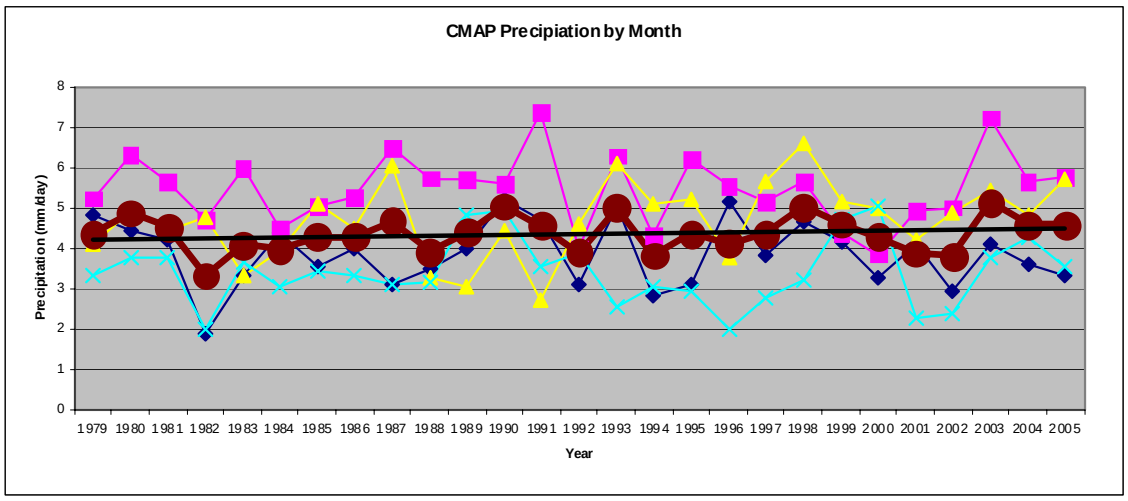

Figure 16. Time series of KSP (mm/day) by month. June – dark blue, July – pink, August – yellow, September – light blue, Jun-Sep (all-summer) – brown, long term trend in all-summer KSP – bold black.

To capture only the monsoonal part of KSP, versus precipitation associated with extratropical influences in early June (pre-monsoon) and late September (post-monsoon),

we separately analyzed pentads 36 (25 June) through 50 (7 September). We refer to precipitation during this period as the Korean summer monsoon (KSM). During this 125-day period, 55% of the annual Korean precipitation total falls. The time series of pentad 36-50, detrended and normalized by the standard deviation, is shown in Figure 17. Again, large interannual variability is apparent.

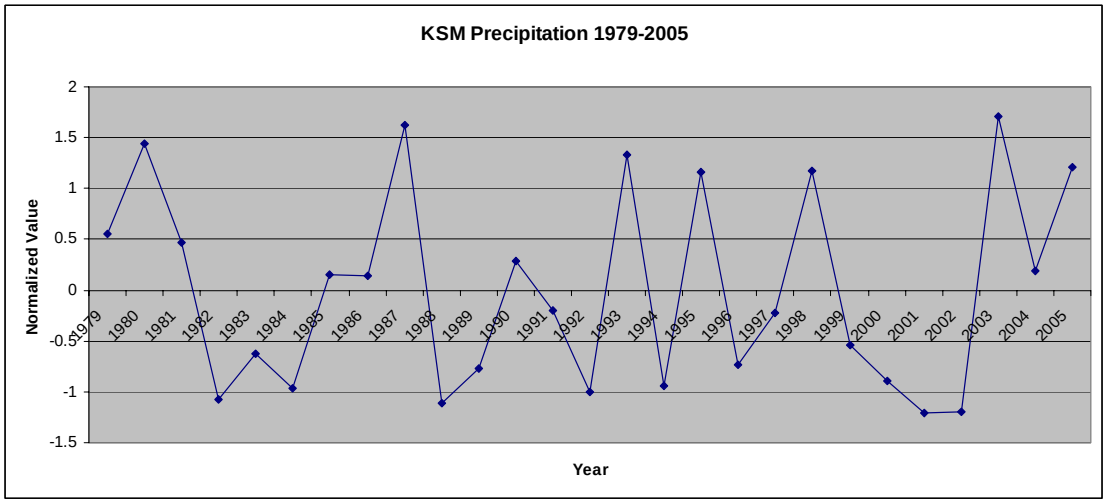

Figure 17. Detrended and normalized time series of the monsoonal part of KSM based on pentads 36-50.

B. RELATIONSHIP BETWEEN KSP AND MAJOR CLIMATE INDICES

To analyze the seasonal predictability of KSP, we correlated the KSP time series shown in Figures 16-17 with the indices of the ENLN, NAO, WP, and IOZM at monthly to seasonal scales. In these correlations, the climate variation indices lead the KSP time series by 0-15 months. The results are shown in Table 3, where yellow shading indicates significance at the 0.95 level or greater using Student's t-test. An initial examination of this table reveals a distinct advantage to working with only the monsoonal part of KSP (25 June – 7 September, Figure 17) versus all-summer values (31 May - 23 September, Figure 16). There are 13 significant correlations between KSM and the climate variation

indices, while there are only two significant correlations between all-summer KSP and the climate variation indices. This suggests that the KSM may be more predictable than all-summer KSP.

The correlations with MEI (Table 3A) show that the only two months in which KSP is significant correlated with MEI are July and August. July KSP shows a positive correlation to MEI in the preceding October - March period, peaking at 0.44 in December, while August KSP shows a positive correlation of 0.34 to MEI in the preceding May. The correlation between the KSM and MEI shows a positive correlation from October to March, peaking at 0.44 in December.

The correlations with the WP index (Table 3B) show a positive correlation of 0.44 between July and August KSP and the WP index in the prior May, and 0.59 between KSM and the WP index in the prior May (the strongest correlation in Table 3).

The correlations with the NAO index (Table 3C) shows negative correlations, between July, August, and KSM and the WP index in the prior May and June, with a maximum negative correlation of -0.44 between KSM and the prior May WP index. However, the correlation switches sign to 0.36 NAO in May and KSP in the following September. Also of note is the high positive correlation between NAO in the prior July and the July, monsoon, and all-summer KSP.

The correlations with the IOZM index (Table 3D) show less coherent correlation patterns. August and September KSP show the greatest number of significant correlations with prior values of the IOZM index. August KSP shows a positive correlation with the prior May and Nov IOZM, at 0.34 and 0.32, respectively. September KSP is oppositely correlated, with statistically significant negative correlations with the prior in January, May, and June IOZM index values.

Correlation between KSP and Maior Climate Indices in the Preceding Year

A.												
MEI	Jul	Aug	Sep	Oct	Nov	Dec	Jan	Feb	Mar	Apr	May	Jun
Jun	-0.06	-0.11	-0.13	-0.21	-0.18	-0.13	-0.12	-0.10	-0.09	-0.12	-0.17	-0.24
Jul	0.05	0.15	0.29	0.35	0.39	0.44	0.40	0.38	0.34	0.20	0.19	0.18
Aug	0.20	0.23	0.27	0.28	0.28	0.27	0.24	0.28	0.26	0.28	0.34	0.29
Sep	-0.31	-0.30	-0.28	-0.28	-0.22	-0.20	-0.15	-0.12	-0.13	-0.16	-0.25	-0.31
Monsoon	0.11	0.19	0.30	0.36	0.41	0.44	0.38	0.40	0.38	0.30	0.26	0.21
Summer	-0.05	0.00	0.09	0.09	0.15	0.20	0.19	0.24	0.20	0.11	0.07	-0.01
B.												
WP	Jul	Aug	Sep	Oct	Nov	Dec	Jan	Feb	Mar	Apr	May	Jun
Jun	0.31	0.19	0.04	0.05	-0.03	-0.32	-0.11	0.34	-0.10	0.00	-0.13	0.12
Jul	0.14	0.16	0.04	-0.16	-0.04	0.15	-0.04	0.00	-0.07	0.33	0.44	0.08
Aug	0.02	0.04	-0.05	-0.20	0.34	0.11	-0.09	0.07	0.10	0.15	0.44	0.24
Sep	-0.41	0.26	0.07	0.07	0.08	-0.14	0.11	0.19	-0.01	0.11	-0.11	0.04
Monsoon	0.20	0.22	-0.06	-0.19	0.22	0.04	-0.09	-0.04	0.00	0.33	0.59	0.23
Summer	0.02	0.30	0.04	-0.13	0.18	-0.08	-0.06	0.27	-0.03	0.29	0.33	0.23
C.												
NAO	Jul	Aug	Sep	Oct	Nov	Dec	Jan	Feb	Mar	Apr	May	Jun
Jun	0.14	0.18	0.34	0.14	-0.26	-0.47	0.10	-0.14	-0.17	-0.12	-0.28	0.01
Jul	0.52	-0.06	0.19	-0.25	0.03	-0.13	0.00	-0.17	-0.09	-0.02	-0.43	-0.26
Aug	0.01	0.03	-0.19	-0.31	0.22	0.13	-0.18	-0.23	0.05	0.19	-0.26	-0.38
Sep	0.05	-0.10	0.25	-0.07	0.07	0.25	0.17	0.21	0.14	0.09	0.36	0.16
Monsoon	0.38	-0.09	0.15	-0.25	0.23	0.05	-0.16	-0.37	-0.12	0.08	-0.44	-0.32
Summer	0.35	0.01	0.27	-0.26	0.04	-0.08	0.03	-0.16	-0.03	0.08	-0.29	-0.24
D.												
IOZM	Jul	Aug	Sep	Oct	Nov	Dec	Jan	Feb	Mar	Apr	May	Jun
Jun	0.01	-0.11	-0.13	-0.09	-0.11	0.04	0.22	0.37	0.16	0.07	-0.17	-0.18
Jul	-0.03	0.02	0.17	0.29	0.22	0.13	-0.07	0.20	-0.04	0.09	0.22	0.30
Aug	-0.01	0.03	0.05	0.22	0.32	0.11	0.11	-0.01	0.05	-0.04	0.34	0.17
Sep	-0.04	-0.08	0.01	-0.11	-0.13	-0.29	-0.37	-0.15	-0.02	-0.08	-0.33	-0.37
Monsoon	-0.03	0.05	0.13	0.32	0.29	0.02	-0.02	0.06	-0.02	0.08	0.29	0.17
Summer	-0.04	-0.06	0.06	0.17	0.16	0.00	-0.06	0.19	0.07	0.01	0.05	-0.02

Table 3. Correlations of KSM and total KSP with climate variation indices, by month and by monsoonal and all-summer periods. KSM is defined as KSP that occurs during 25 June - 7 September. Total KSP is defined as KSP that occurs during 31 May - 23 September. Correlations with the climate variation indices are: (A) MEI, (B) WP index, (C) NAO index. (D) IOZM index. Yellow shading indicates significance at the 95% level or higher.

C. SPATIAL LINEAR CORRELATIONS

1. Simultaneous Correlations with the KSM

Correlating the the KSM with simultaneous July-August 850 hPa GPH (Figure 18) reveals that the most significant feature associated with high (low) precipitation is high (low) heights south of Japan in the area of the Bonin High, with a correlation maximum of 0.72. This positive correlation stretches south and eastward into the central equatorial Pacific. Locally, and secondary to this correlation center is a center of opposite sign north and east of Korea with a minimum correlation of -0.53.

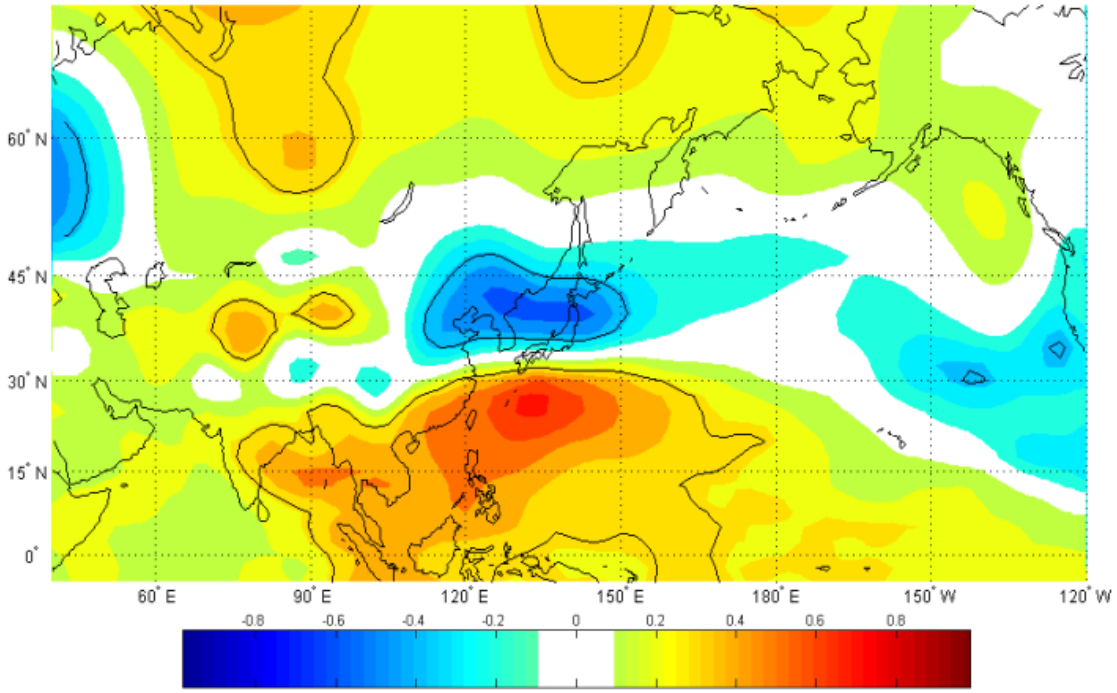

Figure 18. Simultaneous correlations between the KSM and July-August 850 hPa GPH. Correlations in the areas enclosed by black contours are statistically significant at the 95% level using Student's t-test.

The simultaneous correlations of the KSM with 200 hPa GPH (Figure 19) show correlation centers north and south of Korea similar to those in the correlation with 850 hPa GPH and indicate an approximate vertical stacking of the lower and upper

tropospheric GPH patterns associated with high and low KSM. The correlations shown in Figures 18-19 indicate that high (low) KSM is associated with anomalously strong southwesterly (northeasterly) lower tropospheric flow over and near Korea, and anomalously strong upper tropospheric westerlies (easterlies) over and near Korea.

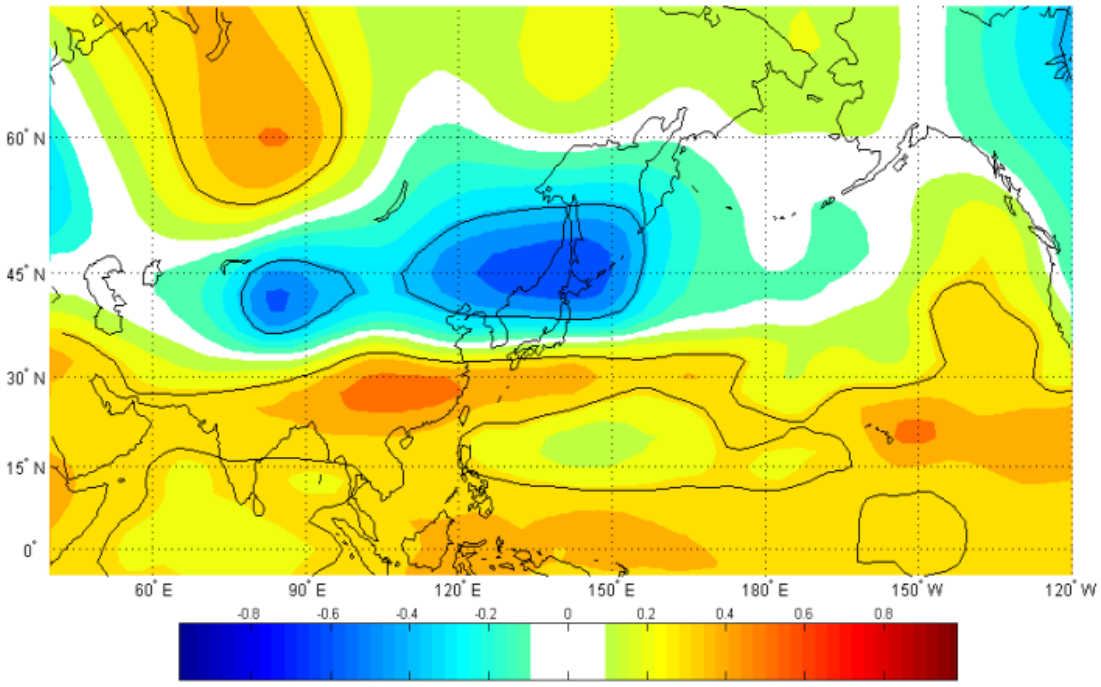

Figure 19. Simultaneous correlation between the KSM and 200 hPa GPH. Correlations in the areas enclosed by black contours are statistically significant at the 95% level using Student's t-test.

The simultaneous correlation of the KSM with SST (Figure 20) reveals positive correlations south of Japan, and negatives correlation east and west of Korea, roughly under the positive and negative correlation centers shown in Figures 18-19. These results indicate that high (low) KSM is associated with anomalously high (low) SST southeast of Korea and anomalously low (high) SST surrounding Korea and much of Japan. .

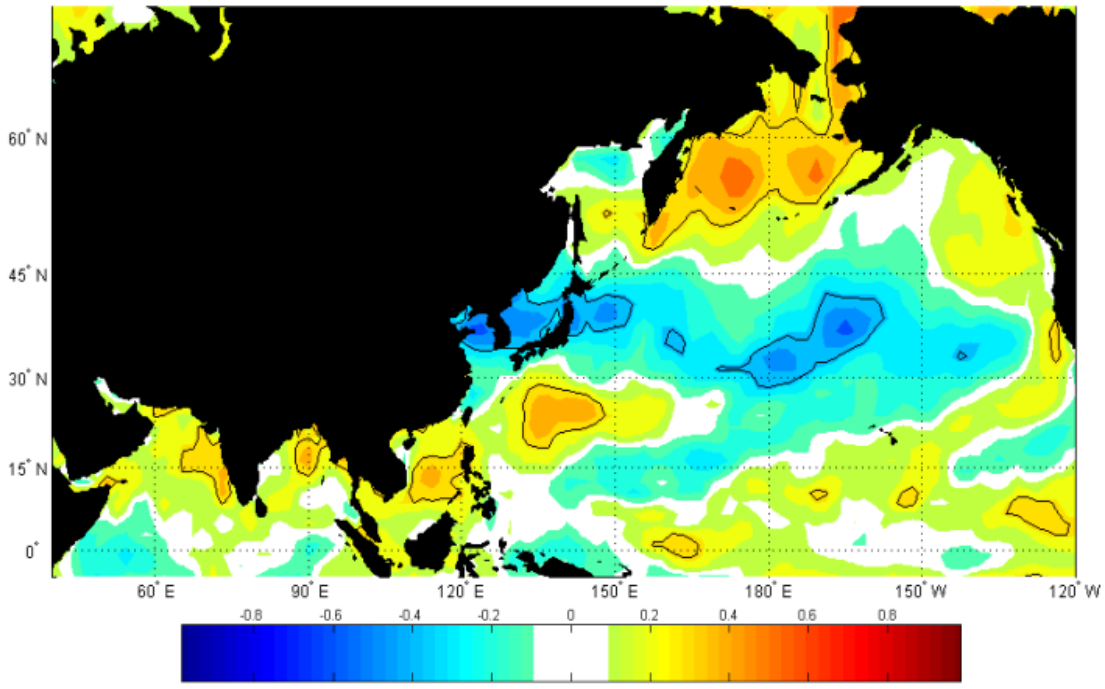

Figure 20. Simultaneous correlation between the KSM and SST. Correlations in the areas enclosed by black contours are statistically significant at the 95% level using Student's t-test.

The correlation between the KSM and Asia-North Pacific precipitation (Figure 21) reveals an area of significant positive correlation to the southwest and northeast of Korea, in a pattern similar to that of the climatological monsoon rain band (Figures 1-5). Significant negative correlations occur in much of the tropical-subtropical North Pacific. There are also areas of significant positive correlation over Tibet, India, Bangladesh, the Maritime Continent, and the central equatorial Pacific. Note that these two areas of significant correlations are roughly coincident with the areas of significant correlations shown in Figures 18-20, suggesting that KSM variations are associated with dynamical processes involving larger scale variations in SST, lower and upper tropospheric circulation, and precipitation in the tropical to midlatitude western North Pacific. To a lesser extent, the results in Figures 18-21 indicate that KSM variations may also be associated with dynamical process in the tropical western and central Pacific (e.g., those associated with ENLN and the MJO).

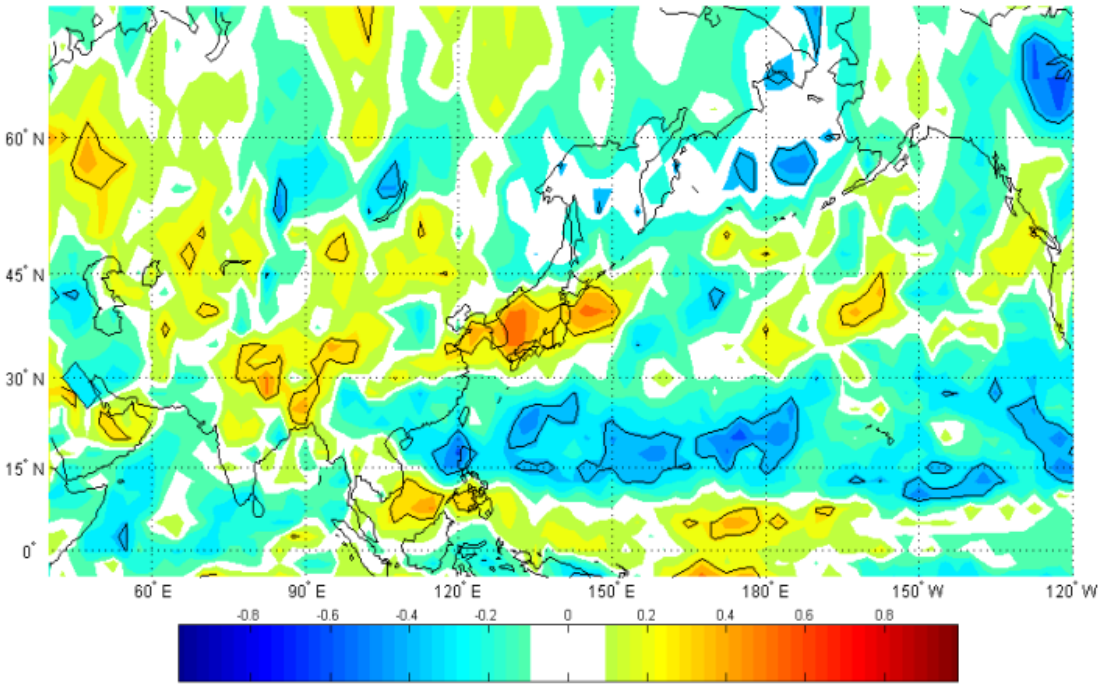

Figure 21. Simultaneous correlation between the KSM and Asia-North Pacific precipitation. Correlations in the areas enclosed by black contours are statistically significant at the 95% level using Student's t-test.

2. Correlations in Which KSM Lags by 1-5 Months

Figure 22 shows the correlation between the KSM and 850 hPa GPH during the prior April-May (i.e., with 850 hPa GPH leading KSM by 1-5 months). Note the area of significant positive correlation south of Japan, similar to the positive simultaneous correlation area (Figure 18). This indicates that there is a tendency for high (low) heights south of Japan one season prior to, and also during, periods of high (low) KSM. Figure 22 shows an area of strong negative correlation centered just east of Kamchatka. These two centers occur in the middle of a south-north quadripole of positive and negative correlation areas between 120 E and 150 W, with weak negative correlations centered near 10 N, strong positive correlations centered near 25 N, strong negative correlations centered near 55 N, and weak positive correlations centered in the Arctic (not shown).

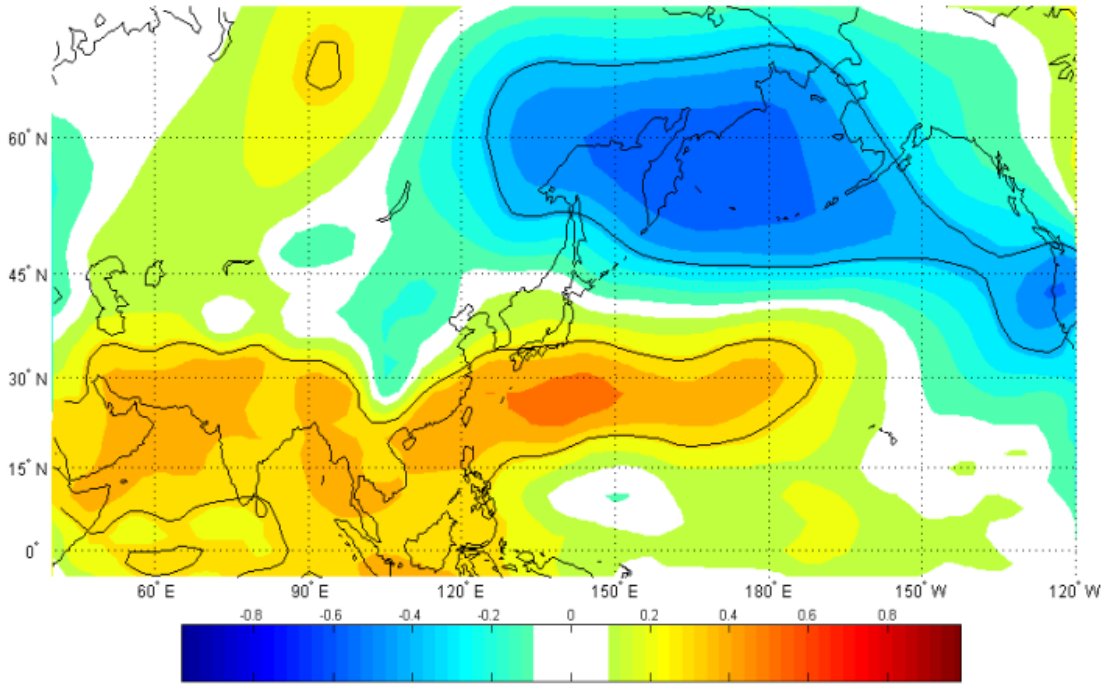

Figure 22. Correlation between the KSM and the preceding April-May 850 hPa GPH. Correlations in the areas enclosed by black contours are statistically significant at the 95% level using Student's t-test.

Figure 23 shows the correlation between the KSM and 300 hPa GPH during the prior April-May (i.e., with 300 hPa GPH leading KSM by 1-5 months). The major positive and negative correlations areas are similar to those in Figure 22, but with a much more longitudinally extensive positive correlation region in the tropics that may indicate a connection to ENLN. EN (LN) events tend to raise (lower upper tropospheric GPH throughout the tropics. This indicates that EN (LN) conditions in the boreal spring tend to precede anomalously high (low) KSM in the following summer.

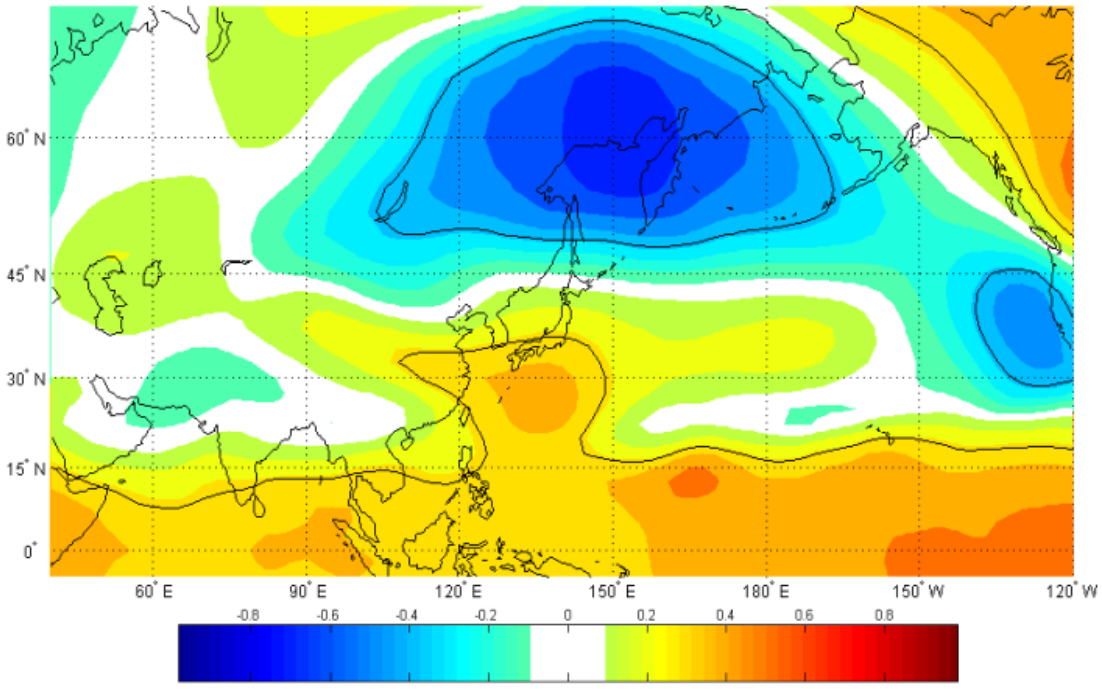

Figure 23. Correlation between the KSM and the preceding April-May 300 hPa GPH. Correlations in the areas enclosed by black contours are statistically significant at the 95% level using Student's t-test.

Figure 24 shows the correlation between the KSM and SST during the prior April-May (i.e., with SST leading KSM by 1-5 months). The correlations with SST are negative near Korea but are mostly not statistically significant. South of Japan there is an area of positive correlations trending from southwest to northeast, indicating that prior to high KSM, SSTs in this area tend to be above (below) average. South of this positive correlation area there is a larger area of negative correlations that extends from the equatorial western Pacific to the central North Pacific north of Hawaii. There is also a positive correlation area in the central and eastern equatorial Pacific that extends along the west coast of North America. These latter two correlation patterns are similar to SST anomaly patterns during ENLN events and indicate that KSM variations are associated with ENLN variations, with EN (LN) conditions in the boreal spring leading to increased (decreased) KSM in the following summer.

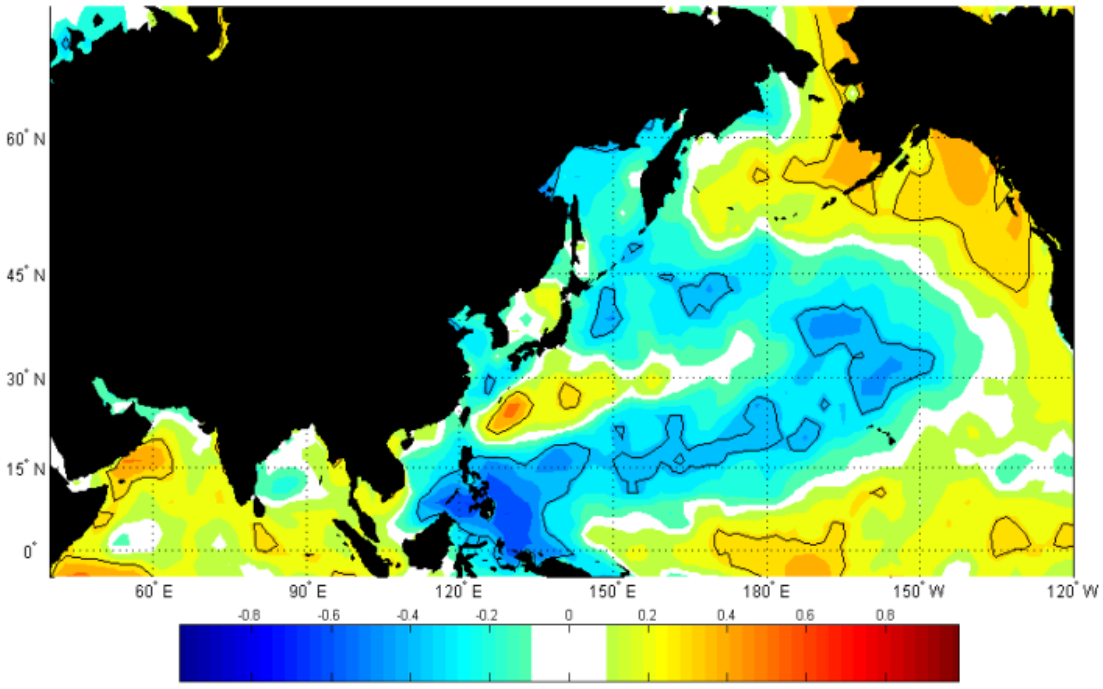

Figure 24. Correlation between the KSM and the preceding April-May SST. Correlations in the areas enclosed by black contours are statistically significant at the 95% level using Student's t-test.

3. Correlations in Which KSM Lags by 7-9 Months

Figure 25 shows the correlation between the KSM and 300 hPa GPH during the prior December-February (i.e., with 300 hPa GPH leading KSM by 7-9 months). Note the Pacific-North American (PNA) like pattern, with correlation centers in the central tropical Pacific, the northeast Pacific, and Canada, along a great circle. This pattern is strongly associated with ENLN, and indicates that ENLN variations in the boreal winter are linked to KSM variations in the following boreal summer.

The correlations between the KSM and SSTs from the prior December-February (Figure 26) show patterns similar to those in Figure 24. In particular, the patterns associated with ENLN (see discussion of Figure 24) are very pronounced in Figure 25, providing evidence that ENLN conditions in the boreal winter influence the KSM in the following summer.

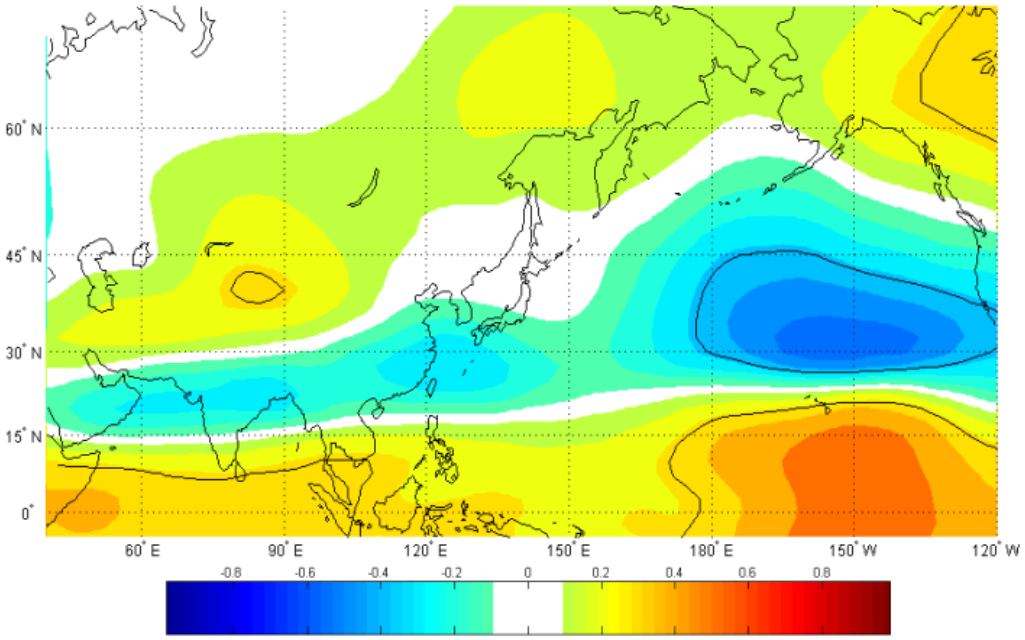

Figure 25. Correlation between the KSM and the preceding December-February 300 hPa GPH. Correlations in the areas enclosed by black contours are statistically significant at the 95% level using Student's t-test.

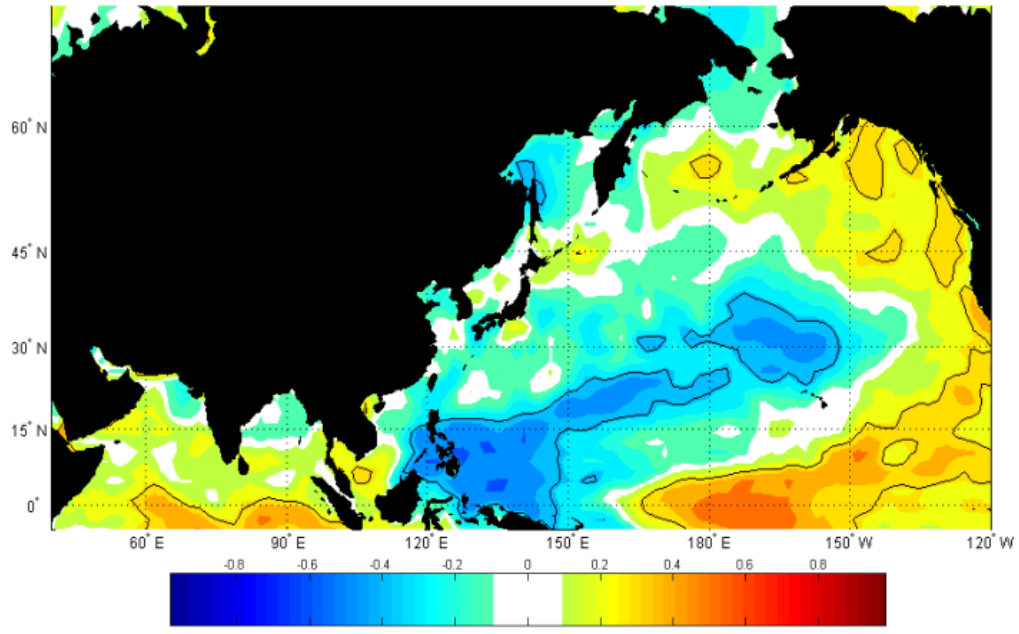

Figure 26. Correlation between the KSM and the preceding December-February SST. Correlations in the areas enclosed by black contours are statistically significant at the 95% level using Student's t-test.

D. COMPOSITE ANALYSES

To gain further insight into the processes that drive variations in KSM, we calculated composite anomalies for months prior to and during periods of anomalously high and low KSM. The composites were based on the top seven years (1980, 1987, 1993, 1995, 1998, 2003, 2005) and bottom seven years (1982, 1984, 1988, 1992, 1994, 2000, 2001) of KSM. We compared and contrasted these composites to gain insights into the differences between high precipitation (HP) and low precipitation (LP) KSP periods. The physical processes identified from the composite analyses were used to develop an index for use in seasonal forecasting of the KSM.

1. Simultaneous Composites

Figure 27 shows HP and LP composites of anomalous precipitation during the KSM period. Note that the HP composite shows positive precipitation anomalies in a southwest to northeast trending band similar to the EASM rain band discussed in chapter I, and a region of negative precipitation anomalies south of Japan in the tropical-subtropical western North Pacific. Similar but opposite and weaker patterns are seen in the LP composite. Note too that the MC and Bay of Bengal precipitation anomalies tend to be opposite between the HP and LP composites. The similarities between the patterns in Figure 27 and those in the correlation figures (see prior sections) support the conclusion that KSP variations, especially positive variations, are closely related to conditions in the EASM rain band, and are affected by atmospheric and oceanic conditions south of Japan.

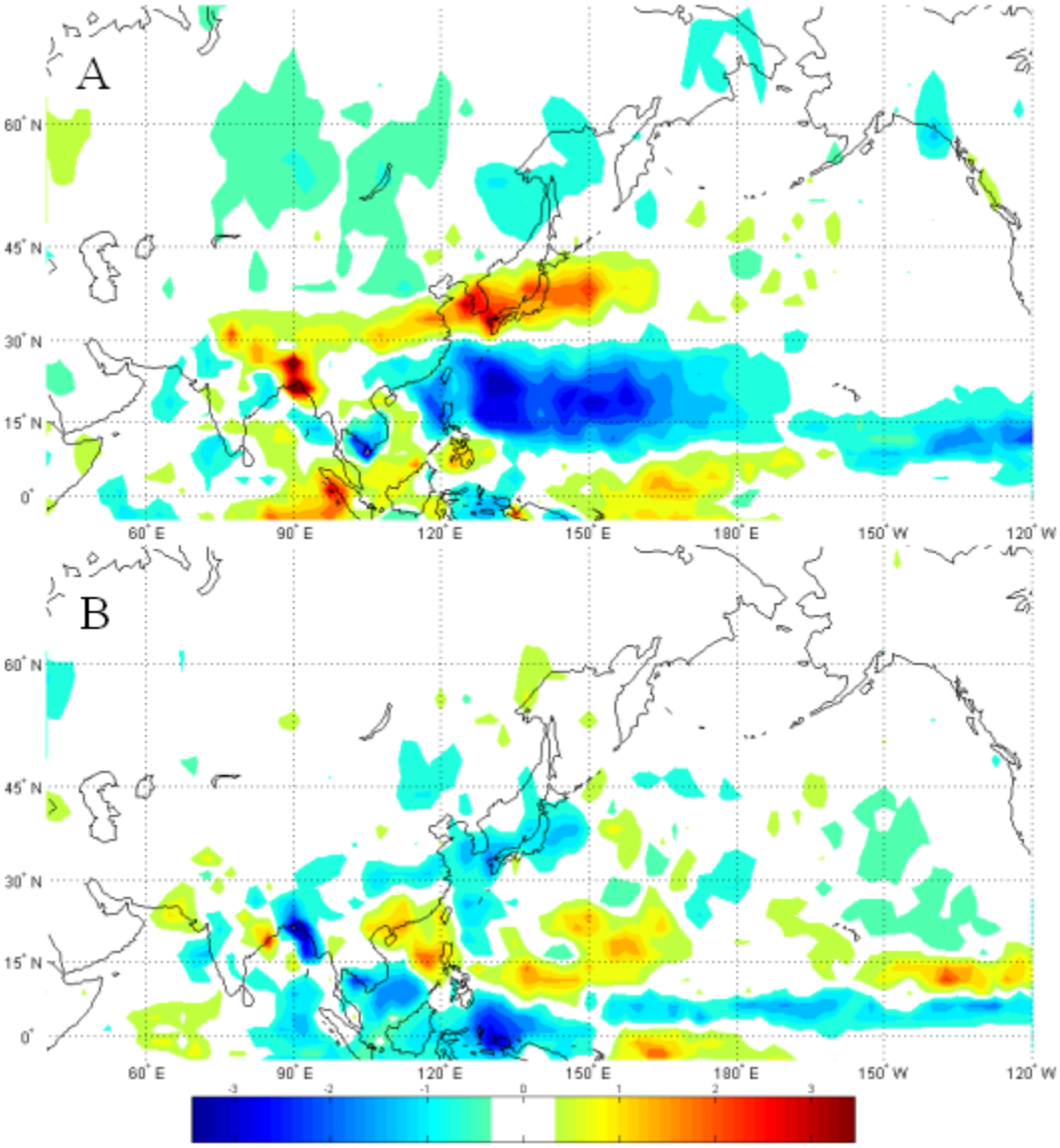

Figure 27. (A) HP and (B) LP composites of anomalous precipitation. Units are millimeters per day.

Figure 28 shows HP and LP composites of anomalous 925 hPa GPH during the KSM period. The most striking patterns and differences between the HP and LP composites are in the positive (negative) GPH anomalies in the tropical-subtropical western North Pacific south of Japan in the HP (LP) composite. In other areas, the anomalies are weak and/or similar in the HP and LP composites. This supports the

conclusion from the prior correlations sections that GPH anomalies to the southeast of Korea lead to anomalous temperature and moisture advection anomalies that influence KSP variations.

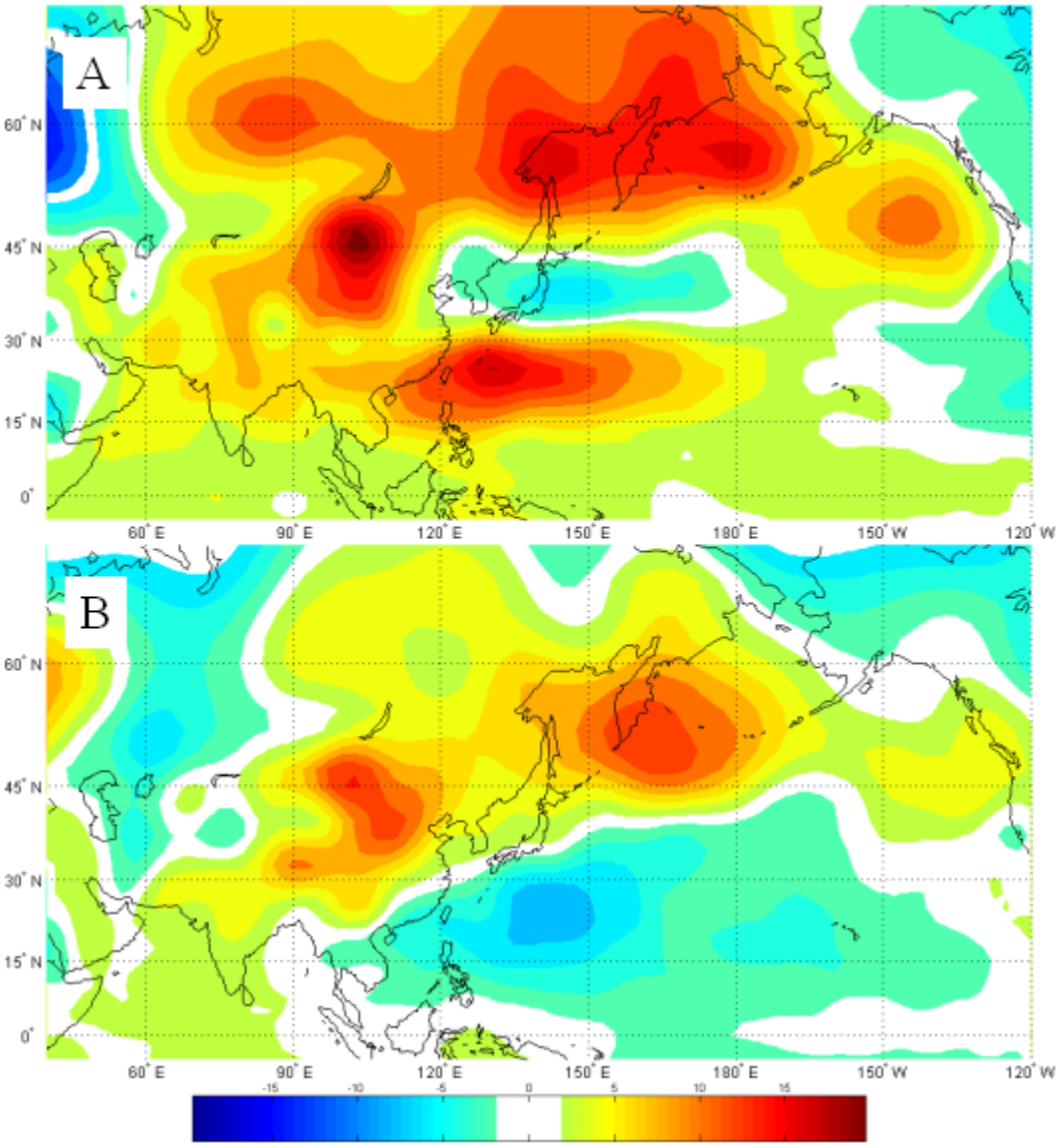

Figure 28. (A) HP and (B) LP composites of anomalous 925 hPa GPH. Units are meters.

2. Leading Composites

Figure 29 shows HP and LP composites of anomalous 925 hPa GPH during the April prior to the KSM. Note that the anomalies in this figure are similar to those in the simultaneous composites (Figure 28) in the tropical-subtropical western North Pacific

south of Korea and Japan. However, outside of this area, the HP and LP anomalies are different from each other and from the simultaneous anomalies, especially over northeast Asia and the extratropical North Pacific. The HP and LP anomalies in these areas are indicative of anomalous wave train activity, with anomalous wave energy propagating northeastward across the North Pacific in the HP case, and southwestward across northeast Asia and the North Pacific in the LP case.

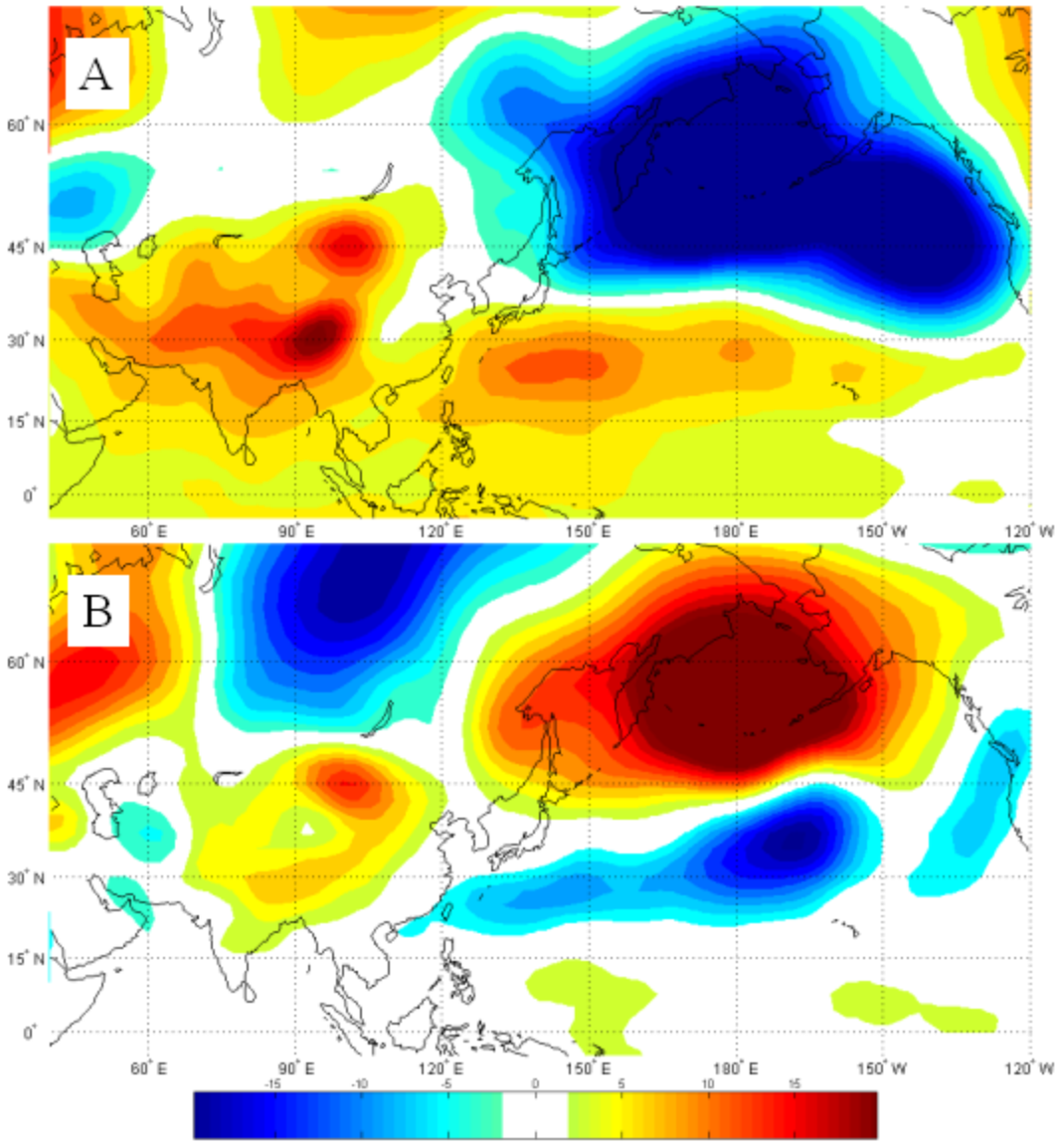

Figure 29. (A) HP and (B) LP composites of anomalous 925 hPa GPH in April prior to the KSM. Units are meters.

Figure 30 shows HP and LP composites of anomalous 925 hPa zonal wind during April prior to the KSM. As expected, the zonal wind anomalies are consistent with the 925 hPa GPH anomalies (Figure 29) and show, for the HP (LP) case, easterly (westerly) anomalies at about 15 N in the western North Pacific south of Japan. These wind anomalies correspond to anomalously strong (weak) trade winds in the HP (LP) case. Strong (weak) trade wind anomalies are, in this part of the western North Pacific, characteristic of EN (LN) periods. So Figures 29-30 provide additional evidence that high (low) KSM is associated with EN (LN) events.

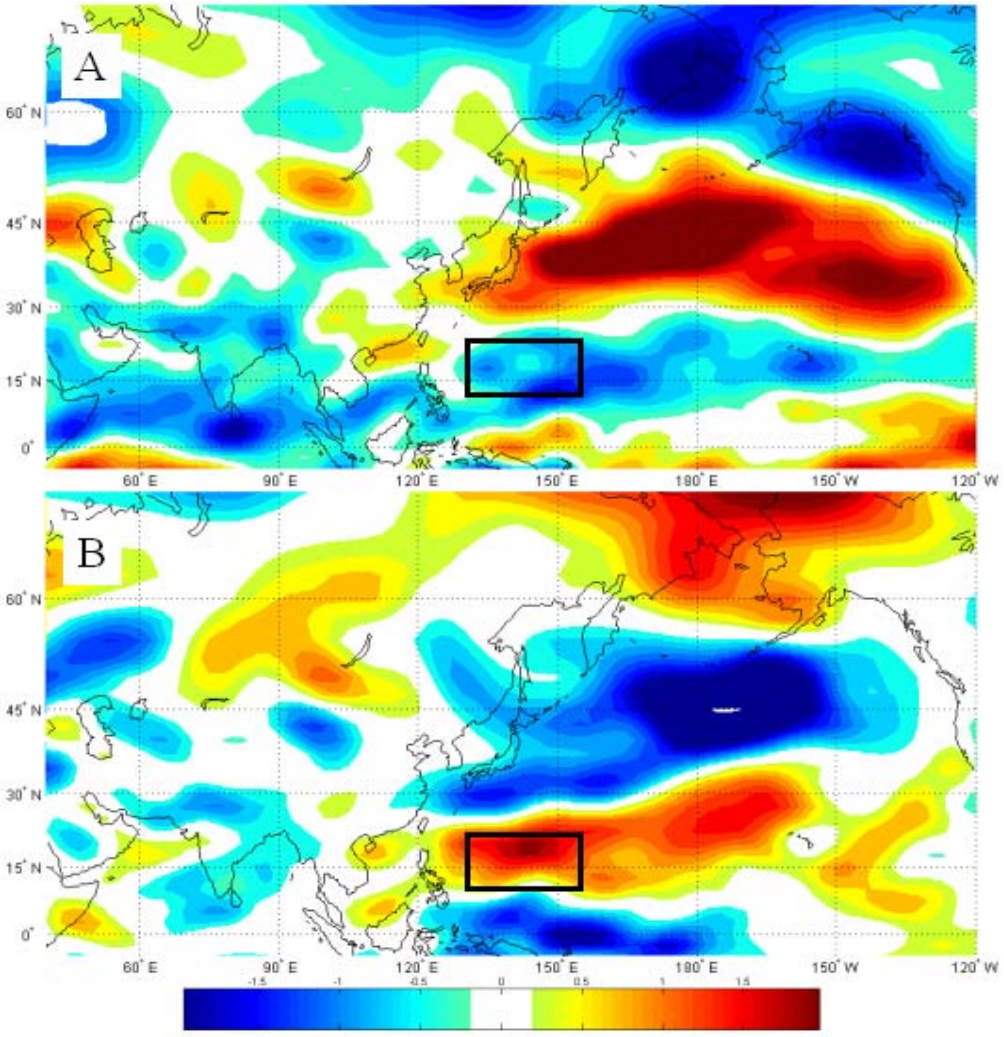

Figure 30. (A) HP and (B) LP composites of anomalous 925 hPa zonal wind in April prior to the KSM. Units are meters per second.

Figure 31 shows that the anomalously strong (weak) trades south of Japan are associated with anomalously low (high) SSTs in the same area. The SST anomalies may be due to the wind anomalies, with increased (decreased) tropical easterlies leading to increased (decreased) wind driven evaporation, sensible heat flux, and turbulent mixing of the upper ocean. Note too the resemblance of the HP composite SST anomalies to the correlations with SST shown in Figures 20 and 24. As for these earlier figures, the patterns in Figure 31 indicate that KSM is associated with ENLN.

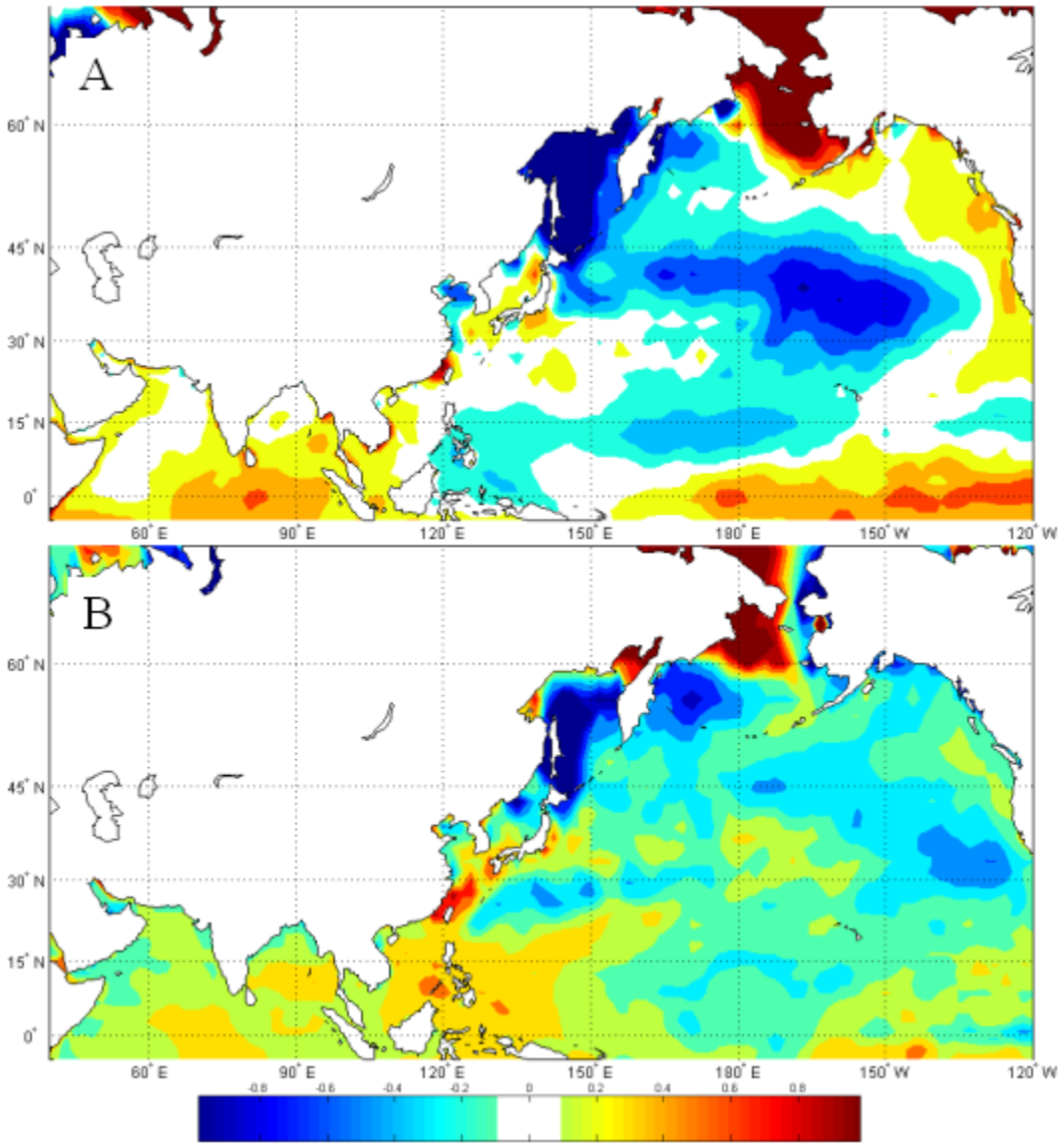

Figure 31. (A) HP and (B) LP composites of anomalous SST in April prior to the KSM. Units are Kelvin.

Figure 32 shows the difference between the HP and LP composites of 925hPa zonal wind anomalies during the prior April and of SST anomalies during the prior April-May (HP composite minus LP composite). Note the large area of positive trade wind anomaly differences in the tropical western North Pacific between 10 and 20 N, and the underlying negative SST anomaly differences. This supports the assertion that anomalously strong (weak) easterly winds in this area during the boreal spring (e.g., April,) prior to the KSM lead to anomalously cool (warm) SSTs, as discussed in the prior paragraph.

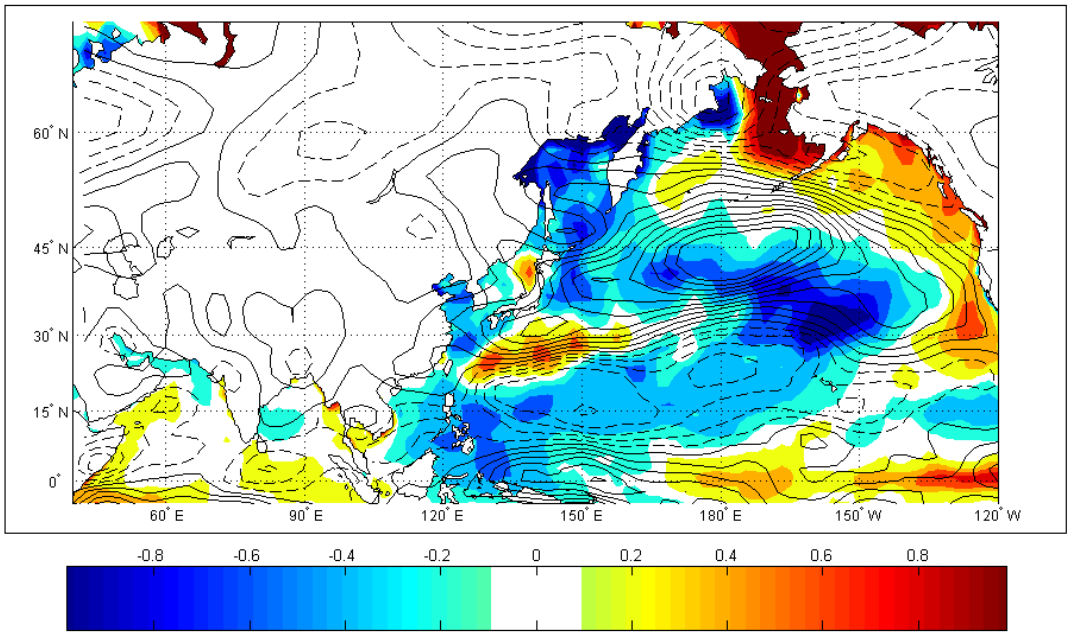

Figure 32. HP minus LP composite differences in: (1) 925hPa zonal wind anomalies during April prior to the KSP period (black contours, solid (negative) indicating positive (negative) anomalies, units: m/s, contours every 0.5 m/s) and (2) SST anomalies during Apr-May prior to the KSM (color shading, units: Kelvin).

Figure 33 is the same as Figure 32, but with April wind anomaly differences replaced by July-August precipitation anomaly differences. The region of cool (warm) SST anomaly differences in the tropical western North Pacific between 10 N and 20 N during April is also a region of negative (positive) precipitation anomaly differences in

the following July-August. This may be the result of the anomalously strong (weak) trade winds in the spring reducing (increasing) the upper ocean thermal energy content in the area, and those thermal energy anomalies persisting into the summer and reducing (increasing) the summer convective activity and precipitation in the area. These results are similar to and support the findings of Wang, Wu, and Fu (2000) and Wang and Zhang (2002).

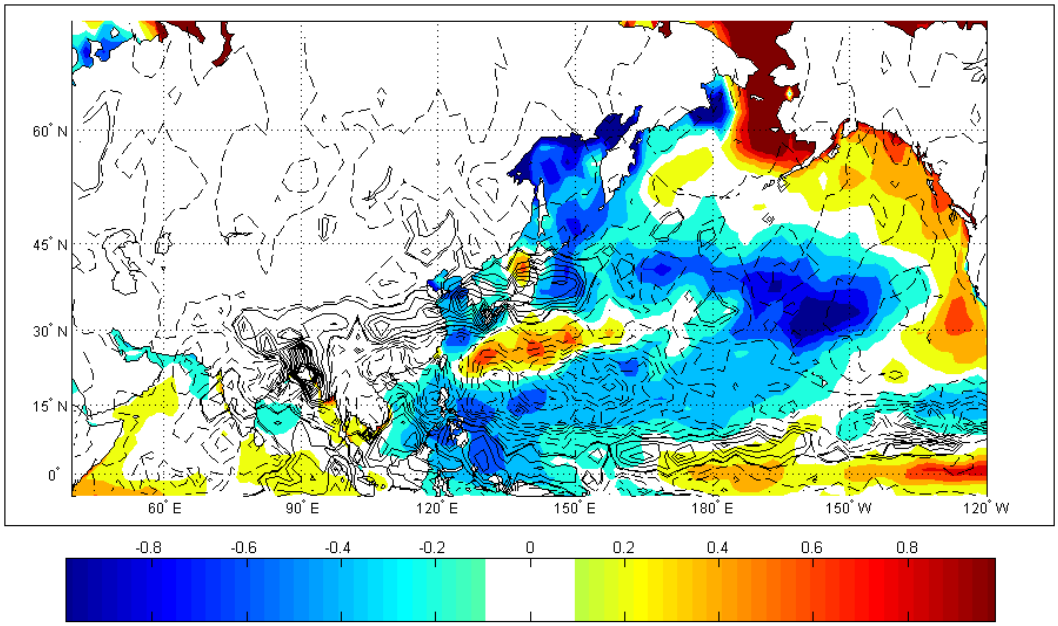

Figure 33. HP minus LP composite differences in: (1) precipitation anomalies during July-August, the KSM period (black contours, solid (negative) indicating positive (negative) anomalies, units: mm/day, contours every 0.5 mm/day) and (2) SST anomalies during Apr-May prior to the KSM (color shading, units: Kelvin).

Figure 34 shows schematically the anomalous atmosphere-ocean interactions that may explain how atmospheric and oceanic anomalies in the tropical-subtropical western North Pacific during spring may lead to anomalies in KSM in the following summer.

A.

B.

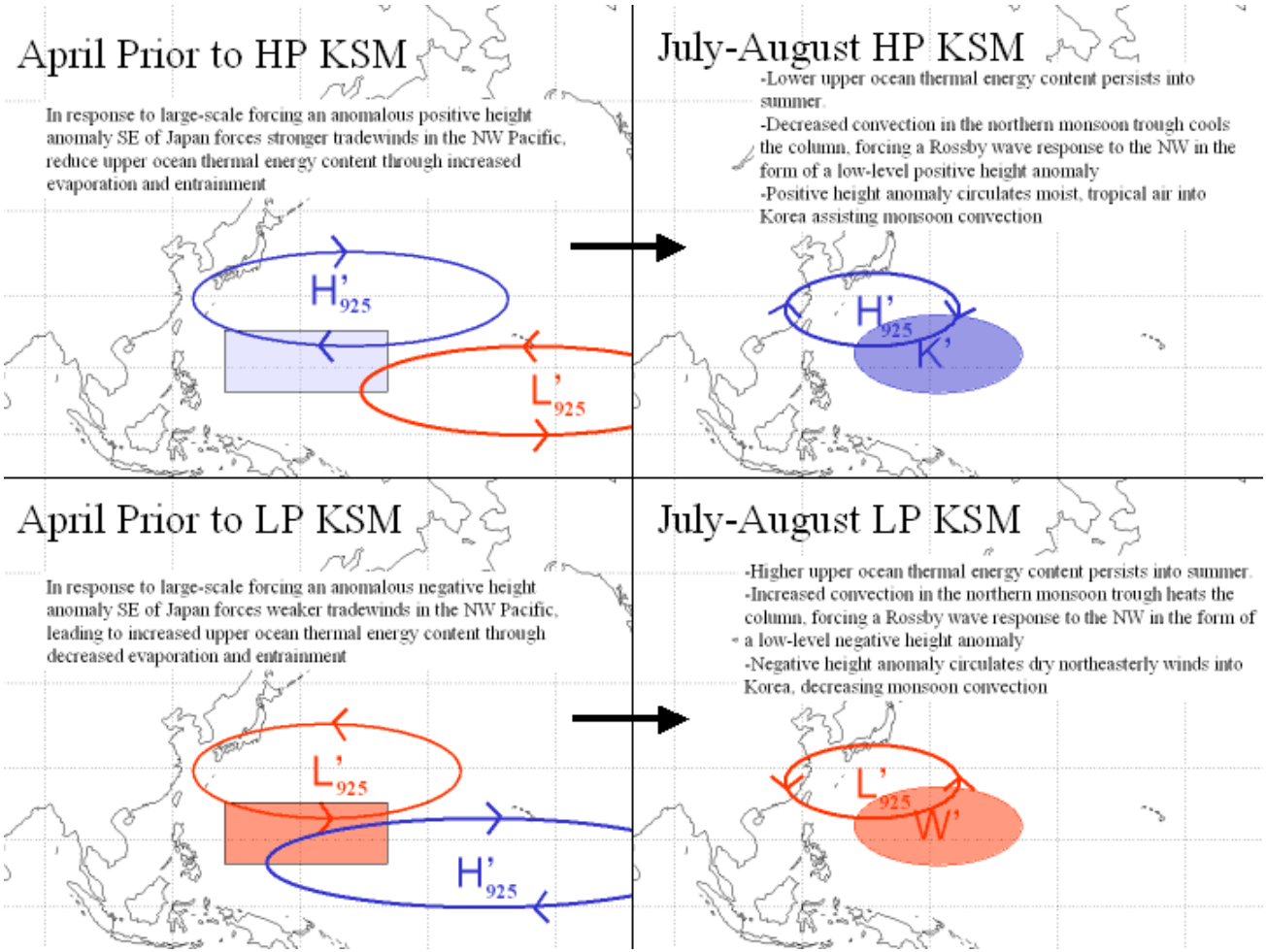

Figure 34. Schematic showing the physical processes during spring (e.g., April) that lead to (A) positive KSM anomalies and (B) negative KSM anomalies (cf. Wang, Wu, and Fu (2000)).

E. KSM FORECASTS FOR JULY-AUGUST BASED ON ZONAL WIND INDEX

It is clear from the preceding correlation and composite analyses that a knowledge of upper ocean thermal energy anomalies in the tropical North Pacific would provide a keen understanding of where tropical convection anomalies would be likely to occur. From this, conclusions on the anomalous Rossby wave response to the convection anomalies could be made, which could lead to a determination of anomalous flow into Korea, and a forecast of KSM anomalies. Unfortunately, basin-wide, ocean thermal energy analyses are not readily available on a daily basis for operational forecasting. However, from the composite analyses, it is clear that the low level zonal wind anomalies in the spring can give an indication of spring and summer upper ocean thermal energy anomalies that then lead to summer convection and circulation anomalies that affect the KSM.

Thus, we developed the normalized time series of area averaged April 925 hPa zonal wind anomalies for the box region 12 N to 22 N and 135E to 155E (see boxes in Figure 30). We refer to this time series as the West Pacific Zonal Index (WPZI). The WPZI for 1979-2005 is shown in Figure 35, along with the corresponding KSM time series. The correlation between WPZI and monsoonal KSM precipitation is -0.65. In this correlation, WPZI leads the KSM by about 2-5 months, since WPZI is based on April values and the KSM is based on July-August values. This leading relationship to the KSM, and the magnitude of the correlation, indicate that WPZI has potential as a predictor of the KSM at leads of 2-5 months.

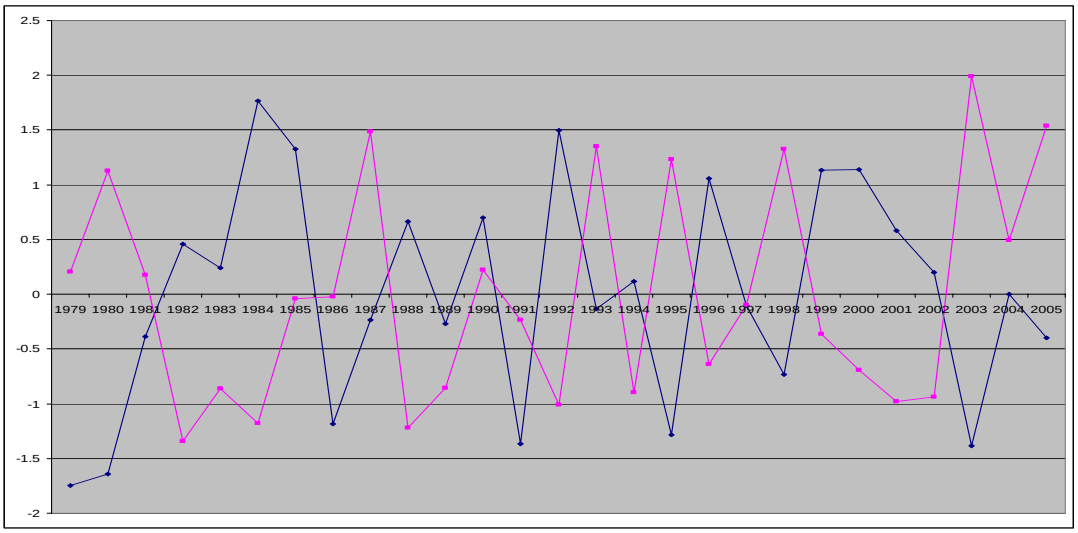

Figure 35. Normalized WPZI (pink) and KSM (blue) for 1979-2005.

Table 4A is the contingency table for hindcasts of the KSM for which the normalized WPZI (Figure 35) was used as the predictor. In this case, all 27 years of the KSP and WPZI time series have been classified as above or below normal. Table 4B shows the hindcast verification scores (see chapter II and Jarry (2005) for explanations of these scores). These scores indicate that the WPZI has skill in predicting the KSM for July-August at leads of 2-5 months.

A.

		OBSERVED	
		Below	Above
FORECAST	Below	12	1
	Above	4	10

B.

ACC	0.81
POD	0.75
FAR	0.08
TS	0.44
HSS	0.63

Table 4. (A) Contingency table and verification statistics for hindcasts of the KSM for July-August using WPZI in the prior April as the predictor. (B) Corresponding hindcast verification scores (ACC - accuracy, POD - probability of detection, FAR - false alarm rate, TS - threat score, HSS - Heidke skill score). For details on forecast statistics see chapter II and Jarry (2005).

F. RELATIONSHIP OF WPZI TO MAJOR CLIMATE INDICES

Table 5 shows the correlation between the WPZI and major climate indices. The only significant correlations in which WPZI lags a climate index are the -0.32 and -0.35 correlations with MEI in November and December, respectively. This supports: (a) the idea that ENLN events during the boreal winter affect the KSM in the following boreal summer (see prior correlation and composite analysis sections); (b) the idea that the impacts of ENLN on the KSM occur via the anomalous processes described in Figure 34; and (c) boreal fall and winter MEI may be a useful predictor of WPZI and may thus increase the lead times at which the KSM can be predicted with skill to 7-10 months. The other significant correlations shown in Table 5 all involve simultaneous correlations,

or correlations in which WPZI leads the climate index by 1-2 months. Thus, they are not useful in extending the KSM lead time over that which can be obtained from the WPZI alone.

	Leading and Lagging Correlations Between WPZI and Major Climate Indices					
	Jul (-)	Aug (-)	Sep (-)	Oct (-)	Nov (-)	Dec (-)
MEI	0.08	-0.03	-0.14	-0.25	-0.32	-0.35
WP	-0.26	-0.25	-0.04	0.18	-0.22	-0.20
NAO	-0.19	0.14	-0.13	0.12	-0.26	0.02
IOZM	-0.03	-0.14	-0.19	-0.24	-0.20	0.00

	Jan (-)	Feb (-)	Mar (-)	Apr	May (+)	Jun (+)
MEI	-0.30	-0.26	-0.19	-0.13	-0.16	-0.18
WP	0.04	0.23	0.13	-0.51	-0.54	-0.14
NAO	0.09	0.21	-0.08	0.18	0.40	0.03
IOZM	-0.06	-0.20	-0.18	-0.34	-0.42	-0.48

	Jul (+)	Aug (+)	Sep (+)	Oct (+)	Nov (+)	Dec (+)
MEI	-0.22	-0.25	-0.27	-0.22	-0.22	-0.27
WP	0.24	0.21	0.08	-0.16	0.07	0.13
NAO	0.07	0.27	-0.11	0.11	-0.10	-0.09
IOZM	-0.07	-0.14	-0.16	-0.14	-0.08	-0.13

Table 5. Correlation between the WPZI based on April values and major climate indices. (-) indicates WPZI lags the climate index leads and (+) indicates WPZI leads the climate index lags. For April, all the correlations are simultaneous.

G. SUMMARY OF KSP FORECASTING FOR JULY-AUGUST

In this chapter, we showed that KSM variations are out of phase with simultaneous precipitation variations occurring in the tropical western North Pacific, in the northern portion of the monsoon trough (MT), similar to Nitta (1987). That is, in summers of below (above) average precipitation in the monsoon trough, Korea is likely to see above (below) average precipitation. This relationship holds true due to the anomalous Rossby wave response to northern MT convection anomalies that induce low

level circulation anomalies to the southeast of Korea, which alters temperature and moisture advection into Korea, thereby altering the KSM.

The correlation and composite analyses showed that northern MT convection in the summer is sensitive to tropical western North Pacific zonal wind anomalies in the spring (e.g., April). A negative (positive) anomaly in these winds leads to anomalous upper ocean cooling (warming) and negative (positive) anomalies in upper ocean thermal energy that persist into summer and produce the summer convection and low level circulation and advection anomalies discussed in the prior paragraph.

Based on these analyses, we developed the WPZI, an index of tropical western North Pacific zonal winds in April to use as a predictor of the KSM. Hindcasts using WPZI as the predictor showed significant skill (e.g., a Heidke Skill Score of 0.63). Correlations in which the MEI leads the WPZI by several months were statistically significant correlation, indicating that: (a) ENLN plays a role in developing the boreal spring zonal wind anomalies that lead to the KSM anomalies; and (b) boreal winter MEI values may be a useful long lead predictor of the KSM in the following summer, especially when combined with the WPZI based on April values.

IV. RESULTS OF INTRASEASONAL ANALYSES AND PREDICTION OF KOREA SUMMER PRECIPITATION

A. OVERVIEW

Our approach to characterizing and predicting intraseasonal variations of Korean summer precipitation (KSP) was divided into three parts. First we used correlation analyses to look at the relationships between climate variations and KSM onset, break periods, and withdrawal. Next, we used contingency table analyses, composite analysis forecasts, and composite anomaly analyses to examine the relationships between KSP and MJO, especially as the MJO and the processes associated with the WPZI interact with each other. Last, we examined the role that tropical cyclones play in KSP.

B. KSM ONSET, BREAK PERIODS, AND WITHDRAWAL

The ability to make a climate forecast of the KSM onset and breaks is desirable for many obvious reasons, both military (mission planning and execution) and civilian (crop planting, event planning). In this section, the methods for analyzing monsoon onset, break, and withdrawal are discussed, and an investigation of the monsoon onset, break, and withdrawal dates over the past 27 years and relationships to climate indices are presented.

1. Monsoon Onset

The KSM onset date can be defined in a number of ways. One way is by the northward movement of the NW Pacific extension of the subtropical ridge, which allows a moist tropical airmass to enter Korean region. Various methods for defining onset have been proposed, involving analyses of GPH or winds at different levels, or precipitation, within the Korean region (Ding and Chan 2005). The definition is complicated by data resolution issues, since the temporal and spatial resolution of available data imposes constraints on operationally applying different definitions. For our study, we chose to define onset in terms of the Korean box average value of CMAP precipitation described in chapters II and III. We defined onset as occurring in the pentad for which this box-

averaged precipitation reached or exceeded 5 mm/day and was immediately followed by a pentad in which precipitation also reached or exceeded 5 mm/day.

Using this definition, we determined the KSM onset pentad) for all the years in our analysis period, 1979-2005 (Table 6).

KSM Onset Pentad by Year	
Year	Pentad
1979	35
1980	36
1981	35
1982	39
1983	39
1984	38
1985	35
1986	34
1987	37
1988	38
1989	32
1990	34
1991	36
1992	39
1993	36
1994	36
1995	37
1996	34
1997	36
1998	36
1999	35
2000	39
2001	34
2002	40
2003	35
2004	34
2005	36

Table 6. Pentad of KSM onset by year.

Figure 36 shows a graph of the onset pentad versus time. The black line shows the linear trend of the pentad onset date. Note there is a slight downward trend in the onset date from just over pentad 36 in 1979 to just under pentad 36 in 2005.

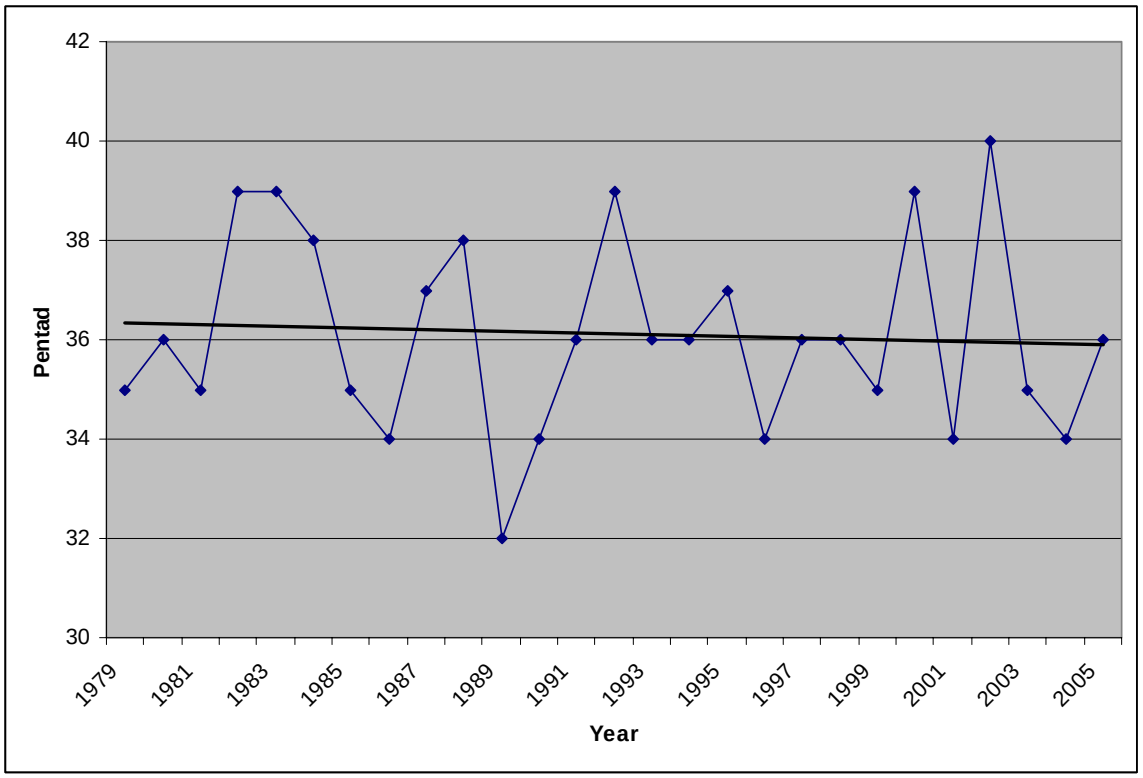

Figure 36. Onset of the KSM by pentad for 1979 through 2005 (blue) and linear trend of in the onset data (black).

2. Monsoon Breaks

The monsoon break is a widely recognized phenomenon in all sectors of the Asian Summer Monsoon (ASM). In the Indian and western North Pacific, active and inactive periods are related to the interaction of the 30-60 day ISO and the 10-20 day ISV. In Korea, break mechanisms are harder to analyze because of inputs from both the overall ASM and midlatitude disturbances. The 1979-2005 long term mean KSP and its standard deviation for each pentad are shown in Figure 37. Note the tendency for intra-pentad variations in precipitation from pentad 36 through pentad 50. These variations are evidence of active and break periods in KSP. The standard deviation curve indicates that active and break periods are more and less consistent at certain times of the KSP period (e.g., more consistent during pentads 39-43).

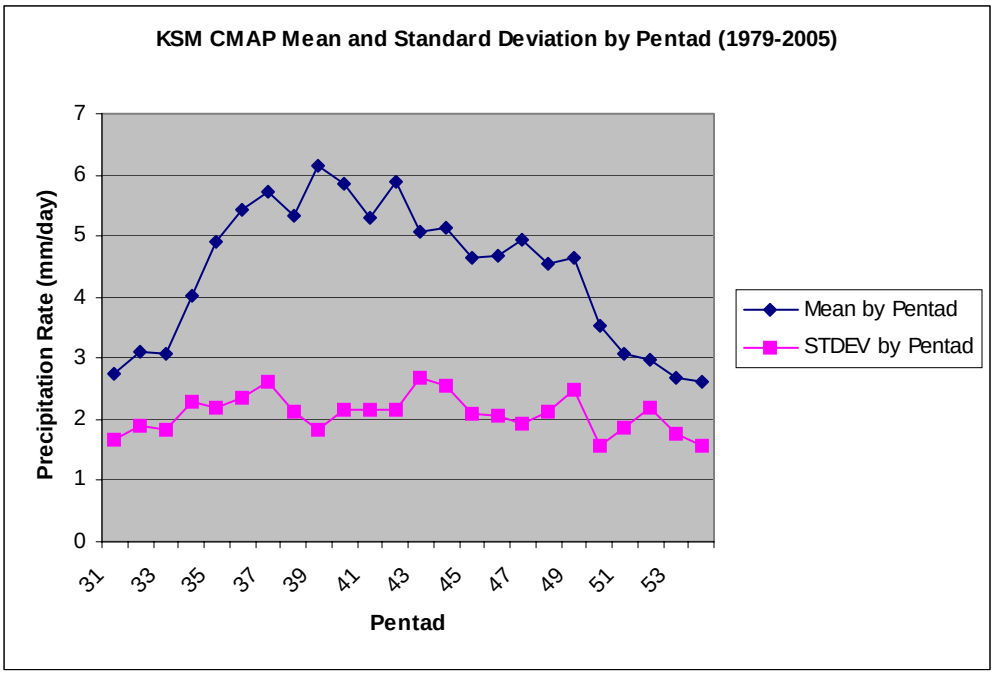

Figure 37. Normalized long term mean Korean summer precipitation (blue) and standard deviation (pink) by pentad based on data from 1979-2005. Pentads shown span the late May through late September period. Units: mm/day.

For this study, we defined a break as any pentad or successive set of pentads, after monsoon onset, in which precipitation is less than 5 mm/day and which is/are followed by one or more pentads in which precipitation is greater than 5 mm/day. Using this definition, we identified the first break start pentad and break length in pentads for each year in our study period, 1979-2005 (Table 7).

	KSM Break Start and Lenth by Year	
	Break Start	Break Length
1979	38	1
1980	43	2
1981	39	3
1982	43	1
1983	42	6
1984	40	5
1985	41	2
1986	37	1
1987	43	1
1988	42	4
1989	34	5
1990	42	4
1991	44	1
1992	42	3
1993	41	1
1994	40	3
1995	44	1
1996	38	2
1997	41	2
1998	45	1
1999	39	3
2000	43	4
2001	40	1
2002	42	2
2003	43	1
2004	36	1
2005	40	2

Table 7. KSM break start pentad and break length in pentads for the first break of each year in the study period.

3. Monsoon Withdrawal

In this study, we defined the monsoon withdrawal as the first of two or more pentads after the monsoon break in which the precipitation rate is less than 4 mm/day averaged over the Korean region box defined in Figure 15. Table 8 shows the pentad of monsoon withdrawal for each year, 1979-2005.

	KSM Withdrawal Pentad by Year
	Pentad
1979	46
1980	51
1981	49
1982	48
1983	51
1984	49
1985	46
1986	43
1987	50
1988	47
1989	42
1990	52
1991	44
1992	49
1993	47
1994	46
1995	49
1996	45
1997	49
1998	47
1999	43
2000	52
2001	44
2002	45
2003	51
2004	43
2005	50

Table 8. KSM withdrawal pentad by year.

4. Relationship between Climate Variations and KSM Onset, Break, and Withdrawal

Table 9 shows the leading and lagging correlations between the major climate indices (i.e., the indices for ENLN, WP, NAO, IOZM; see chapter II) and the KSM onset, break start, break length, and withdrawal. Yellow shading indicates statistical significance at the 95% level using Student's t-test. Starting with MEI, we see a large number of statistically significant positive correlations for the MEI leading the KSM start, with a maximum correlation of 0.45 for the prior May MEI. Table 9 also indicates

that that the MEI is a leading indicator of the: (a) KSM break start, with positive correlations peaking at 0.51 for the prior January MEI; and (b) the KSM withdrawal, with positive correlations peaking at 0.49 for the prior March MEI. This indicates that EN (LN) tends to lead to a later (earlier) KSM onset, break start, and withdrawal. Interestingly, there is no statistically significant correlation between prior MEI and break length (but there is a statistically significant negative correlation with MEI lagging, in September-December). Compared to the MEI, the other climate indices show little month-to-month consistency in signs of and strength of leading correlations. However, there is a significant positive correlation between prior May-June NAO and KSP break length and a significant negative correlation between prior March-June IOZM and KSM break length.

Correlations Between Major Climate Indices in Months Prior to and During KSM Onset, Break, and Withdrawal

A. MEI	Jan	Feb	Mar	Apr	May	Jun	Jul	Aug	Sep
Onset	0.36	0.33	0.36	0.43	0.45	0.38	0.31	0.24	0.13
Break Start	0.52	0.49	0.51	0.47	0.45	0.39	0.30	0.20	0.07
Break Length	-0.01	-0.01	0.05	0.06	-0.03	-0.11	-0.22	-0.31	-0.32
Withdrawal	0.38	0.40	0.49	0.45	0.38	0.31	0.26	0.19	0.16
B. WP	Jan	Feb	Mar	Apr	May	Jun	Jul	Aug	Sep
Onset	-0.01	-0.24	0.29	-0.08	-0.10	-0.09	-0.12	-0.26	-0.14
Break Start	0.00	-0.17	0.44	0.22	0.30	0.04	-0.36	-0.42	-0.09
Break Length	0.18	0.05	-0.27	-0.25	-0.32	-0.24	0.20	0.29	-0.20
Withdrawal	-0.04	-0.21	-0.01	-0.10	0.12	0.06	0.03	-0.29	-0.28
C. NAO	Jan	Feb	Mar	Apr	May	Jun	Jul	Aug	Sep
Onset	0.05	0.16	0.00	0.04	0.19	-0.04	-0.07	0.20	-0.20
Break Start	-0.07	0.13	-0.09	0.10	-0.23	-0.37	-0.26	0.03	-0.23
Break Length	0.47	0.28	0.17	-0.04	0.32	0.34	0.17	0.32	0.11
Withdrawal	0.00	0.14	-0.12	0.16	-0.17	-0.17	-0.11	0.04	-0.03
D. IOZM	Jan	Feb	Mar	Apr	May	Jun	Jul	Aug	Sep
Onset	0.01	-0.27	-0.30	-0.11	0.01	0.14	0.25	0.27	0.17
Break Start	0.30	0.07	-0.02	0.15	0.33	0.28	0.22	0.20	0.13
Break Length	-0.31	-0.31	-0.37	-0.35	-0.48	-0.27	0.21	0.10	-0.07
Withdrawal	0.04	-0.14	-0.15	-0.08	0.06	0.17	0.28	0.24	-0.01

Table 9. Correlations between KSM onset, break start, break length, and withdrawal and: (A) MEI, (B) WP, (C) NAO, and (D) IOZM for the months listed. The main KSM period is July-September, so the January-June columns represent correlations in which the climate indices lead the KSM variables. Values highlighted in yellow are statistically significant to the 95% level using Student's t-test.

5. Summary

Examining the relationships between precipitation totals and KSM onset, break, and withdrawal dates yields interesting results. Table 10 shows the cross correlations between these values. There is a strong positive correlation between the onset date of the KSM, the start of the KSM break, and KSM withdrawal. This means the later the onset, the later the break will start, and the later the monsoon will end, and vice versa. No significant correlations exist between the break length and KSM onset, break start, and KSM withdrawal. The strong negative correlation between monsoon onset and June precipitation suggests that a later onset date, most probably in July, will lead to light June precipitation totals. The monsoon break is negatively correlated to July and August precipitation but positively correlated to September precipitation. The July and August relationship is an intuitive one; one can picture how a long break would likely persist in July and August and drive down these months' precipitation totals. For the September relationship, the long breaks tend to last through August, and by definition, must be followed by a local maxima in that summer's precipitation curve, and this maxima will tend to be in September.

Cross Correlation Between KSM Characteristics and Precipitation Totals

	Break Start	Break Length	Withdrawal	JUN CMAP	JUL CMAP	AUG CMAP	SEP CMAP	Total CMAP
Onset	0.63	0.19	0.46	-0.63	-0.30	0.11	-0.16	-0.20
Break Start		-0.17	0.61	-0.18	0.16	0.35	-0.17	0.21
Break Length			0.23	-0.18	-0.35	-0.44	0.44	-0.22
Withdrawal				-0.13	0.09	0.23	0.18	0.31

Table 10. Cross correlation table between monsoon onset, break start, break length, withdrawal and total monthly CMAP precipitation in June-September, and total all-summer precipitation (i.e., total KSP). Values shaded in yellow are statistically significant to the 95% level using Student's t-test.

C. MJO AND KOREAN SUMMER PRECIPITATION

We examined the interactions between KSP and the intensity and phase of the MJO, based on the RMMI index of MJO activity (see chapter II). A typical RMMI diagram (e.g., Figure 38) represents MJO's eastward propagation by a set of the chronologically ordered points in the diagram that delineate a counterclockwise oriented

curve extending from phase one through phase eight. The MJO intensity is represented by the distance of the points from the origin of the diagram (greater distance indicates greater intensity). Working from this diagram, we reduced the number of MJO phases to four phases by combining the phases in each of the four main sectors (Indian Ocean, Maritime Continent, western Pacific, and western hemisphere and Africa). That is, we combined phase 2 with phase 3, 4 with 5, 6 with 7, and 8 with 1. To match the temporal resolutions of the CMAP precipitation data and the RMMI data, we downscaled the RMMI in time to the pentad scale by using the mode of the phase for the given pentad (e.g., we created 5-day averages of the RMMI intensity data).

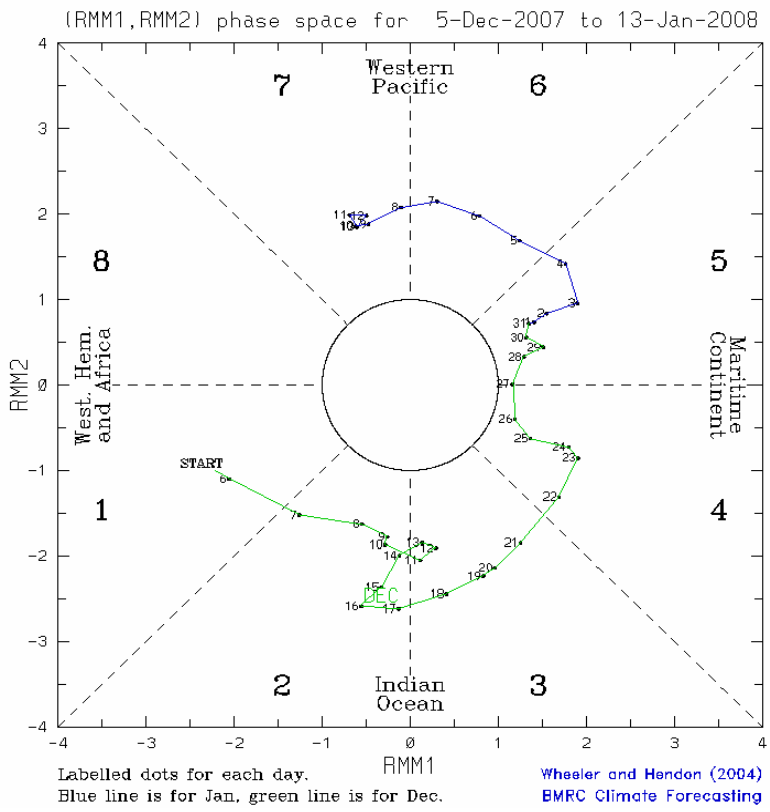

Figure 38. A typical 40-day RMMI phase space diagram. Each point in the diagram represents the data and the longitude of the convective component of the MJO. An MJO is classified by phases, representing eight longitudinal sectors through which the convective component tends to propagate, from phase 1 to phase 8. MJO intensity is indicated for each point by the point's distance from the center of the diagram (from http://www.bom.gov.au/bmrc/clfor/cfstaff/matw/maproom/RMM/phase.Last40days.html accessed 21 March 2008).

1. Relationship of MJO to KSM Onset

Using the previously determined KSM onset dates, we examined the lead and lag relationships between the MJO and KSM onset using correlation and conditional forecasting techniques. Pentads 31 through 42 were considered, with the earliest onset date in pentad 33 and the latest in pentad 40. For all summer pentads during 1979-2005, there were nearly equal numbers of all four phases of the MJO, with a slight skew toward lower phases, with phase 1 occurring in 28% of pentads, phase 2 in 27%, phase 3 in 22% and phase 4 in 23%. For the intensity, the average value over the summer was 1.1.

MJO Phase Leading, Simultaneous With, and Lagging the KSM Onset Pentad

			Leading		Sim	Lagging	
			-2	-1	0	1	2
A. Raw percentages	MJO Phase	1	30	37	33	30	19
		2	22	33	22	33	26
		3	15	11	33	19	15
		4	33	19	11	19	41
			-2	-1	0	1	2
B. Raw percentages minus average percentages	MJO Phase	1	1	9	5	1	-10
		2	-4	7	-4	7	-1
		3	-7	-11	11	-3	-7
		4	10	-5	-12	-5	18
			-2	-1	0	1	2
C. Raw minus average divided by average	MJO Phase	1	4	30	17	4	-35
		2	-16	26	-16	26	-2
		3	-32	-49	52	-15	-32
		4	44	-20	-52	-20	76

Table 11. Raw percentages for leading (left) to lagging (right) values of MJO phase (A), raw percentage minus mean (B) and raw percentage minus average percentage divided by average percentage (C) with respect to KSM onset.

Table 11 shows that two pentads prior to the onset of the KSM, there is: (a) a 10% greater chance than average (44% greater chance proportionally) of phase 4 of the MJO (RMMI phases 6 and 7) occurring; and (b) and a 7% lower chance than average (32% lower chance proportionally) of phase 3 of the MJO (RMMI phases 4 and 5). Simultaneous with the onset of the KSM, there is an 11% increased chance of phase 3 of the MJO (52% increase proportionally), and a 12% decreased chance of phase 4 of the MJO (52% decrease proportionally). Two pentads after the KSM onset, the greatest

increase from average is in phase 4, with an 18% increase or 76% increase proportionally, while the greatest decrease is in phase 1 at -10% (-35% proportionally). While the largest increase over the average appears to move randomly between leading and lagging the KSM, there may be a physical basis for the relationships, since the greatest decrease from average moves similarly to what might be expected from a typical MJO, with the greatest deficit moving through phases 3, 3, 4, 4, 1 at -2, -1, simultaneous, +1, and +2 pentads.

With regard to intensity, the results are not as conclusive apart from the simultaneous relationships between MJO and KSM onset. Table 12 is the same as Table 11 above, but for intensity, conditioned on whether the intensity in the pentad was above or below the average value of 1.1.

MJO Intensity Leading, Simultaneous With, and Lagging the KSM Onset Pentad

		Leading		Sim	Lagging	
A. Raw percentages	Intensity	-2	-1	0	1	2
	>1.1	52	56	52	37	41
	<1.1	48	44	48	63	59
B. Raw percentages minus average percentages	Intensity	-2	-1	0	1	2
	>1.1	2	6	2	-13	-9
	<1.1	-2	-6	-2	13	9
C. Raw minus average divided by average percentage	Intensity	-2	-1	0	1	2
	>1.1	4	12	4	-26	-18
	<1.1	-4	-12	-4	26	18

Table 12. Raw percentages for leading (left) to lagging (right) values of MJO intensity (A), raw percentage minus mean (B) and raw percentage minus average percentage divided by average percentage (C) with respect to KSM onset.

Table 12 indicates that: (a) there is a propensity of above average intensity MJO events prior to and during the KSM onset; and (b) there is a propensity of below average intensity MJO events after the KSM onset. This suggests that the tropical atmosphere is convectively more active before and during KSM onset. This makes sense intuitively: in the weeks prior to KSM start, we would expect the stepwise, northward progression of the EASM to be south of Korea, presumably in the tropics where the tropical western

North Pacific would be experiencing positive convective anomalies, which could be due in part to the convective phase of the MJO traversing trough the MC and western tropical Pacific region.

2. Relationship of MJO to KSM Withdrawal

Table 13 shows the percent occurrence of each of the four phases of MJO for pentads before, simultaneous with, and after the withdrawal of the KSM. The second set of rows shows the raw percentage minus the average percentage of phase occurrence and the final set of rows shows this subtracted number divided by the average.

MJO Phase Leading, Simultaneous With, and Lagging the KSM Withdrawal Pentad

			Leading		Sim	Lagging	
			-2	-1	0	1	2
A. Raw percentages	MJO Phase	1	30	33	22	26	26
		2	22	26	26	22	22
		3	33	22	37	22	22
		4	15	19	15	30	30
			-2	-1	0	1	2
B. Raw percentages minus average percentages	MJO Phase	1	3	6	-5	-1	-1
		2	-4	0	0	-4	-4
		3	9	-2	13	-2	-2
		4	-8	-5	-8	6	6
			-2	-1	0	1	2
C. Raw minus average divided by average percentage	MJO Phase	1	10	24	-17	-3	-3
		2	-14	0	0	-14	-14
		3	38	-8	54	-8	-8
		4	-36	-20	-36	28	28

Table 13. Raw percentages for leading (left) to lagging (right) values of MJO intensity (A), raw percentage minus mean (B) and raw percentage minus average percentage divided by average percentage (C) with respect to KSM withdrawal.

Table 13 does not show a clear MJO cycle in the changes of the phase with the greatest increase over the average (phases 3, 1, 3, 4, 4 in pentads -2, -1, 0, 1, 2 before and after KSM withdrawal). There is some evidence of an MJO cycle in the changes of the phase with the greatest decrease below average (phases 4, 4, 4, 2, 2 in pentads -2, -1, 0, 1, 2 before and after KSM withdrawal).

Table 14 shows that the relationships between MJO intensity and KSM withdrawal are nearly opposite to those for KSM onset. That is, there is a propensity for less (more) intense than average MJO activity prior to and during (after) KSM withdrawal.

MJO Intensity Leading, Simultaneous With, and Lagging the KSM Withdrawal Pentad

		Leading		Sim	Lagging	
A. Raw percentages	Intensity	-2	-1	0	1	2
	>1.1	44	52	59	63	70
	<1.1	56	48	41	37	30
B. Raw percentages minus average percentages	Intensity	-2	-1	0	1	2
	>1.1	-6	2	9	13	20
	<1.1	6	-2	-9	-13	-20
C. Raw minus average divided by average percentage	Intensity	-2	-1	0	1	2
	>1.1	-12	4	18	26	40
	<1.1	12	-4	-18	-26	-40

Table 14. Raw percentages for leading (left) to lagging (right) values of MJO intensity (A), raw percentage minus mean (B) and raw percentage minus average percentage divided by average percentage (C) with respect to KSM withdrawal.

3. Relationship of MJO Phase and Intensity to KSP Intensity

Table 15 shows the leading, simultaneous, and lagging relationships between MJO phase and intensity and normalized precipitation KSP. The three parts of the table show the relationships for KSP that was above average (I, 0.5 standard deviation (SD) above the mean), average (II, within 0.5 SD of the mean), and below average (III, 0,5 SD below the mean). These three groupings represent the division of all summer pentads (31 through 54, or June through September) into three groups of roughly equal membership: above average with 229 members), average with 199 members, and below average with 220 members.

Pentads with above average precipitation (Table 15-I) showed little departure from average with respect to MJO phase leading, simultaneous with, and lagging KSP. With MJO phase leading, phase 1 showed a slight increase above average, while phases 2 and 4 were below average. Pentads with average KSP showed a propensity for MJO phases 2 and 4 two pentads prior (12% and 9%, respectively) and phase 2 one pentad prior (6%, or 12% above the mean percentage). During average KSP pentads, phase 1 was seen in greater numbers (19% above mean) and phase 4 in lower numbers (13% under mean). After average KSP pentads, phase 1 was relatively common.

One to two pentads before the average KSP pentads (Table 15-II), phase 2 (phase 3) was relatively common (uncommon). During average KSP pentads, phase 1 (3 and 4) was relatively common, while phases 3 and 4 were relatively uncommon. One to two pentads prior to the below average pentads (Table 15-III), MJO phases 3 and 4 (1 and 2) are relatively common (uncommon). During below average KSP pentads, phase 4 is relatively common, and phases 1 and 3 are relatively uncommon.

Percentage of Pentads Leading, Simultaneous With, and Lagging the Given MJO Phase for Above Average, Average, and Below Average Pentads

I.			Leading		Sim	Lagging	
			-2	-1	0	1	2
A. Raw percentages	MJO Phase	1	31	31	25	27	27
		2	25	24	29	26	28
		3	23	24	27	23	21
		4	21	21	20	24	24
			-2	-1	0	1	2
B. Raw percentages minus average	MJO Phase	1	4	3	-2	-1	0
		2	-1	-2	2	0	2
		3	0	1	4	0	-2
		4	-2	-2	-4	1	1
			-2	-1	0	1	2
C. Raw minus average divided by	MJO Phase	1	14	11	-9	-3	-1
		2	-5	-8	9	0	6
		3	-1	5	16	-2	-10
		4	-9	-9	-15	5	4

II.			Leading		Sim	Lagging	
			-2	-1	0	1	2
Raw percentages	MJO Phase	1	28	28	33	31	31
		2	29	28	24	24	23
		3	18	21	23	23	22
		4	25	23	20	22	24
			-2	-1	0	1	2
Raw percentages minus average	MJO Phase	1	0	0	5	3	3
		2	3	2	-2	-2	-3
		3	-5	-2	0	0	-1
		4	2	0	-3	-1	1
			-2	-1	0	1	2
Raw minus average divided by average	MJO Phase	1	0	1	19	11	12
		2	12	6	-7	-9	-13
		3	-24	-8	-1	1	-5
		4	9	-1	-13	-3	5
III.			Leading		Sim	Lagging	
			-2	-1	0	1	2
A. Raw percentages	MJO Phase	1	23	24	25	25	26
		2	22	24	26	27	24
		3	30	24	20	23	26
		4	25	27	30	24	23
			-2	-1	0	1	2
B. Raw percentages minus average	MJO Phase	1	-4	-3	-3	-2	-1
		2	-4	-2	0	1	-2
		3	7	1	-3	0	3
		4	2	4	6	1	0
			-2	-1	0	1	2
C. Raw minus average divided by	MJO Phase	1	-15	-12	-11	-8	-5
		2	-16	-7	-1	4	-7
		3	29	6	-13	1	13
		4	8	16	28	4	1

Table 15. Raw percentages for leading (left) to lagging (right) values of MJO intensity (A), raw percentage minus mean (B) and raw percentage minus average percentage divided by average percentage (C) for pentads greater than 0.5 SD (I), 0.5 to –0.5 SD (II) and less than –0.5 SD (III), all with respect to KSP intensity.

Table 16 summarizes these results by showing which phases saw a surplus or deficit of a particular MJO phase for above average, average, and below average KSP.

	Summary of Table 15 Results					
	MJO Leading		Simultaneous		MJO Lagging	
	Surplus	Deficit	Surplus	Deficit	Surplus	Deficit
> 0.50	1	--	2,3	4	3	2,4
0.50 to -0.50	2	3	1	4	1	2
<-0.50	3,4	1,2	4	1,3	1	3

Table 16. Summary of results in Table 15.

4. Relationship of MJO / WPZI to KSP

The following section investigates the utility of conditioning the MJO relationship to KSP on the state of the WPZI. For this investigation, we developed contingency tables in which MJO phase, MJO intensity, and WPZI state were matched to KSP (in particular, KSP above or below different standard deviation levels). In this analysis, MJO phase, MJO intensity, and WPZI were treated as predictors and KSP was treated as the predictand, with the predictors leading the predictor by two to four pentads (10-20 days). We also developed composite anomalies from which physical processes were identified that appear to explain the MJO/WPZI relationships to intraseasonal KSP variations.

a. Simultaneous Relationships between MJO, WPZI, and KSP

We analyzed the KSP data to classify each KSP pentad during 1979-2005 with MJO phase, MJO intensity, and WPZI state. We then developed contingency tables to represent the results of this analysis, with different tables for different lead/lag relationships, and different KSP values (above average, average, and below average KSP). We also identified the results in the table that were statistically significant at the 90% level using the hypergeometric distribution Fisher's exact test (Wilkis 2006; green shading in Tables 17-20).

Contingency Table Results for MJO Simultaneous with KSP

	Count of KSM Pentads Above Mean			
	MJO Phase			
	1	2	3	4
Negative WPZI, Intense MJO	**24**	**30**	**30**	**12**
Negative WPZI, Weak MJO	**19**	**26**	**18**	**20**
Positive WPZI, Intense MJO	**13**	**12**	**14**	**13**
Positive WPZI, Weak MJO	**25**	**14**	**15**	**16**

	Count of KSM Pentads Below Mean			
	MJO Phase			
	1	2	3	4
Negative WPZI, Intense MJO	**27**	**17**	**20**	**17**
Negative WPZI, Weak MJO	**18**	**29**	**15**	**14**
Positive WPZI, Intense MJO	**30**	**18**	**18**	**34**
Positive WPZI, Weak MJO	**23**	**24**	**19**	**24**

	Percentage of KSM Values Below Mean			
	MJO Phase			
	1	2	3	4
Negative WPZI, Intense MJO	**0.53**	**0.36**	**0.40**	**0.59**
Negative WPZI, Weak MJO	**0.49**	**0.53**	**0.45**	**0.41**
Positive WPZI, Intense MJO	**0.70**	**0.60**	**0.56**	**0.72**
Positive WPZI, Weak MJO	**0.48**	**0.63**	**0.56**	**0.60**

Table 17. Count of all pentads fitting the given contingency table criteria for above mean KSP cases (top), below mean KSP cases (middle); and the percentage of below mean values (bottom). In the bottom table, percentages meeting the 90% significance level using Fisher's exact test are shaded green.

Table 17 shows the results for the simultaneous relationships between MJO/WPZI and KSP. As an example, when the WPZI was negative, the MJO was in phase 2, and the MJO intensity was above average, there were 30 pentads with above average KSP and 17 pentads with below average KSP, and 36% of these pentads had below average KSP. As another example, when the WPZI was positive, the MJO was in phase 2, and the MJO intensity was below average, 63% of the pentads had below average KSP.

The results in Table 17 are consistent with those in Tables 15-16, which dealt with just MJO phase versus KSP. For example, Table 17 shows that the bulk of above average precipitation pentads occur in phases 2 and 3 of the MJO, especially high intensity MJOs. But Table 17 also shows that these pentads are associated with negative WPZI, and that low precipitation pentads tend to occur during positive WPZI. These low KSP pentads are also associated with phase 4 of the MJO, in agreement with Tables 15-16.

b. Relationships between MJO / WPZI with MJO Leading by Two Pentads

To study the ability of the MJO conditioned by WPZI state to predict KSP, we examined the cases in which MJO led KSP by two pentads. This allowed us to investigate how the MJO phase, conditioned by the MJO intensity and WPZI state (an indicator of ENLN state), affects KSP 5-10 days into the future.

Contingency Table Results for MJO Leading KSP by Two Pentads				
	Number of KSM Pentads Above Mean			
	MJO Phase			
	1	2	3	4
Negative WPZI, Intense MJO	**25**	**30**	**25**	**15**
Negative WPZI, Weak MJO	**23**	**32**	**15**	**14**
Positive WPZI, Intense MJO	**16**	**15**	**11**	**18**
Positive WPZI, Weak MJO	**22**	**14**	**8**	**18**
	Number of KSM Pentads Below Mean			
	MJO Phase			
	1	2	3	4
Negative WPZI, Intense MJO	**29**	**17**	**22**	**18**
Negative WPZI, Weak MJO	**13**	**22**	**19**	**17**
Positive WPZI, Intense MJO	**28**	**10**	**19**	**30**
Positive WPZI, Weak MJO	**27**	**25**	**27**	**24**
	Percentage of KSM Values Below Mean			
	MJO Phase			
	1	2	3	4
Negative WPZI, Intense MJO	**0.54**	**0.36**	**0.47**	**0.55**
Negative WPZI, Weak MJO	**0.36**	**0.41**	**0.56**	**0.55**
Positive WPZI, Intense MJO	**0.64**	**0.40**	**0.63**	**0.63**
Positive WPZI, Weak MJO	**0.55**	**0.64**	**0.77**	**0.57**

Table 18. Same as Table 17 except that MJO leads KSP by two pentads.

Table 18 shows the relationships between MJO/WPZI two pentads prior to pentads with above or below average KSP. This table shows that a high percentage of below average KSP pentads occur two pentads after pentads with MJO phases 3 and 4 and positive WPZI. A high percentage of above average KSP pentads occur two pentads after pentads with MJO phase 2, unless the MJO is weak and the WPZI is positive. Table 18 also shows that the MJO/WPZI conditions associated with above and below average KSP shift to the left in the table compared to the simultaneous case (Table 17), with some variations according to MJO intensity and WPZI state. For the simultaneous relationships, the greatest percentage of low KSP pentads are associated with MJO

phases 1 and 4, but for the MJO/WPZI leading relationships they are associated with MJO phases 3 and 4. And the greatest percentage of high KSP pentads are simultaneously associated with MJO phases 2 and 3, but for the MJO/WPZI leading relationships they are associated with MJO phases 2.

c. Relationship between KSP, MJO, and WPZI with MJO Leading by Three Pentads

With MJO state leading KSP by three pentads (11-15 days) we see a continuing shift to the left (compare Tables 17-19). Clearly, the MJO phase 3 is associated with the greatest proportion of below average KSP pentads three pentads prior to the below average KSP. This holds for all combinations of WPZI/intensity states.

Contingency Table Results for MJO Leading KSP by Three Pentads				
	Sum KSM Pentads Above Mean			
	MJO Phase			
	1	2	3	4
Negative WPZI, Intense MJO	**31**	**29**	**18**	**22**
Negative WPZI, Weak MJO	**20**	**25**	**16**	**18**
Positive WPZI, Intense MJO	**21**	**9**	**9**	**20**
Positive WPZI, Weak MJO	**18**	**15**	**11**	**19**
	Sum KSM Pentads Below Mean			
	MJO Phase			
	1	2	3	4
Negative WPZI, Intense MJO	**24**	**17**	**28**	**14**
Negative WPZI, Weak MJO	**19**	**26**	**16**	**13**
Positive WPZI, Intense MJO	**25**	**16**	**20**	**28**
Positive WPZI, Weak MJO	**30**	**23**	**26**	**22**
	Percentage of KSM Values Below Mean			
	MJO Phase			
	1	2	3	4
Negative WPZI, Intense MJO	**0.44**	**0.37**	**0.61**	**0.39**
Negative WPZI, Weak MJO	**0.49**	**0.51**	**0.50**	**0.42**
Positive WPZI, Intense MJO	**0.54**	**0.64**	**0.69**	**0.58**
Positive WPZI, Weak MJO	**0.63**	**0.61**	**0.70**	**0.54**

Table 19. Same as Table 17 except that MJO leads KSP by three pentads.

d. Relationship between KSP, MJO and WPZI with MJO Leading by Four Pentads

With MJO leading KSP by four pentads (16-20 days; Table 20), a: (1) high percentage of low KSP pentads is associated with all MJO phases and with positive WPZI; and (2) a moderately high percentage of high KSP pentads are associated with MJO phases 1 and 4, and with negative WPZI. These results are roughly opposite to those shown in Table 17 for simultaneous relationships between MJO/WPZI and KSP.

Contingency Table Results for MJO Leading KSP by Four Pentads

	Sum KSM Pentads Above Mean			
	MJO Phase			
	1	2	3	4
Negative WPZI, Intense MJO	**31**	**21**	**22**	**24**
Negative WPZI, Weak MJO	**17**	**34**	**16**	**14**
Positive WPZI, Intense MJO	**24**	**11**	**8**	**20**
Positive WPZI, Weak MJO	**12**	**13**	**12**	**22**

	Sum KSM Pentads Below Mean			
	MJO Phase			
	1	2	3	4
Negative WPZI, Intense MJO	**24**	**22**	**22**	**18**
Negative WPZI, Weak MJO	**23**	**15**	**17**	**16**
Positive WPZI, Intense MJO	**20**	**15**	**20**	**30**
Positive WPZI, Weak MJO	**33**	**26**	**25**	**21**

	Percentage of KSM Values Below Mean			
	MJO Phase			
	1	2	3	4
Negative WPZI, Intense MJO	**0.44**	**0.51**	**0.50**	**0.43**
Negative WPZI, Weak MJO	**0.58**	**0.31**	**0.52**	**0.53**
Positive WPZI, Intense MJO	**0.45**	**0.58**	**0.71**	**0.60**
Positive WPZI, Weak MJO	**0.73**	**0.67**	**0.68**	**0.49**

Table 20. Same as Table 17 except that MJO leads KSP by four pentads.

e. Hindcast Statistics

Using data from Tables 17-20, verification statistics were compiled using the tabular data as hindcasts in which MJO and WPZI values were used as predictors of above or below average KSP, with MJO and WPZI leading KSP by zero, two, three, and four pentads. Tables 21-24 include contingency tables for the four lead times (zero, 2, 3, and 4 pentads). The contingency table cells were filled using values from the percentage sections in Tables 17-20. If a percentage value met the statistical significance criteria and

the majority of cases were below average, then the number of below average cases was placed in the below average forecasted and observed cells. A similar procedure was used to determine the number of cases in which above average KSP was forecasted and observed. Two sub-tables, A and B, were developed for each of the four lead times. The A (B) tables are based only cases for which the statistical significant reached the 85% (90%) level. The tables were developed for forecasting below average pentads, so the main diagonal values, in which the forecasted and observed values were the same, represent a correct forecast of a below average KSP pentad. For an explanation of the verification statistics shown in sub-tables C and D of Tables 21-24, see chapter II and Jarry (2005).

A.

		OBSEVED	
		Below	Above
FORECAST	Below	205	135
	Above	141	167

B.

		OBSEVED	
		Below	Above
FORECAST	Below	112	56
	Above	89	123

C.

ACC	0.57
POD	0.59
FAR	0.40
TS	0.32
HSS	0.15

D.

ACC	0.62
POD	0.56
FAR	0.33
TS	0.29
HSS	0.24

Table 21. Hindcast contingency tables and verification statistics for MJO predictor leading KSP by zero pentads. A and C represent only Table 17 cases meeting the 85% significance level, while B and D represent only Table 17 cases meeting the 90% significance level. ACC – accuracy, POD – probability of detection, FAR – false alarm rate, TS – threat score, HSS – Heidke skill score.

A.

		OBSERVED	
		Below	Above
FORECAST	Below	263	176
	Above	84	125

B.

		OBSERVED	
		Below	Above
FORECAST	Below	129	67
	Above	84	125

C.

ACC	0.60
POD	0.76
FAR	0.40
TS	0.41
HSS	0.18

D.

ACC	0.63
POD	0.61
FAR	0.34
TS	0.32
HSS	0.26

Table 22. Same as Table 21 but for MJO predictor leading KSP by two pentads (6-10 days).

A.

		OBSERVED	
		Below	Above
FORECAST	Below	260	181
	Above	87	120

B.

		OBSERVED	
		Below	Above
FORECAST	Below	171	100
	Above	68	100

C.

ACC	0.59
POD	0.75
FAR	0.41
TS	0.40
HSS	0.15

D.

ACC	0.62
POD	0.72
FAR	0.37
TS	0.39
HSS	0.22

Table 23. Same as Table 21 but for MJO predictor leading KSP by three pentads (11-15 days).

A.

		OBSERVED	
		Below	Above
FORECAST	Below	270	188
	Above	77	113

B.

		OBSERVED	
		Below	Above
FORECAST	Below	134	65
	Above	77	113

C.

ACC	0.59
POD	0.78
FAR	0.41
TS	0.42
HSS	0.16

D.

ACC	0.63
POD	0.64
FAR	0.33
TS	0.34
HSS	0.27

Table 24. Same as Table 21 but for MJO predictor leading KSP by two pentads (16-20 days).

Tables 21-24 show that at all four leads, the hindcasts had skill (e.g., the Heidke skill scores and threat scores are above zero). The sub-table C verification scores (based on the 85% significance criterion) are similar to those obtained when using only WPZI as the predictor (see chapter III, section F). However, the sub-table D scores (based on the 90% significance criterion) show a notable improvement over hindcasts based on using just the WPZI as the predictor. The hindcasts based on MJO/WPZI leading by four pentads have the best hindcast statistics (e.g., highest HSS and POD, the lowest FAR). These results indicate that forecasts in which both MJO and WPZI are used as predictors have a high potential to produce skillful forecasts at leads of 5-20 days. However, these results also indicate that there are some situations for which the predictability is relatively low (e.g., those situations for which statistically insignificant results are shown in Tables 17-20). Thus, forecasting systems based on MJO/WPZI predictors must be used with caution, and should be limited to cases for which statistically significant relationships between MJO, WPZI, and KSP have been identified.

f. Physical Basis for Statistical Relationships between MJO, WPZI, and KSP

The results shown in Tables 17-20 indicate that above average KSP is associated with MJO phases 2 and 3, average KSP is associated with MJO phase 1, and below average KSP is associated with MJO phase 4. Based on these results, we constructed, for each MJO phase, composite anomaly maps of precipitation and 850 hPa GPH (Figure 39) based on data for the KSP period (late May- late September) during 1979-2005. Note that over much of the Asian – North Pacific region, the precipitation and GPH anomalies for phase 1 are approximately opposite to those for phase 3, and that those for phase 2 are approximately opposite to those for phase 4. These composites help reveal the physical processes by which MJO phase and WPZI variations lead to intraseasonal variations in KSP. For example, the phase 2 (4) panel shows anomalously anticyclonic (cyclonic) flow over the western tropical-subtropical North Pacific that leads to anomalously positive (negative) temperature and moisture advection into Korea. This helps explain the results of the prior section that showed that expected KSP varies noticeably from phase 2 to phase 4.

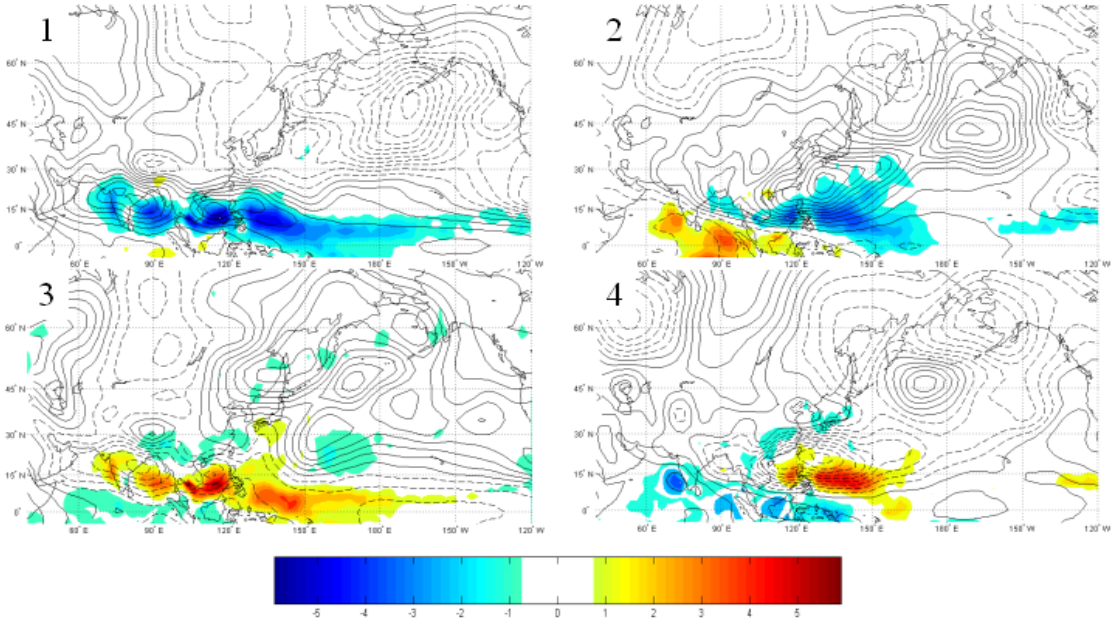

Figure 39. Composite anomaly maps of precipitation (color shading; units: mm/day) and 850 hPa GPH (black contours, solid (dashed) indicates positive (negative), contour interval = 1 gpm) for MJO phases 1-4. Based on data for the KSP period (late May-late September) during 1979-2005.

Figure 40 is similar to Figure 39 but focuses on just MJO phases 2 and 4 according to the MJO intensity (high or low). The high intensity phase 2 composite shows a focused positive height anomaly to the south of Korea that helps circulate warm, moist tropical air into the area and assists monsoon precipitation. Broadly similar features occur in the low intensity phase 2 composite, but the positive height anomaly extends further northward over Korea, preventing warm, moist advection into Korea. Thus, the intensity of the MJO appears to be a factor in shaping the positive height anomaly and the resulting advections into Korea. In the high intensity phase 4 composite, there is a strong negative height anomaly centered south of Korea that acts to inhibit moisture advection into and precipitation in Korea. By contrast, in the low intensity phase 4 composite, the negative height anomaly south of Korea is much weaker and shifted northward, creating a near neutral state over Korea. Note that Figure 40 supports the Table 17 indication that high intensity MJOs and negative WPZI tend to be associated with above average KSP.

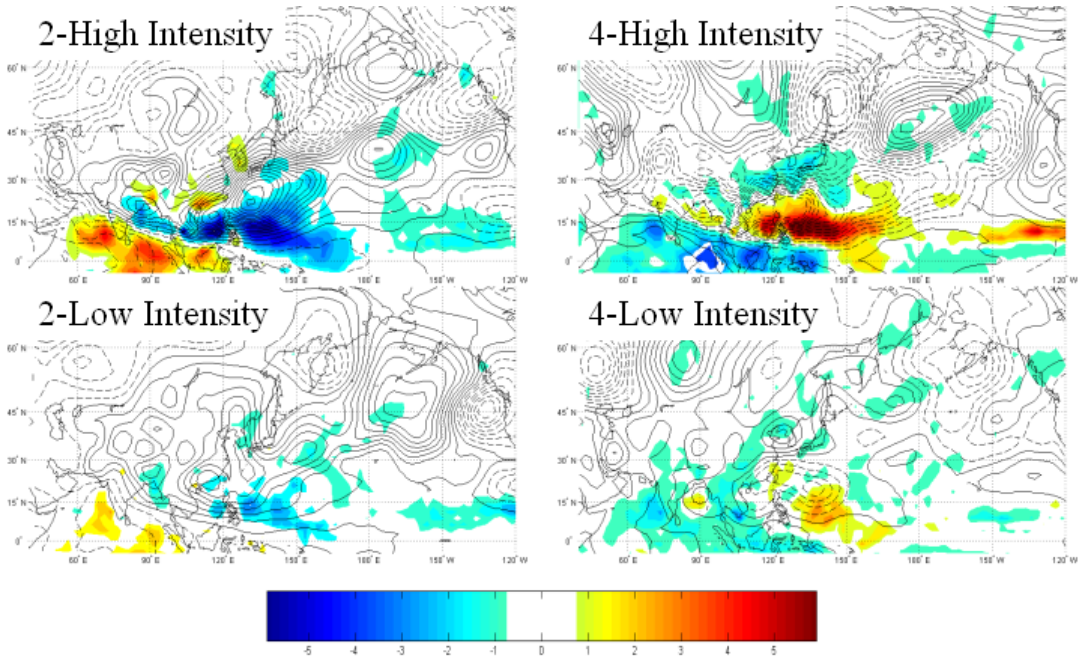

Figure 40. Composite anomaly maps of precipitation (color shading; units: mm/day) and 850 hPa GPH (black contours, solid (dashed) indicates positive (negative), contour interval = 1 gpm) for MJO phases 2 and 4, and for high and low intensity MJO cases. Based on data for the KSP period (late May-late September) during 1979-2005.

Figure 41 shows the influence of WPZI state on the processes by which MJO influences intraseasonal variations of KSP. Note the stark differences between the negative WPZI composites (lower four panels of Figure 41) and positive WPZI composites (lower four panels of Figure 41). For example, the phase 2, negative WPZI composite has much stronger positive height anomaly and negative precipitation anomaly south of Korea. This leads to a stronger anomalous southwesterly flow into Korea and a positive KSP anomaly. In the phase 3, positive WPZI composite, we see a much stronger negative height anomaly in the tropical-subtropical western North Pacific that inhibits precipitation in the EASM region, while in the phase 3, negative WPZI composite, there the corresponding height anomalies are weak and there is a positive precipitation anomaly in South Korea. In the phase 4, positive WPZI case, the negative height anomaly in tropical-subtropical western North Pacific is better developed than I the corresponding negative WPZI composite, leading to stronger negative KSP anomalies

than in the negative WPZI case. Comparing the results of Figure 41 and Figure 28, it is clear that the WPZI is providing a background anomalous circulation, which can constructively or destructively interfere with the circulation anomalies associated with the MJO. This interference can be modified by the intensity of the MJO (see Figure 40). Also, since the WPZI is related to the ENLN variations (see chapter III), the results shown in Figure 41 can be thought of as representing the combined effects of the MJO and ENL on the tropical and western North Pacific during the KSP period (June-September).

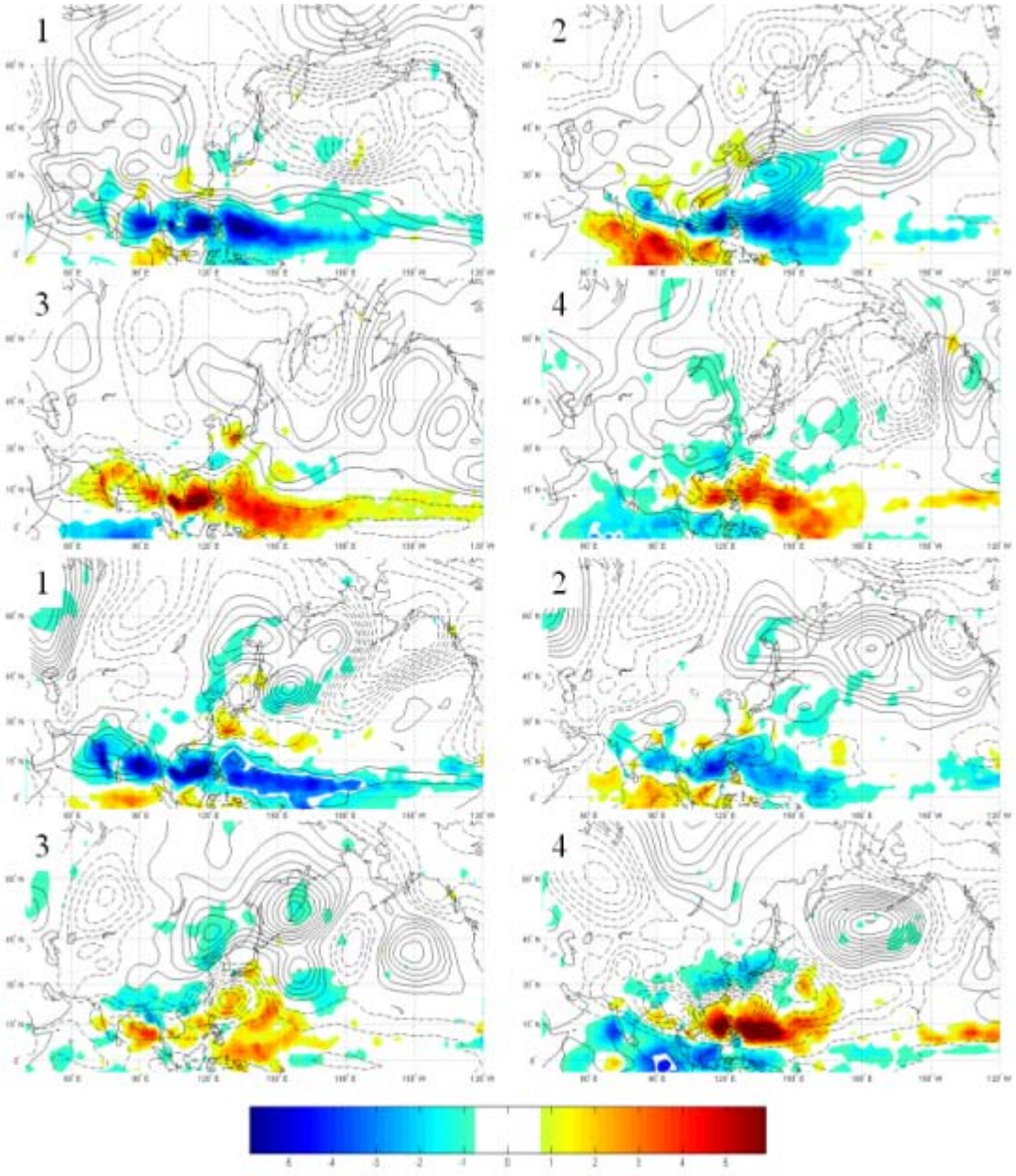

Figure 41. Composite anomaly maps of precipitation (color shading; units: mm/day) and 850 hPa GPH (black contours, solid (dashed) indicates positive (negative), contour interval = 2 gpm) for MJO phases 1-4, and for negative WPZI cases (upper four panels) and positive WPZI cases (lower four panels). Based on data for the KSP period (late May-late September) during 1979-2005.

To investigate the lag lead relationships between MJO, WPZI, and KSP, we constructed composite anomalies similar to those in Figures 39-41, but for 0-4 pentads following those composites. These composites of the trailing pentads show the time evolution of the anomalies associated with the different phases, and also reveal how the anomalies associated with one phase transition to those associated with the next. Figure 42 is an example of such a sequence of composite anomalies. Note how the negative height anomaly in the tropical-subtropical western North Pacific during phase 4 (upper left panel of Figure 42) evolves during the next one to four pentads, so that four pentads later, a positive height anomaly occurs where the negative height anomaly was located during phase 4). The time evolution of the anomalies also reveals how an MJO phase can be a leading indicator. For example, during phase 4, Korean precipitation is near average, but one pentad later it is above average, and three pentads later it is below average or average.

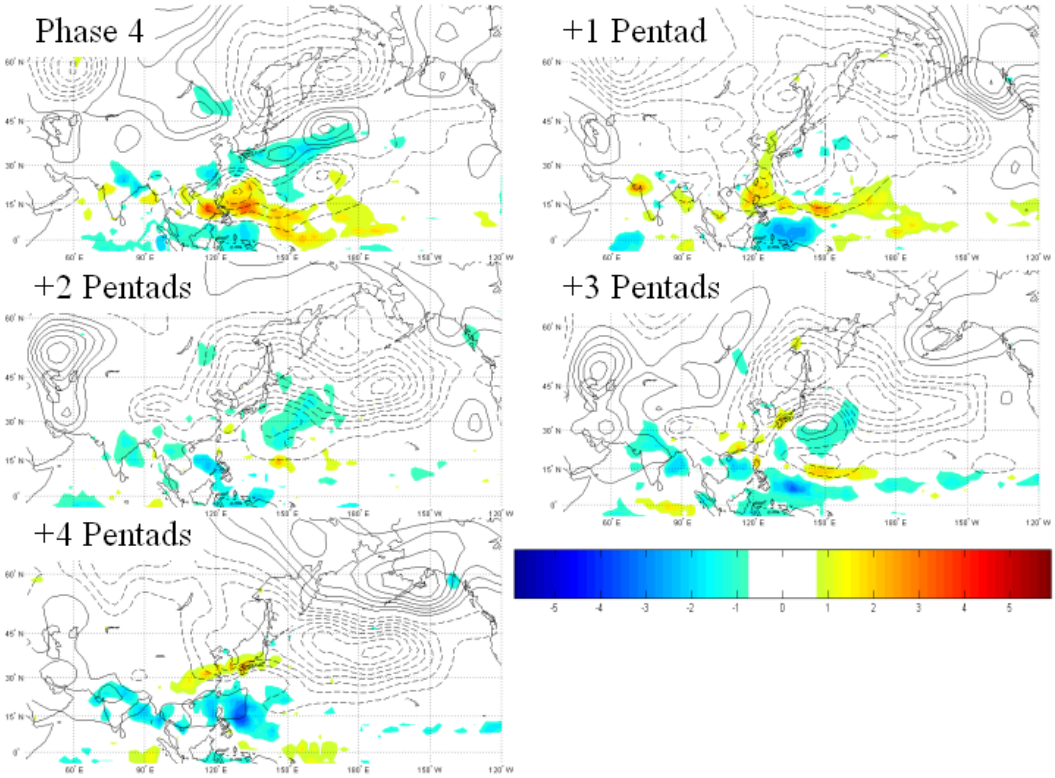

Figure 42. Composite anomaly maps of precipitation (color shading; units: mm/day) and 850 hPa GPH (black contours, solid (dashed) indicates positive (negative), contour interval = 1 gpm) for high intensity phase 4 of MJO, for negative WPZI cases (upper four panels), and for 0, 1, 2, 3, and 4 pentads after the occurrence of the high intensity, phase 4, negative WPZI state. Based on data for the KSP period (late May-late September) during 1979-2005.

g. An Automated WPZI/MJO KSP Prediction Scheme

The results shown in the prior sections indicate that a conditional forecasting system can be developed for intraseasonal variations of KSP based on MJO phase and intensity, and the WPZI. Such a system would predict the probability of KSP being above or below average during a given pentad. Three general approaches can be taken in the development of a forecasting scheme. One method would be to use analyses of the current MJO/WPZI state --- plus the lead relationships between MJO, WPZI, and KSP described in the prior sections --- to statistically predict how KSP will evolve in subsequent pentads. Another method would be to use a climate forecasting center's (e.g.,

CPC's) predictions of the MJO and zonal wind (from which WPZI forecasts could be generated) --- plus the simultaneous relationships between MJO, WPZI, and KSP described in the prior sections ---to dynamically and statistically predict how the KSP evolve in subsequent pentads. A third method would be to combine methods one and two.

A simple program could easily be developed through which the user chooses one of the three forecast schemes. Then, information is entered on the current MJO state, WPZI state, and (if needed) climate center forecasts of the MJO and the zonal winds used to calculate the WPZI. This information is then matched with data from Tables 17-24. The outputs from the program are probabilities of above or below average area averaged KSP for the Korean box shown in Figure 15 being above or below average. The program would also warns the user when outputs produced are not statistically significant at the 90% level. This forecast system could be used at various lead times to and initiation times to determine the confidence and uncertainty associated with the forecast.

An example of how the program engages the user and produces output is given below (program prompts for information are in black, user inputs are in red, and program outputs are in blue).

> Which forecast method would you like to use? (1: Use current MJO state to forecast future KSP. 2: Use climate center forecast of MJO for given day range to forecast KSP during that day range. 3: Use both 1 and 2.): 3
>
> Enter day range of forecast (1: 10 to 15 days in future. 2: 5 to 10 days into the future): 1
>
> Enter current MJO phase given by Australian BOM: 7
>
> Enter current MJO intensity given by Australian BOM: 1.5
>
> Enter WPZI value: -1.2
>
> Enter climate center forecasted MJO phase: 3

Enter climate center forecasted MJO intensity: 1.25

**********OUTPUT**********

Given the past relationships between MJO, WPZI, and KSP, and given the user-provided information (on-going MJO in phase 7 with above average intensity of 1.5 during a negative WPZI), there is a 61% chance of KSP being above average 11-15 days from now.

Given the past relationships between MJO, WPZI, and KSP, and given the user-provided information (forecasted MJO in phase 2 with above average intensity of 1.25 during and negative WPZI) there is a 64% chance of KSP being above average 11-15 days from now.

D. KOREAN SUMMER MONSOON AND TROPICAL CYCLONES

The Korean peninsula is frequently impacted by tropical cyclones (TCs). A total of 48 TCs impacted Korea (i.e., had a Joint Typhoon Warning Center best track position pass through the Korean box shown in Figure 15) during 1970-2006, for an average of 1.27 TCs per year. Figure 43 shows all of these 48 TC tracks in red, with the origin of each TC designated with a green star. The average position of formation for Korean landfalling TCs is 15 N, 143 E. Nearly all of the 48 TCs are weakly recurving storms, staying west of the recurving track that occurs over or east of Japan.

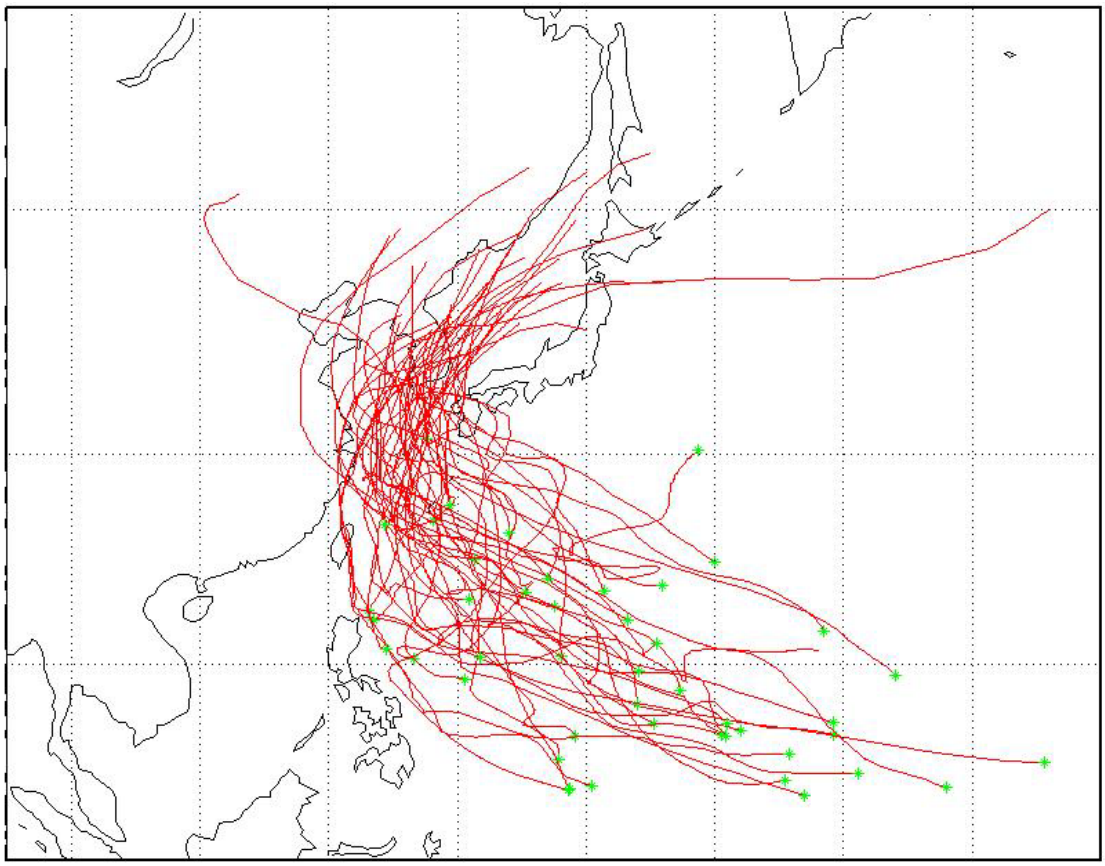

Figure 43. Tracks for all TCs impacting the Korean peninsula from 1970 to 2006 in red. Initial position is signified with a green star. Based on best track data from the Joint Typhoon Warning Center.

A total of 10 TCs were typhoons when they impacted Korea, while 14 were tropical storms, and 24 were tropical depressions. Figure 44 shows the preponderance of TC activity occurs in July and August with lesser activity in June, September, and October.

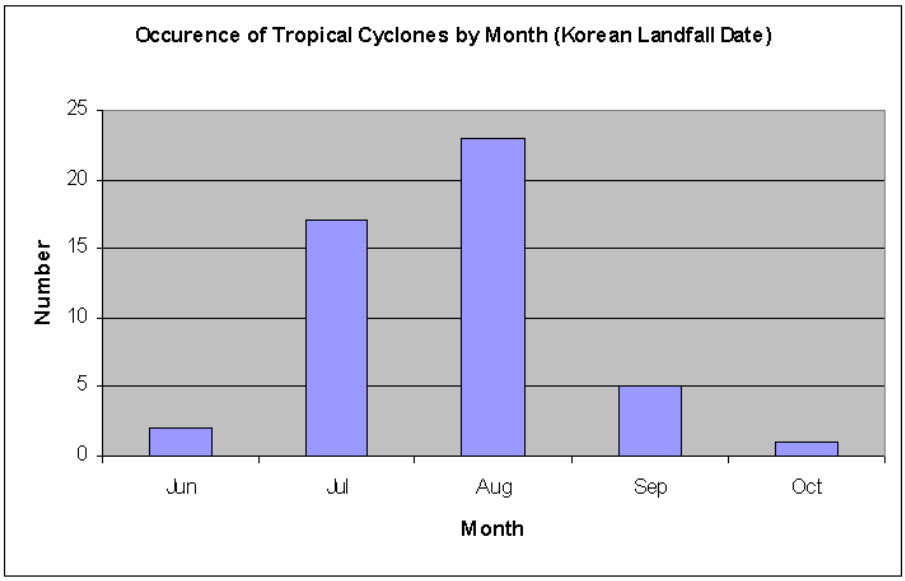

Figure 44. Number of TCs impacting Korea by month from 1970 to 2006.

Breaking the summer into three intraseasonal periods (15 Jun – 15 Jul, 15 Jul – Aug and 15 Aug – 15 Sep) reveals that the great majority of Korean impacting TCs occur during 15 Jul – 15 Sep (Figure 45).

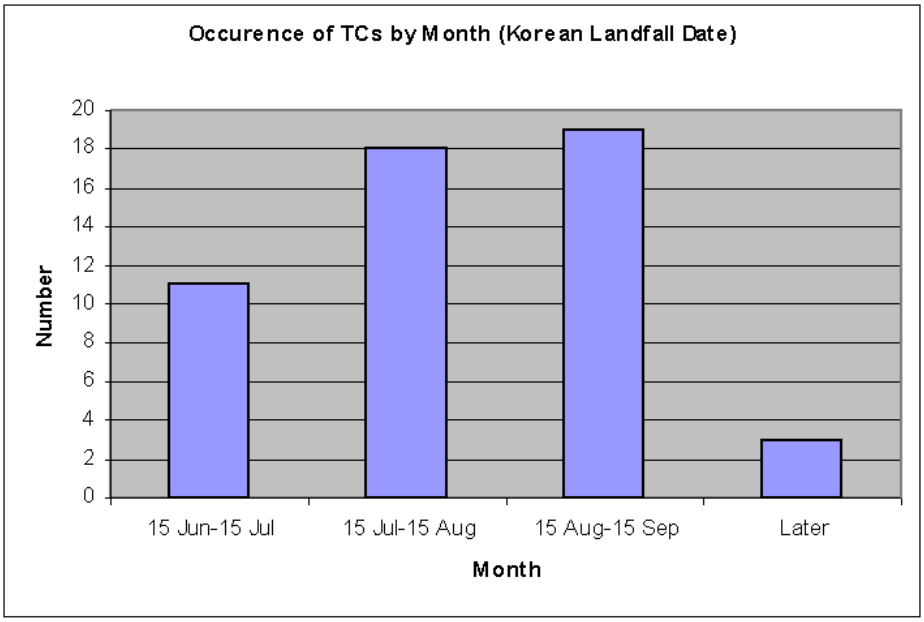

Figure 45. Number of Korean impacting TCs by intraseasonal period for 1970-2006.

Looking at the number of TCs per year from 1970 to 2006 (Figure 46) shows a steady increase from one per year at the beginning of the record to two per year at the end year. The 5-year moving average shows an increase along the linear regression line, but also shows a distinct decadal (7 to 9-year) oscillation.

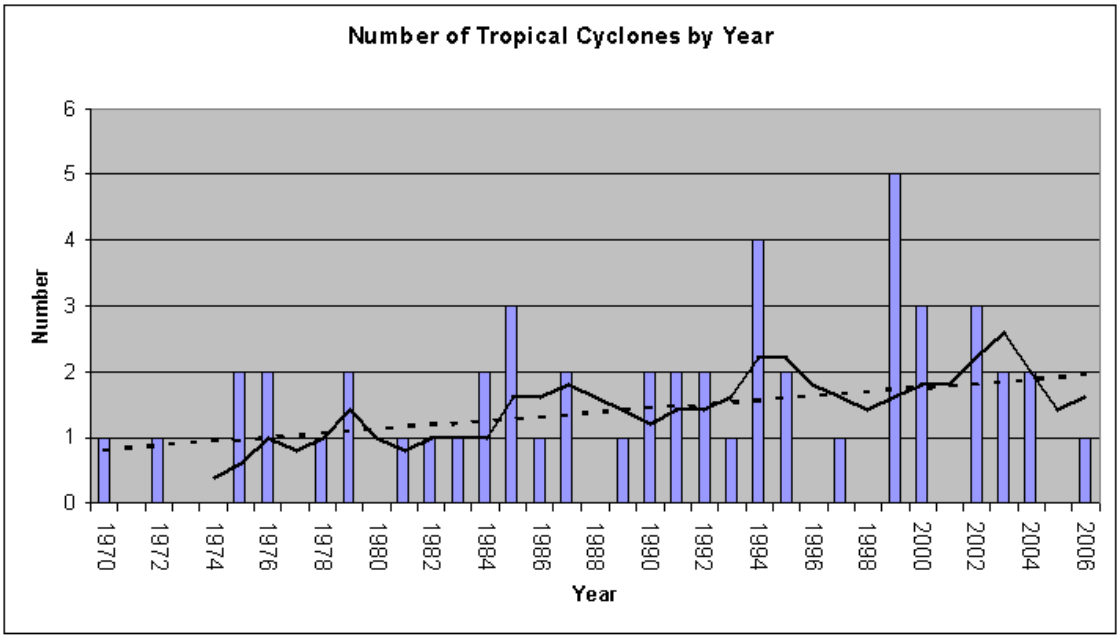

Figure 46. Number of Korean impacting TCs per year t from 1970 to 2006. Dashed black line is a linear trend. Solid black line is a 5-year moving average. Dotted balc line shows the long term trend.

Figure 47 shows that the probabilities of having zero, one, or two Korean impacting TCs in a year are about equal, with each of the three categories having occurred in about 25-30% of the last 37 years. Only 14% of the years had more than two Korean impacting TCs.

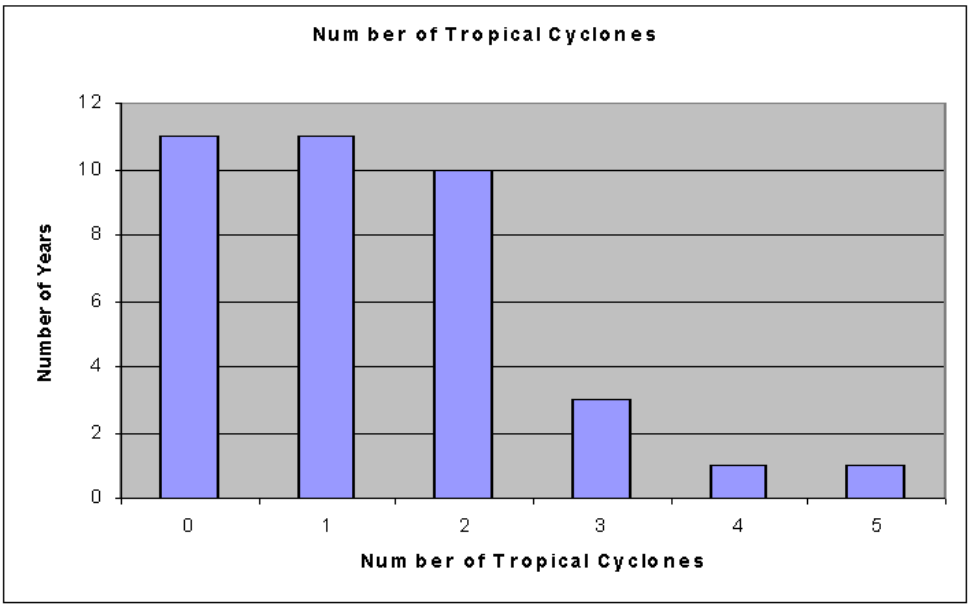

Figure 47. Number of years in which a given number of TCs impacted Korea in one year.

1. Relationship of Korean TC Landfall to El Niño

Previous research has shown that ENLN influences TC formation locations, intensities, and tracks in the western North Pacific (e.g., Lander 1994; Ford 2000). Steering flow is influenced by the anomalous Rossby wave response to the NW of the equatorial tropospheric warming (cooling) during EN (LN). This response tends to lead to a higher (lower) percentage of recurving TCs during EN (LN), and a lower (higher) percentage of straight running TCs during EN (LN). Korea lies between the main recurving and straight running tracks, which complicates the process of trying to tie TC activity in the Korea region to ENLN.

Figure 48 shows the percentage of years in which a given number of TCs impacted Korea, categorized by the ENLN state (EN, LN, or neutral). We defined this state according to the June-August average value of the MEI, with MEI greater than 0.5 indicating EN, less than -0.5 indicating LN, and in between values indicating neutral. During LN years, Korean impacting TCs are relatively uncommon (57% of LN years had zero Korean impacting TCs), but only 12% of EN years had zero TCs, and 31% of

neutral years had zero TCs. Only 14% of LN years had one TC, compared to 41% of EN years, and 23% of neutral years. The trend continues in the high-TC number years, with only 29% of LN years having more than 2 TCs per year, 47% of EN years, and 46% of neutral years. There were very few cases of more than 3 TCs per year, and so there was little difference between EN, LN, and neutral years.

The results from Figure 48 agree with the research from Ford (2000). Ford showed the difference in shear conditions and steering flow associated with EN versus LN led to more recurving TCs during EN. This leads to a greater chance of having at least one TC impact Korea, which is supported by Figure 48.

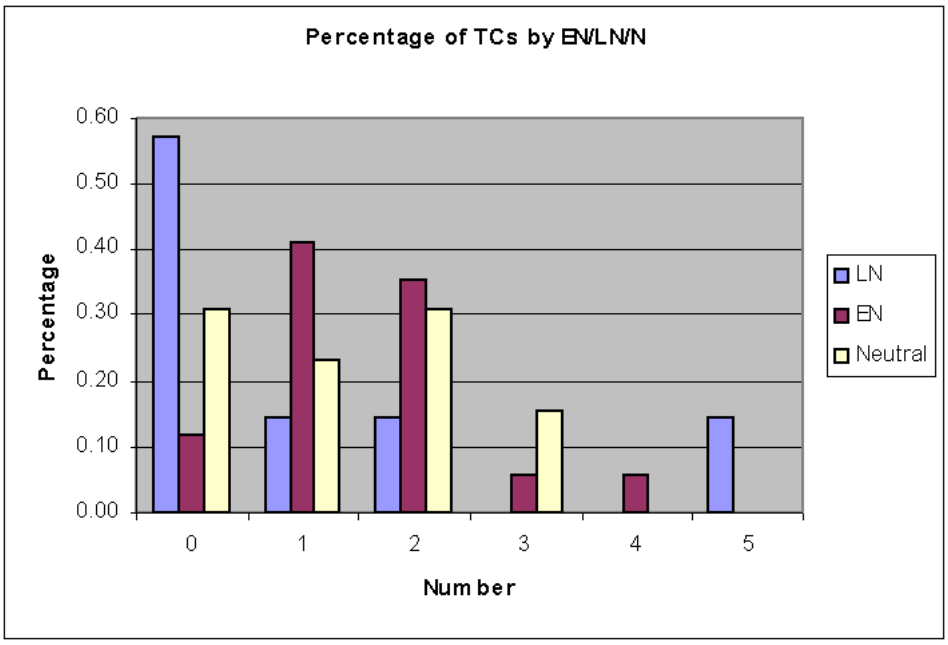

Figure 48. Percentage of years in which Korea was impacted by the given number of TCs, by the ENLN state (LN, EN, or Neutral).

The change in intensity of EN during the summer appears to influence the number of TCs impacting Korea. During 13 (35%) of the 37 summers studied, there was a strengthening EN, but in those summers, 43% of all the Korean TCs occurred and only one zero-TC year occurred. During five (14%) of the summers studied, there was a weakening EN. During these summers, only 7% of Korean impacting TCs occurred, while two years showed zero Korean impacting TCs. The number of LN years was small

(only seven of the 37 years). In five of these seven years, LN was strengthening and in two of the seven years LN was weakening. Three of the LN strengthening years had TCs and two had no TCs, and in the two weakening years there were no TCs. These results are consistent with those of Ford (2000) who showed that EN and LN impacts on TC activity in the western North Pacific occur mainly in the TC season that immediately follows the development of an EN or LN event. Since ENLN development tends to occur in the boreal spring, the following TC season occurs as the EN or LN is developing. A total of 12 (32%) years were neutral, and 33% of the Korean impacting TCs occurred in these years and in three of these years there were no Korean impacting TCs.

2. Relationship of Korean TC Landfall to MJO

We compared the state of the MJO prior to and during the days on which TCs impacted Korea. Figure 49 shows the number of days for which a given MJO phase (the eight phases of the RMMI) occurred on the Korean impact day, and at 5, 10 and 15 days before the impact day. This figure shows, for example, that 10-15 days prior to TC impact, the MJO is most likely to be in phases 5 through 8. Of course, 10-15 days prior to impact is when TC that eventually impact Korea are likely to be forming. This suggests that the influence of MJO on Korean impacting TCs may occur, at least in part, through modifications of the tropical environment in which TCs that impact Korea form.

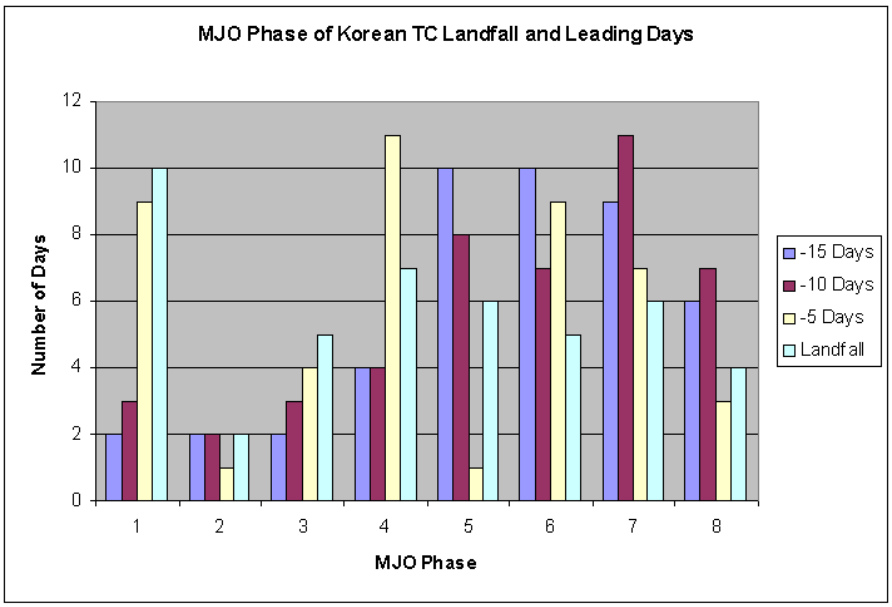

Figure 49. Number of days for which a given MJO phase (1-8) occurred at the day of TC impact in Korea (light blue bar), 5 days before the impact day (yellow), 10 days before the impact day (purple), and 15 days before the impact (blue). For example, 15 days prior to impact day (purple bars), it was common for MJO to be in phase 5, 6, or 7.

To investigate this further, we examined the MJO anomaly composites created by the Australian BOM (Figure 50). The phase 5-7 composites show a marked decrease in average outgoing longwave radiation (OLR) values and higher convective activity in the tropical western North Pacific, indicating a relatively favorable environment for TC formation and intensification.

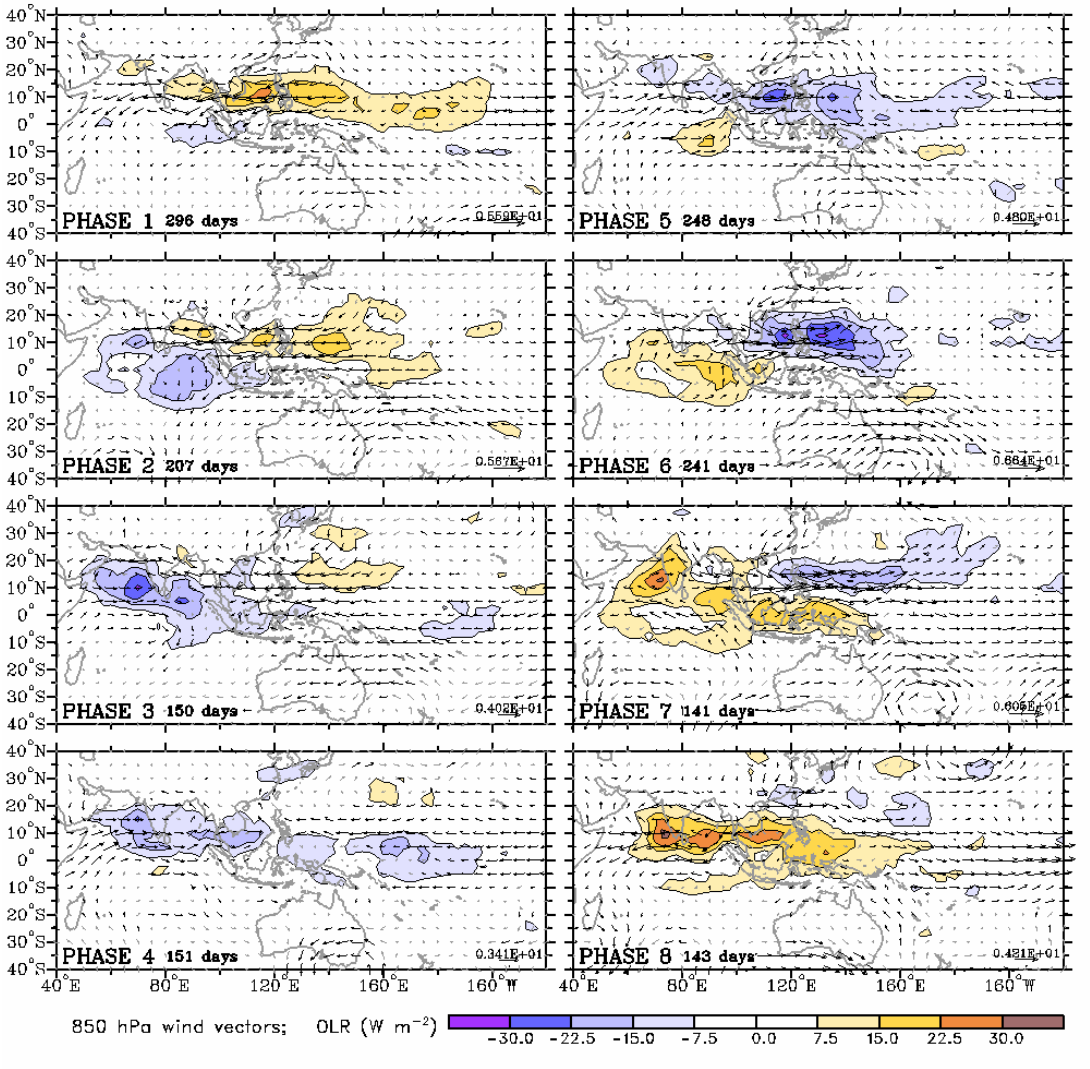

Figure 50. Composites of OLR and 850 hPa wind vector anomalies for each phase of the MJO (From Australian BOM, accessed Jan 2008).

V. SUMMARY AND CONCLUSIONS

A. SUMMARY

This study investigated statistical techniques for forecasting Korean summer precipitation on seasonal and intraseasonal time scales. A review of literature on the Asian summer monsoon showed little research on Korea portion of the summer monsoon specifically, and even less on predictive techniques for the Korean summer monsoon or the more general East Asian summer monsoon. This study showed that, through climate analyses and index development, skillful forecasts of the Korean summer monsoon at leads of one week to several months are possible. In particular, once the Korean summer has begun, MJO phase and intensity, combined with a zonal wind index for the tropical western North Pacific, are useful predictors of Korean summer precipitation at lead times of five to 20 days. The relationship between ENLN and tropical cyclones that impact Korea can also be used to make long lead forecasts of TC impacts on Korea.

For seasonal forecasts of the KSM, the West Pacific Zonal Index was developed. This index uses the box averaged April 925 hPa zonal wind in the tropical western North Pacific, east of the Philippines, as a predictor of the coming KSM. The strength of the zonal wind in this box leads to alterations in upper ocean thermal energy content, which impacts the amount of precipitation in the monsoon trough, which then impacts the amount of precipitation seen over Korea through low level height anomalies to the south of Korea that assist or inhibit KSM convection via favorable or unfavorable low level advections of temperature and moisture.

On the intraseasonal scale, ENLN was shown to have a strong relationship with KSM start, breaks, and withdrawal, possibly through the Philippine Sea Anomalous Anticylone (PSAC) (Wang and Wu 2002). The MJO, when couple with the WPZI, showed skill in hindcasts of Korea summer precipitation at lead times of up to 20 days. The forecast ability lies in the MJOs inherent 30-60 day cycle. This allows the MJO state

at 16 to 20 days prior to the forecast period to impact KSP by changing, in a relativbely predictable way, the lower tropospheric circulations to the south of Korea that then influence precipitation in Korea.

Tropical cyclones that impact Korea were shown to occur preferentially during summers in which El Niño events are intensifying. This appears to be due to the alteration of the background steering flow that leads to more recurving TCs during these EN summers (Ford 2000). We also determined 10-15 days prior to TCs impact Korea, there was a tendency for MJO to be in phase 5, 6, 7, or 8. This appears to be due to the increased convective activity in the monsoon trough associated with these MJO phases, which makes TC formation, and subsequent TC motion toward Korea, more likely.

B. MILITARY USE

As stated in Chapter I, 14 WS develops products that are nearly exclusively based on LTM conditions. Such products do not allow for the consideration of climate variations that can lead to considerable deviations from the LTM. These deviations can have significant effects on military operations. Although not as accurate or precise as most short-range forecasts, the long range forecasting methods presented in this study have the potential to provide more comprehensive and accurate forecasts than is possible form the current practice of using LTM based products for long-range military planning.

This study began with an account of the Korean floods of 1998, floods which caused great damage and loss of both civilian and military lives. To show the possible operational capabilities of the methods created in this study, the summer of 1998 is used as a case study.

In the beginning of May 1998, several judgments could have been be made about the coming Korea summer precipitation. For one, there was a major El Niño event in the prior winter that was still quite strong but was decaying rapidly and was forecasted to continue decaying. Second, low-level normalized zonal wind anomalies in the tropical western North Pacific had been consistently negative throughout the spring. With the

findings in this thesis, climate forecast could have been developed for the coming Korean summer precipitation. A summary and discussion of this hypothetical forecast is presented below.

> Late May 1998: We are emerging from a major El Niño event. As a result of El Niño conditions during January-May 1998, the Korean summer monsoon is forecasted to start one to two weeks later than the first week in July average. Monsoon precipitation is also expected to continue longer in the season, into late August through early September.
>
> Strong El Niño conditions during September 1997 – March 1998, and moderate El Niño conditions during April-May 1998, have led to stronger than normal trade winds in the tropical western North Pacific east of the Philippines. These strong trade winds have, in turn, led to stronger than normal cooling of the ocean surface and upper ocean thermal energy content. As a result, the northern monsoon trough region south of Korea is expected to have less convection than normal, and the Bonin High ridging is expected to be stronger than normal during June-September 1998. These unusual conditions in the Bonin High are expected to increase Korean summer monsoon precipitation, starting in July and extending into mid-September 1998.

The 1998 KSM started earlier, rather than later, than expected, beginning in the last week of June, rather than the second or third week of July. The KSM did last longer than average, into early September. And of course, the monsoon did produce more precipitation, and did so for the reasons presented above.

For intraseasonal forecasts for 1998, using the WPZI as the predictor of pentad KSP would have yielded a forecast accuracy of 14 out of 24 pentads correct, or 58% forecast accuracy. Using the MJO conditioned with the WPZI in the automated program described in chapter IV would have yielded a forecast accuracy of 17 out of 24 pentads correct, or 74% accuracy. If we had only generated forecasts based on relationships for which there is at least 90% statistical significance, our accuracy would have been 10 out of 13, or 77% forecast accuracy.

Another operational use is to include the results of this study in war plans for the Korean Peninsula --- in particular, by using the environmental forecasts to generate

forecasts of the environmental impacts on military operations. The information in this study could be easily folded into the current war plans that are dominated by LTM descriptions of the environment.

C. RECOMMENDATIONS TO THE DEPARTMENT OF DEFENSE

1. Develop Physically-Based Indices for Climate Prediction for Other Regions Important to DoD

Simple, physical indices can be developed, verified and implemented by operational and strategic forecast centers. 14 WS would presumably be in the best position to produce these forecasts.

2. Generalize Conditional MJO Forecasting Technique to Other Regions

The conditional MJO forecasts described in chapter V of this thesis can be easily extended to other regions of the globe with suspected MJO influences on climate and weather patterns. In the same way that the WPZI was used to modify the impacts of MJO, other new or existing indices (e.g., those for MEI, NAO, IOZM, etc.) could be used.

D. FUTURE WORK AND RESEARCH

1. Extrapolate study to examine and forecast precipitation year-round in Korea. Investigate how the impacts of different climate variations on Korea with the time of year.

2. Conduct a more careful examination of how additional Asian monsoon features besides the monsoon trough in the tropical western North Pacific influence

Korean precipitation. In particular, the interactions between the Indian summer monsoon and the northeast Asian summer monsoon must be clarified to improve intraseasonal forecasts for Korea.

3. The relationships between tropical cyclones and the northeast Asian summer monsoon should be better quantified, through a more detailed accounting of circulation patterns and use of climate indices.

4. More advanced methods should be explored to improve the climate forecasting techniques presented in this thesis. Non-linear methods could be used to help develop a better understanding of the complex monsoon environment.

5. Develop standard operating procedures and forecast reference notebook material based on this study for use by all levels of military forecasters.

THIS PAGE INTENTIONALLY LEFT BLANK

LIST OF REFERENCES

Ambaum, M. H. P., and B. J. Hoskins, 2002: The NAO troposphere-stratosphere connection. *J. Climate*, 15, 1969-1978.

Annamalai, H., J. Slingo, 2001: Active/Break Cycles: Diagnosis of the Intraseasonal Variability of the Asian Summer Monsoon. *Climate Dynamics*, 18, 85-102.

Barnston, A.G., and R.E. Livezey, 1987: Classification, Seasonality and Persistence of Low-Frequency Atmospheric Circulation Patterns. *Mon. Wea. Rev.*, 115, 1083–1126.

Black, E., J. Slingo, and K. Sperber, 2003: An observational study of the relationship between excessively strong short rains in coastal east Africa and Indian Ocean SST. *Mon. Wea. Rev*., 131, 74-94.

Bond, N.A., and G.A. Vecchi, 2003: The Influence of the Madden–Julian Oscillation on Precipitation in Oregon and Washington. *Wea. Forecasting*, 18, 600–613.

Chen, T.J.G., and C.P. Chang, 1980: The Structure and Vorticity Budget of an Early Summer Monsoon Trough (Mei-Yu) over Southeastern China and Japan. *Mon. Wea. Rev.*, 108, 942–953.

Chang, C.P., S.C. Hou, H.C. Kuo, and G.T.J. Chen, 1998: The Development of an Intense East Asian Summer Monsoon Disturbance with Strong Vertical Coupling. *Mon. Wea. Rev.*, 126, 2692–2712.

Chang, C.P., P. Harr, and J. Ju, 2001: Possible Roles of Atlantic Circulations on the Weakening Indian Monsoon Rainfall–ENSO Relationship. *J. Climate*, 14, 2376–2380.

Ding, Y.H., 1992: Summer monsoon rainfall in China. *J. Meteor. Soc. Japan*, 70, 373-396.

Ding, Y.H. and C.L. Chan, 2005: The East Asian summer monsoon: an overview. *Meteor. Atmos. Phys.*, 89, 117-142.

Ding, Q. and B. Wang, 2005: Circumglobal teleconnection in the Northern Hemisphere Summer. *J. Climate*, 18, 3483-3505.

Ding, Q., and B. Wang: 2007: Intraseasonal teleconnection between the Eurasian wavetrain and Indian summer monsoon. *J. Climate*, 20, 3751-3767.

Dugam, S.S., Kakade, S.B. and Verma, R.K.,1997. 'Interannual and long-term variability in the North Atlantic Oscillation and Indian summer monsoon rainfall', *Theor. Appl. Climatol.* 58, 21-29.

Dugam, S. 2006: Monsoon Variability in Relation to ENSO and NAO. Proceedings of 8 ICSHMO, Foz do Iguaçu, Brazil.

Ford, B. W., 2000: El Niño and La Niña Effects on Tropical Cyclones: The mechanisms. M. S. thesis, Dept of Meteorology, Naval Postgraduate School, 190 pp.

Gill, A. E., 1980: Some simple solutions for heat induced tropical circulation. *Quart. J. Roy. Meteor. Soc*., 106, 447-462.

Gong, D., and C. Ho (2003), Arctic oscillation signals in the East Asian summer monsoon, *J. Geophys. Res*., 108(2), 4066-4072

Goswami, B. N., 2005: The Asian monsoon: Interdecadal variability. Springer, pp 285-327.

Ha, K. J., Park, S. K. and K. Y. Kim, 2005: On interannual characteristics of Climate Prediction Center merged analysis precipitation over the Korean peninsula during the summer monsoon season. *Int. J. Climatol.* 25: 99–116

Hanson, C. 2007. Long Range Operational Military Forecasts for Iraq. M.S. Thesis, Dept. of Meteorology, Naval Postgraduate School, 59 pp.

Ha, K. J., Park, S. K., Kim, K. Y. 2005. On Interannual Characteristics of Climate Prediction Center Merged Analysis Precipitation over the Korean Peninsula During the Summer Monsoon Season. *Int. J. Climatol*., 25, 99-116.

Ha, K. J. and S. S. Lee, 2007: On the interannual variability of the Bonin high associated with the East Asian summer monsoon rain. *Climate Dynamics*, 28, 67-83.

Hawthorne, L., Stanley, G., and B. Tate, cited 2008. [Accessed online at http://www.hq.usace.army.mil/cepa/pubs/sep98/story2.htm]. Accessed March 2008.

Hendon, H.H., and B. Liebmann, 1990: The Intraseasonal (30–50 day) Oscillation of the Australian Summer Monsoon. *J. Atmos. Sci.*, 47, 2909–2924.

Hendon, H.H., and M.L. Salby, 1994: The Life Cycle of the Madden–Julian Oscillation. *J. Atmos. Sci.*, 51, 2225–2237.

Horel, J. D., and J. M. Wallace, 1981: Planetary-scale atmospheric phenomena associated with the Southern Oscillation. *Mon. Wea. Rev*., 109, 813-829.

Hurrell, J. W., Y. Kushnir, G. Ottersen, and M. Visbeck, 2003: An overview of the North Atlantic Oscillation. *The North Atlantic Oscillation: Climatic Significance and Environmental Impact. Geophys. Monogr.*, No. 134, Amer. Geophys. Union, 1-34.

Huang, R., and Y. Wu, 1989: The influence of ENSO on the summer climate change in China and its mechanism. *Adv. Atmos. Sci.,* 6, 21–32.

Hwang, S.O., J.K.E. Schemm, A.G. Barnston, and W.T. Kwon, 2001: Long-Lead Seasonal Forecast Skill in Far Eastern Asia Using Canonical Correlation Analysis. *J. Climate*, 14, 3005–3016.

Jarry, J., 2005. Analysis of Air Mobility Command Weather Mission Execution Forecasts: Metrics of Forecast Performance and Impacts on War Fighting Operations. M.S. Thesis, Naval Postgraduate School, 170 pp.

Jhun, J. G. and B. K. Moon, 1997: Restoration and analyses of rainfall amount observed by Chugugi. *J. Korean Meteor. Soc*, 33, 692-707.

Kalnay, E. et al. 1996: The NCEP/NCAR 40-Year Reanalysis Project. *Bull. Amer. Meteor. Soc.*, 77, 437–471.

Kawamura, R., 1998: A Possible Mechanism of the Asian Summer Monsoon-ENSO Coupling. *J. Meteor. Soc. Japan*, 76, 1009-1027.

Kemball-Cook, S., and B. Wang, 2001: Equatorial Waves and Air–Sea Interaction in the Boreal Summer Intraseasonal Oscillation. *J. Climate*, 14, 2923–2942.

Kim, M. K., Kim, Y. H., Lee, W. S. Seasonal prediction of Korean regional climate from preceding large-scale climate indices *Int. J. Climatol.* 2006.

Kripalani, R. H., Oh, J. H., Kang, J. H., Sabade, S. S., and A. Kulkarni, 2005: Extreme monsoons over East Asia: Possible role of Indian Ocean Zonal Mode. *Theor. Appl. Climatol*., 82, 81–94

Lamb, P. J. and R. A. Peppler, 1987: North Atlantic Oscillation: Concept and an Application. *Bull. Amer. Meteor. Soc.*, 68, 1218-1225.

Lau, K.M., and P.H. Chan, 1988: Intraseasonal and Interannual Variations of Tropical Convection: A Possible Link between the 40–50 Day Oscillation and ENSO? *J. Atmos. Sci.,* 45, 506–521.

Legates, D.R. and C.J. Willmott, 1990. Mean seasonal and spatial variability in gauge-corrected, global precipitation. *International Journal of Climatology*, 10, 111-127.

Lim, Y.K., and K.Y. Kim, 2007: ENSO Impact on the Space–Time Evolution of the Regional Asian Summer Monsoons. *J. Climate*, 20, 2397–2415.

Liu, Y.J., Ding, Y. H. and J. H. He, 2003: A study of a typical Meiyu front. *Acta Meteorol. Sinica*, 61, 291-301.

Madden, R. A., and P. R. Julian, 1971: Description of a 40-50 day oscillation in the zonal wind in the tropical Pacific. *J. Atmos. Sci*., 28, 702-708.

Madden, R. A., and P. R. Julian, 1994: Observations of the 40-50-day tropical oscillation—a review. *Mon. Wea. Rev*., 122, 814-837.

Matsuno, T., 1966: Quasi-geostrophic motions in the equatorial area. *J. Meteor. Soc. Japan*, 44, 25-42.

Moss, S. 2007. Long Range Operational Military Forecasts for Afghanistan. M.S. Thesis, Dept. of Meteorology, Naval Postgraduate School, 77 pp.

Neelin, J. D., D. S. Battisti, A. C. Hirst, F. F. Jin, Y. Wakata, T. Yamagata, and S. E. Zebiak, 1998: ENSO theory. *J. Geophys. Res*., 103, 14 261-14 290.

Nitta, T., 1987: Convective activities in the tropical western Pacific and their impact on the Northern Hemisphere summer circulation, *J. Meteor. Soc. Japan*, 65, 373-390.

Ramage, C. S., 1971: *Monsoon Meteorology*. International Geophysical Series, Vol. 15, Academic Press, 296 pp.

Saji, N. H. and T. Yamagata, 2003: Possible impacts of the Indian Ocean Dipole mode events on global climate. *Clim. Res*., 25, 151-169.

Saji, N. H., B. N. Goswami, P. N. Vinayachandran, and T. Yamagata, 1999: A dipole mode in the tropical Indian Ocean. *Nature*, 401, 360-363.

Sardeshmukh, P. D., and B. J. Hoskins, 1988: The generation of global rotational flow by steady idealized tropical divergence. *J. Atmos. Sci*., 45, 1228-1251.

Stepanek, A., 2006. Improving Medium-Range Forecasts in North America Using Teleconnections Associated with the Madden-Julian Oscillation. M.S. Thesis, Dept. of Meteorology, Naval Postgraduate School, 119 pp.

Sun, J., Lee, T. Y., 2002: A Numerical Study of an Intense Quasi-stationary Convection Band over the Korean Peninsula, *J. Meteor. Soc. Japan*, 80, 1221-1245.

Tanaka, M., 1992: Intraseasonal oscillation and the onset and retreat dates of the summer monsoon over East, Southeast Asia and the Western Pacific region using GMS high cloud amount data, *J. Meteor. Soc. Japan*, 70, 613-629.

Tao S., and L. Chen, 1987: A review of recent research on the East Asian summer monsoon in China. *Monsoon Meteorology*, C.-P. Chang and T. N. Krishnamurti, Eds., Oxford University Press, 60–92.

Teng, H. and B. Wang, 2003: Interannual Variations of the Boreal Summer Intraseasonal Oscillation in the Asian–Pacific Region. *J. of Climate*, 16, 3572-3584

Thompson, D. W. J., and J. M. Wallace, 1998: The Arctic Oscillation signature in the wintertime geopotential height and temperature fields. *Geophys. Res. Lett*., 25, 1297-1300.

Thompson, D. W. J., and J. M. Wallace, 2000: Annular modes in the extratropical circulation, Part I: Month-to-month variability. *J. Climate*, 13, 1000-1016.

Trigo, R. M., T. J. Osborn, J. M. Corte-Real, 2002: The North Atlantic Oscillation influence on Europe: climate impacts and associated physical mechanisms. *Clim. Res.*, 20, 9-17.

Twigg, K., 2007: A Smart Climatology of Evaporation Duct Heights and Surface Radar Propagation for the Northwest Indian Ocean and Nearby Regions. M. S. Thesis, Dept. of Meteorology, Naval Postgraduate School, 159 pp.

Vorhees, D., 2006: The impacts of global scale climate variations on Southwest Asia. M.S. Thesis, Dept. of Meteorology, Naval Postgraduate School, 175 pp.

Waliser, D. E., 2005: The Asian monsoon: Interdecadal variability. Springer, pp 203-257.

Wang, B., R. Wu, and X. Fu, 2000: Pacific-East Asia teleconnection: How does ENSO affect East Asian climate? *J. Climate*, 13, 1517-1536.

Wang, B. and LinHo, 2002: Rainy seasons of the Asian-Pacific monsoon. *J. Climate*, 15, 386-398.

Wang, B., and Q. Zhang, 2002: Pacific-East Asian teleconnection, part II: How the Philippine Sea anticyclone established during development of El Niño. *J. Climate*, 15, 3252-3265.

Wang, B., Lin Ho, Yongsheng Zhang, and M.-M. Lu, 2004: Definition of South China Sea Monsoon Onset and Commencement of the East Asia Summer Monsoon. *J. Climate*, 17, 699–710.

Wang, B., 2005: *Asian Summer Monsoon*, Springer, 750 pp

Wang, B., Jhun, J.G., and B.K. Moon, 2007: Variability and Singularity of Seoul, South Korea, Rainy Season (1778–2004). *J. Climate*, 20, 2572–2580.

Webster, P. and S. Yang, 1992: Monsoon and ENSO: Selectively interactive systems. *Quarterly Journal of the Royal Meteorological Society*. 118(507), 877-926.

Wilks, D., 2006: *Statistical Methods in the Atmospheric Sciences*, Academic Press, 627 pp.

Wheeler, M.C., and H.H. Hendon, 2004: An All-Season Real-Time Multivariate MJO Index: Development of an Index for Monitoring and Prediction. *Mon. Wea. Rev.*, 132, 1917–1932.

Whitaker, J.S., and K.M. Weickmann, 2001: Subseasonal Variations of Tropical Convection and Week-2 Prediction of Wintertime Western North American Rainfall. *J. Climate*, 14, 3279–3288.

Willmott, C.J., S.M. Robeson and J.J. Feddema, 1994. Estimating continental and terrestrial precipitation averages from rain-gauge networks. *International Journal of Climatology*, 14(4), 403-414.

Wolter, K. and M. S. Timlin, 1993: Monitoring ENSO in COADS with a seasonally adjusted principal component index. *Proc. 17th Climate Diagnostics Workshop*

Xie, P., and P. A. Arkin, 1997: Global precipitation: A 17-year monthly analysis based on gauge observations, satellite estimates, and numerical model outputs. *Bull. Amer. Meteor. Soc.*, 78, 2539–2558.

Yang, S., K.M. Lau, S.H. Yoo, J.L. Kinter, K. Miyakoda, and C.H. Ho, 2004: Upstream Subtropical Signals Preceding the Asian Summer Monsoon Circulation. *J. Climate*, 17, 4213–4229.

Yasunari T., 1979: Cloudiness fluctuations associated with the Northern Hemisphere summer monsoon. *J. Meteor. Soc. Japan*, 57, 227–242.

Yu, L., Weller, R. A., and W. T. Liu, 2003: Case analysis of a role of ENSO in regulating the generation of westerly wind bursts in the western equatorial Pacific. *J. Geophys. Res.*, 108(4), 3128

Zhang, C., 1996: Atmospheric Intraseasonal Variability at the Surface in the Tropical Western Pacific Ocean. *J. Atmos. Sci.*, 53, 739–758.

INITIAL DISTRIBUTION LIST

1. Defense Technical Information Center
   Ft. Belvoir, Virginia

2. Dudley Knox Library
   Naval Postgraduate School
   Monterey, California

3. Prof. Tom Murphree
   Code MR/WA
   Naval Postgraduate School
   Monterey, California

4. Col Dave Smarsh
   Naval Postgraduate School
   Monterey, California

5. Dr. Zhuo Wang
   Code MR/WA
   Naval Postgraduate School
   Monterey, California

6. Air Force Weather Technical Library
   Asheville, North Carolina